NASA CR-159,543

DOE/NASA 0022 - 79/1
NASA CR-159543
SRC-78TR-39

NASA-CR-159543
19790015258

EXPERIMENTAL AND ANALYTICAL TOOLS FOR EVALUATION OF STIRLING ENGINE ROD SEAL BEHAVIOR

Allan I. Krauter
Shaker Research Corporation

Herbert S. Cheng
Northwestern University

February 1979

Prepared for
NATIONAL AERONAUTICS AND SPACE ADMINISTRATION
Lewis Research Center
Cleveland, OH 44135
Under Contract DEN3-22

for
U.S. DEPARTMENT OF ENERGY
Office of Conservation and Solar Applications
Division of Transportation Energy Conservation
Washington, DC 20545

DOE/NASA 0022 - 79/1
NASA CR-159543
ED-77-A-31-1040

EXPERIMENTAL AND ANALYTICAL TOOLS FOR EVALUATION OF STIRLING ENGINE ROD SEAL BEHAVIOR

Allan I. Krauter
Shaker Research Corporation
Ballston Lake, New York 12019
Herbert S. Cheng
Department of Mechanical Engineering
Northwestern University
Evanston, Illinois 60201

February 1979

Prepared for
NATIONAL AERONAUTICS AND SPACE ADMINISTRATION
Lewis Research Center
Cleveland, OH 44135
Under Contract DEN3-22

for
U.S. DEPARTMENT OF ENERGY
Office of Conservation and Solar Applications
Division of Transportation Energy Conservation
Washington, DC 20545

TABLE OF CONTENTS

LIST OF FIGURES

LIST OF FIGURES (Continued)

LIST OF TABLES

INTRODUCTION

The Stirling engine is currently the subject of intensive study by the Department of Energy. This engine has the potential to provide clean and efficient propulsive power for the automobile and for other highway vehicles. In order to do so, however, several technical problems associated with such use of the Stirling engine must be solved.

One of the technical problems that must be addressed is the rod seal. This seal has the function of separating the high pressure gas from the low pressure crank case oil. The seal can be either a sliding seal or a roll sock seal. The sliding seal is simpler, less expensive, and possesses a more gradual failure mode than the roll sock seal. However, the sliding seal, unlike the roll sock seal, is not hermetic. Additionally, the sliding seal is subject to wear and can produce undesirable levels of friction force.

The performance of the sliding seal with respect to leakage, wear, and friction can be improved from its present level. To do so requires that the details of the behavior of the seal in the Stirling engine be understood. Additionally, it is necessary to be able to treat the behavior of the seal in a quantitative manner. It is the objective of the work under the current NASA Contract DEN3-22 to progress substantially toward these ends. Specifically, the contract is directed at applying hydrodynamic and elastohydrodynamic theory to the rod seal. The contract is also concerned with the experimental determination of film thickness, fluid leakage, and power loss. The contract entails both producing correlation of experimental and theoretical results and developing tools appropriate for evaluation of rod seal behavior.

The present document is an interim report of work completed in the first year of the two year effort. During the year tools for evaluating rod seal behavior have been developed. Analytically, a computer model of the elastohydrodynamic behavior of the rod seal for reciprocating motion is available. The model permits the large initial radial squeeze, which is typically used for elastomeric seals, to exist. The model determines both the pressure distribution and the oil film thickness distribution in the seal/cylinder contact zone. In this, the calculations are made with time as the independent parameter; consequently, the computer model provides film thickness and pressure results as a function of cyclic position.

Experimentally, a rugged apparatus capable of providing film thickness, friction force, and seal leakage data has been completed. The apparatus contains a moving transparent cylinder (guided by precision hydrostatic bearings) and a stationary elastomeric test seal. A pressure gradient of 690 kPa (100 psi) can be applied across the seal. Frequencies from 10 Hz to 50 Hz with a 0.254 m (1.000 inch) total stroke can be employed. Film thickness is measured with interferometry,

fluid leakage by level and pressure changes, and power (friction) loss by force cells.

This report describes both the experimental and the analytical work completed to date. The experimental effort is discussed in the next section. Included in the section are descriptions of the experimental apparatus, of its capabilities, and of preliminary results from its use. Also included in the section is a discussion of the technique, developed under the contract work, for producing interferometry fringes at the seal/cylinder interface. The special attention given in this report to interferometry is due to the importance of film thickness measurement in the contract work.

The analytical effort is covered both in the section following that for the experimental work and in the Appendices. The section presents the rod seal analysis which is implemented in the computer program given in the Appendixes. (A description of how the program is used is also given in the Appendixes.) In addition, the section presents results obtained from use of the computer program.

The Conclusions and Recommendations section concerns the application during the ensuing year of the analytical and experimental tools developed during the past year and described in this report.

Page 3 intentionally left blank.

EXPERIMENTAL REPORT

This section discusses the experimental apparatus that was designed and constructed during the past year. The capabilities of the device and the results obtained from its preliminary use are described. In addition, measurement of film thickness, accomplished by interferometric techniques, is considered. The separate treatment is given to interferometry because of the importance of film thickness measurement to the contract work.

The experimental device has not as yet been used to evaluate the behavior of the rod seal or to produce experimental/analytical correlations. Work in these areas is planned for the ensuing year and is described in the Conclusions and Recommendations section.

The Experimental Apparatus

The experimental apparatus is designed to facilitate the measurement of film thickness, seal friction force, and fluid leakage. The greatest experimental difficulties are associated with determining film thickness. Consequently, the design of the apparatus is based on the technique selected for this measurement.

A review of the available techniques for film thickness measurements was made in order to select that method most appropriate to the elastomeric seal/cylinder wall interface. Some details of that review are presented in the subsection below entitled "Interferometry." The result of the review was the selection of optical interferometry. Accordingly, the experimental apparatus contains a transparent cylinder. In addition, in order to minimize the difficulties of using the interferometric technique, it is this cylinder, rather than the rod seal, that reciprocates. The use of a reciprocating transparent cylinder and a stationary elastomeric rod seal was the most important feature that affected the design of the device.

Other features also affected the design. These features can be grouped in three categories: Measurement capabilities, performance capabilities and characteristics, and ease of use. Each of these categories is considered below.

In the measurement category, it is desirable to be able to determine the instantaneous seal friction force and the instantaneous pressure on the gas side of the seal. It is also desirable that some indication be obtained of the temperature near the seal/cylinder interface. Finally, it is desirable for the apparatus to produce direct macroscopic indications of oil and gas leakage.

In the category of performance capabilities and characteristics, a rather lenghtly list of desirable features can be developed. Some of the more significant ones are:

- capability for a reasonable magnitude of pressure drop across the seal
- compression (rather than tension) in the transparent cylinder (to utilize its strength characteristics)
- minimum variation of the gas pressure during each cycle of the cylinder
- precise guidance of the cylinder and minimum cylinder runout
- infinitely variable speed in the range from 10 to 50 Hz
- provision for water cooling
- accurate alignment of the seal with respect to the transparent cylinder
- long life span (low stress levels)
- rigid mounting structure
- few static seals
- oil above the test seal (to insure fully flooded conditions)
- vertical rod axis (to insure axisymmetric seal behavior)
- balanced dynamic forces, and
- synchronization of optics with cylinder motion.

In the category of ease of use, significant features are:

- ease of testing various types of seals
- ease of replacing the seal and maintaining alignment
- ease of removing the test seal from the transparent cylinder, and
- ease of parts replacement.

The experimental apparatus constructed during the past year was designed to incorporate the features in the three categories above. The design is centered around the transparent cylinder which reciprocates with a 25.4 mm (1.000 inch) peak to peak displacement. The transparent cylinder has a 76 mm (3 inch) I. D. This I. D. was chosen large enough to prevent excessive difficulties in producing optical interferometry measurements, and small enough to keep the size of the apparatus (and the associated internal forces) reasonable. In addition, the cylinder bore was chosen such that the seal size is standard and relatively common.

The overall apparatus is shown in the photograph of Figure 1. In the photograph can be seen the stationary plunger which holds the test seal and the oscillating assembly which contains the transparent cylinder. The photograph also shows, at the lower left, a pump and pressure tank. This pump and pressure tank provide high pressure oil to precision hydrostatic bearings which guide the reciprocating parts. The large motor in the center of the photograph is the prime mover which drives the apparatus. Its output speed can be varied continuously from less than 10 Hz to more than 50 Hz. The lattice cage which encloses the rotating and reciprocating parts provides a measure of operator safety. The framework for the apparatus is constructed of thick steel plate and I beams with relatively large cross sections.

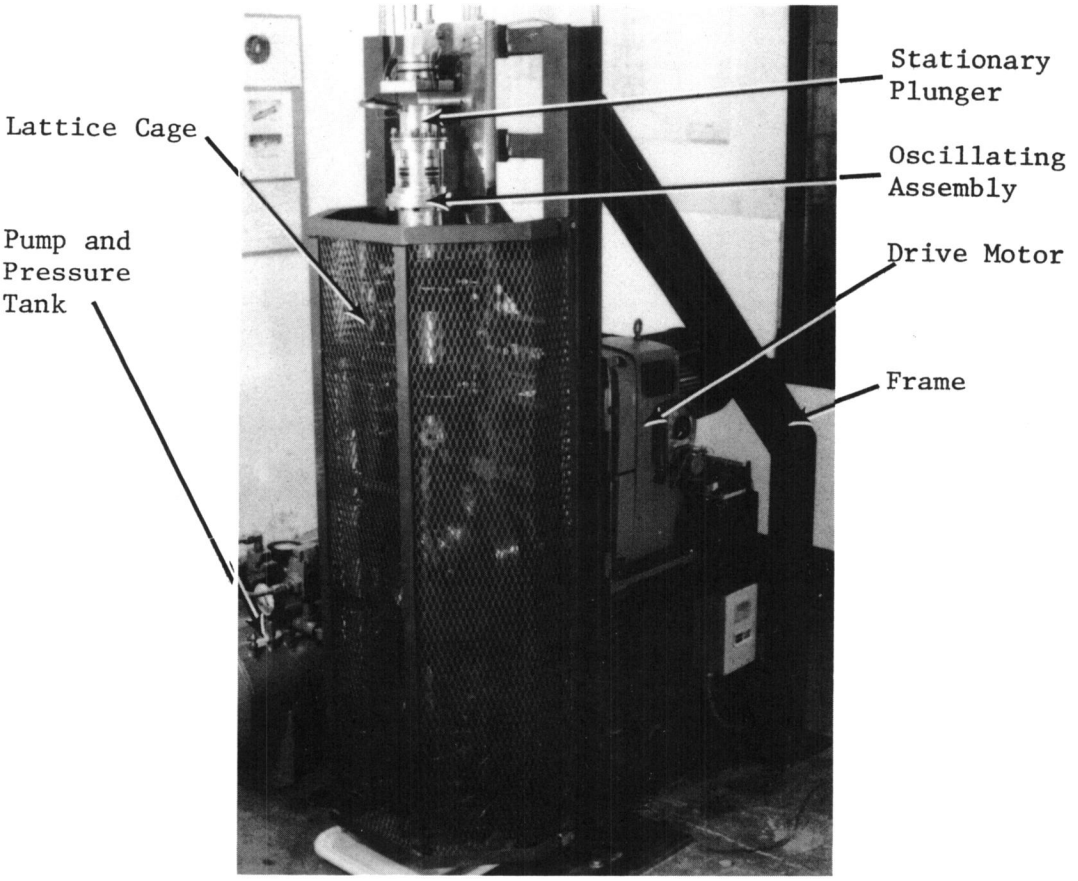

Figure 1 Overall View of
Experimental Apparatus

The frame stands about 1.8 m (6 feet) tall. As pictured in Figure 1, the device has a mass of approximately 500 kg (1,100 pounds mass).

Removal of the guard cage allows components of the drive system to be seen. This has been done in Figure 2, which shows the flywheel, two connecting rods, and 4 hydrostatic bearings with their associated plumbing. These components can also be identified by referring to Figure 3, which is a schematic drawing of the apparatus.

The lower connecting rod is attached to a shaft which moves downward when the upper assembly (which contains the transparent cylinder) moves upward. The sole function of this lower shaft is to balance the vertical forces in the rig. Each shaft is guided by two precision hydrostatic oil bearings which are of a four pad design and contain rubber seals at top and bottom. The shafts are constructed of aluminum. They are attached to their respective connecting rods by needle bearings.

Figure 4 shows some details of the upper end of the apparatus. A schematic drawing which corresponds generally to this photograph is presented in Figure 5. The schematic shows both the exterior outline of this end of the apparatus (on the left in the figure) and some internal details (on the right in the figure).

Referring to both Figures 4 and 5, the hydrostatic bearings and the plunger which holds the test seal are mounted to a backing plate. This backing plate and the one for the lower shaft were assembled to the framework (against the machined tabs, Figure 4) and the bores of all four hydrostatic bearings were machined together. This process insured that the axes of all four hydrostatic bearings became coincident upon assembly of the apparatus. During this machining process, the stationary plate was milled. This procedure resulted in the top surface of the stationary plate being perpendicular to the axis of the four hydrostatic bearings. Doweling of the stationary plate to the backing plate and of the hydrostatic bearings to the backing plate allowed for disassembly of the apparatus subsequent to the machining operation for insertion of the moving shaft.

Several additional components in Figure 4 are worthy of discussion. The vertical pipe at the lower left of the photograph is the manifold for the hydrostatic oil supply. The three small pipes just to the left of center at the top of the photograph are the supply lines to the oil side of the seal, to the gas side of the seal, and for the water cooling. The return water leaves the apparatus through the threaded pipe at the top center of the photograph.

The plunger is connected to the stationary plate with four bolts (three of which can be seen in Figure 4). This arrangement can be readily described by referring to Figures 6 and 7. Figure 6 shows the

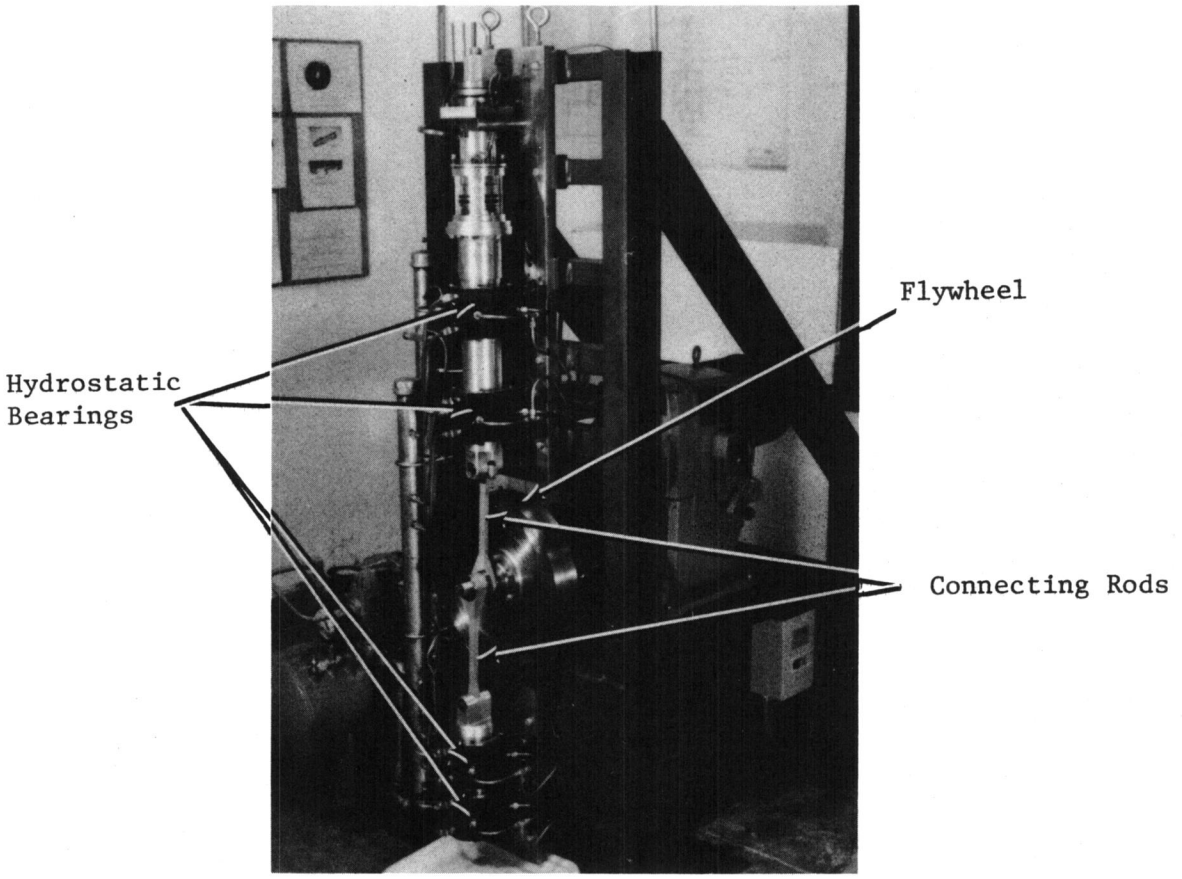

Figure 2 Overall View of Experimental Apparatus
With Guard Cage Removed

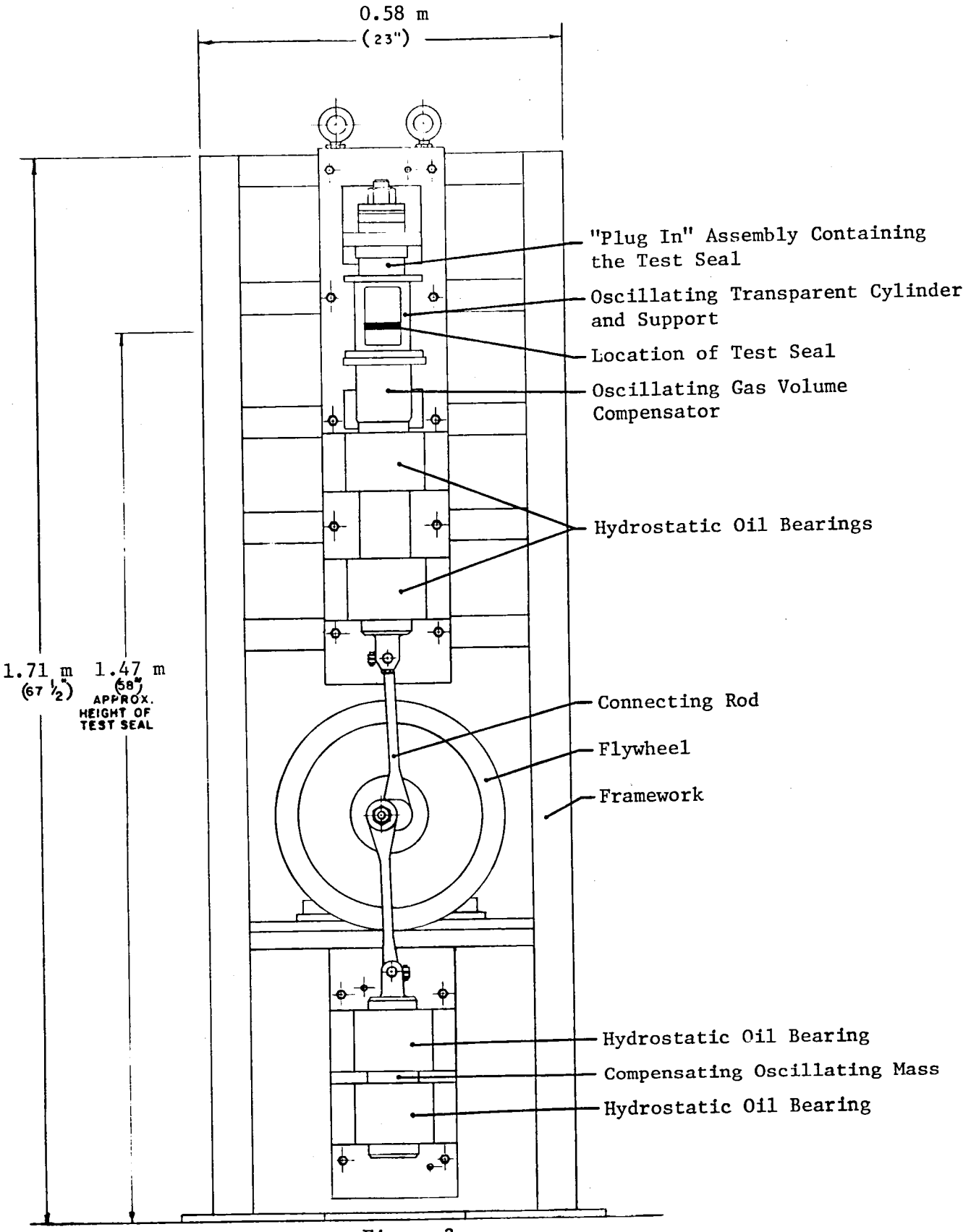

Figure 3
Layout of the Experimental Device

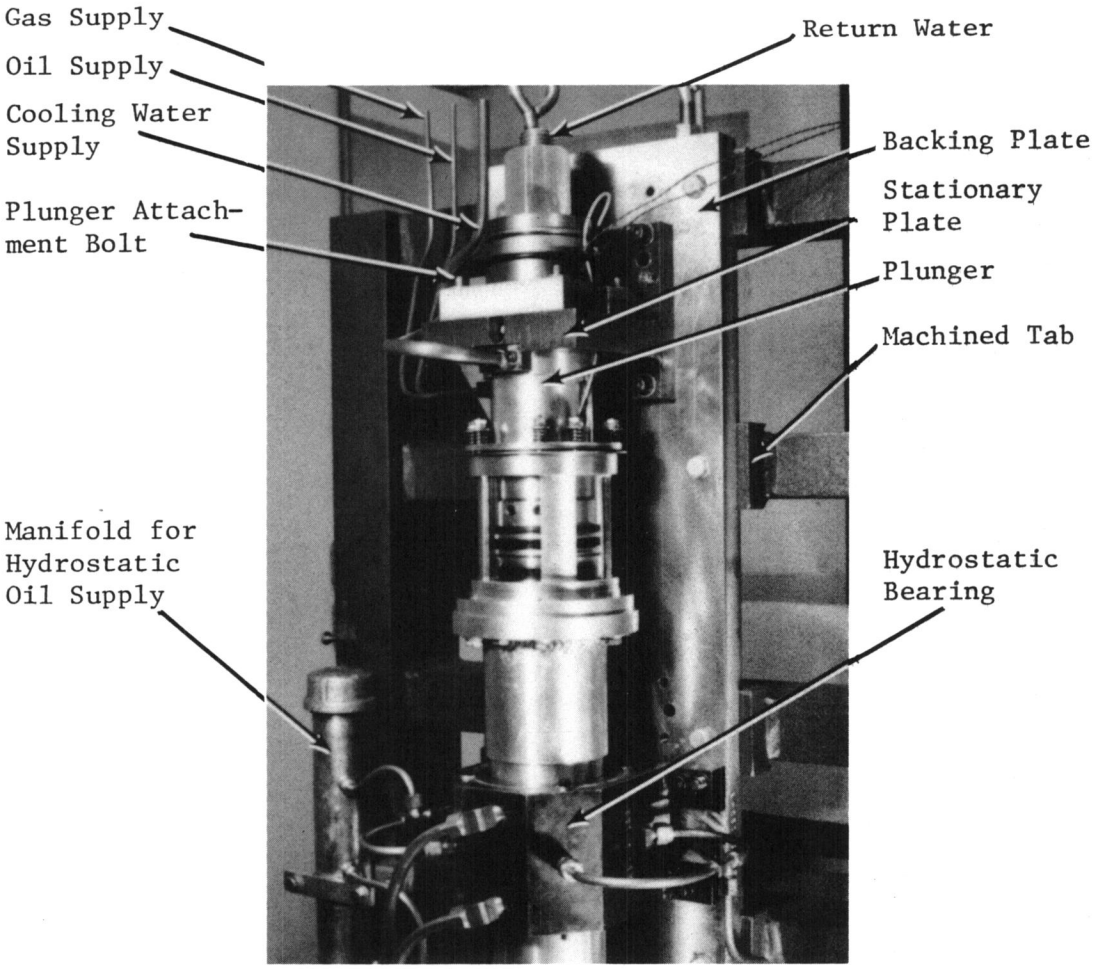

Figure 4 Close-up of Upper End of Experimental Apparatus

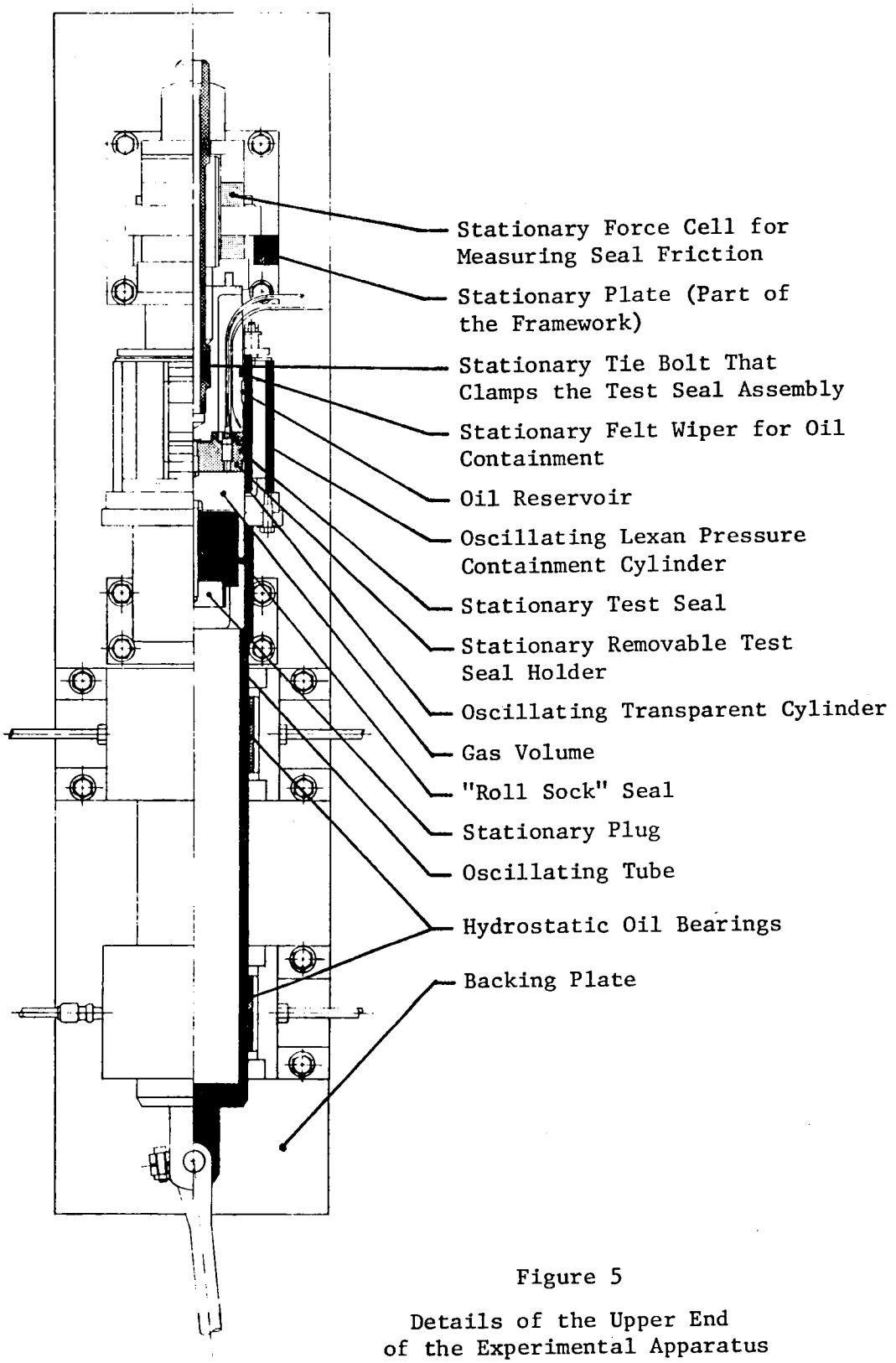

Figure 5

Details of the Upper End
of the Experimental Apparatus

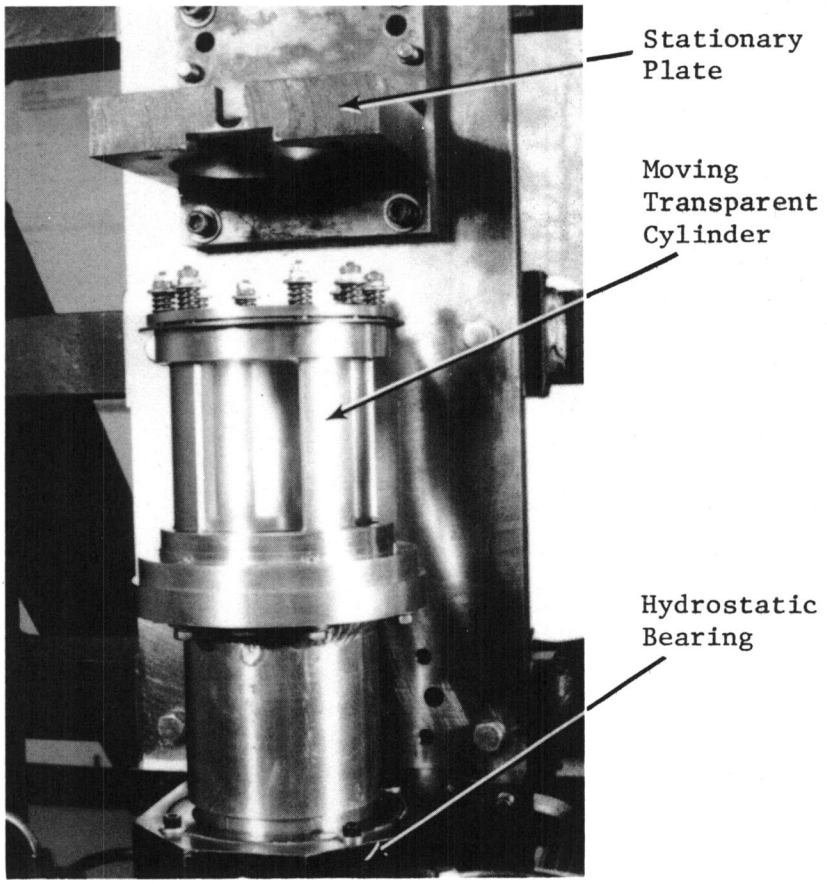

Figure 6 Transparent Cylinder Region of Apparatus With Plunger Removed

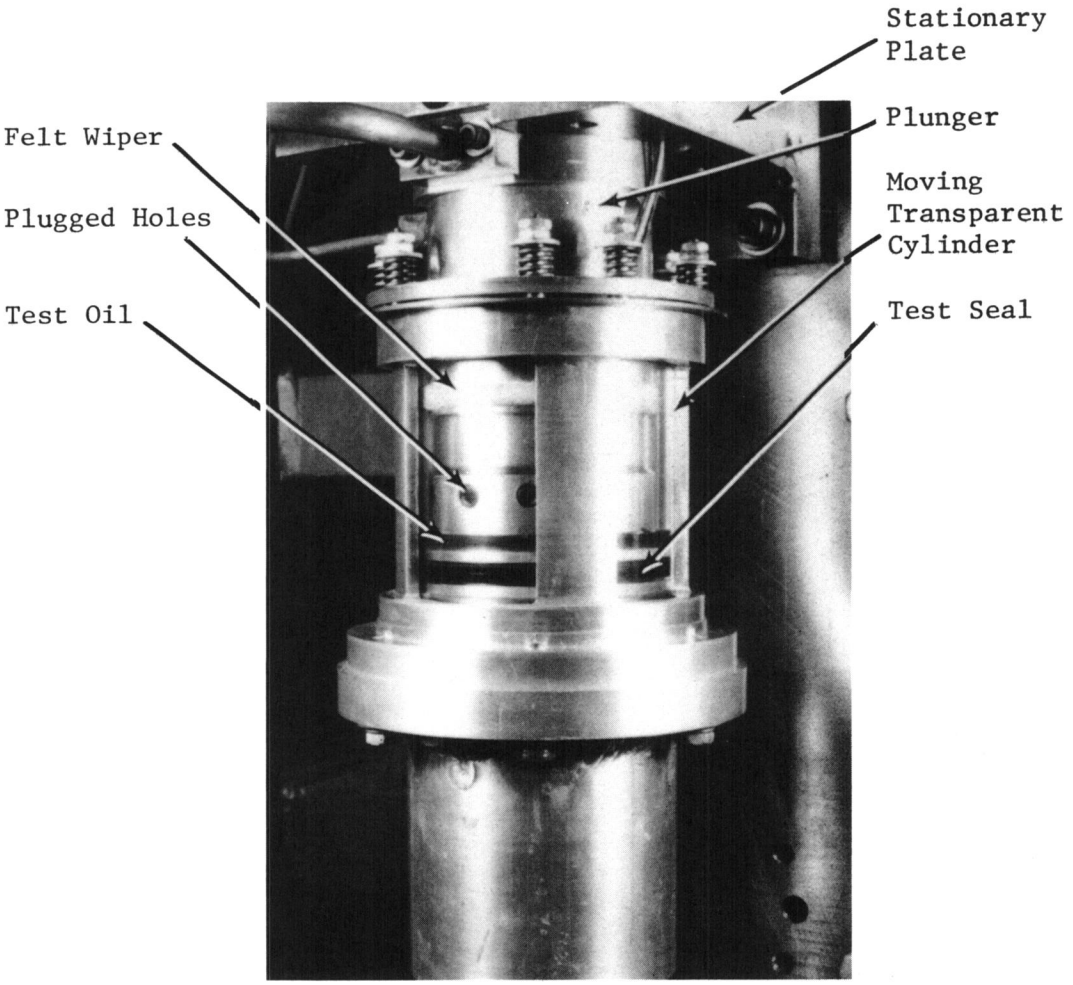

Figure 7 Transparent Cylinder Region of Apparatus With Plunger Installed

apparatus with the plunger removed. The stationary plate is at the top of the picture, the moving transparent cylinder (and its housing) are at the center of the picture, and the uppermost hydrostatic bearing is at the bottom of the picture. Figure 7 is a similar view with the plunger installed. In Figure 7, the bottom of the stationary plate can be seen at the very top of this photograph.

Figures 6 and 7 (as well as the schematic of Figure 5) indicate how the transparent cylinder is supported in its housing. The cylinder is inside the webs of this aluminum housing and is compressed axially by the 8 springs. Alignment is produced by boring the cylinder at the same time as the bottom face is cut. Not shown in the photographs (but included in Figure 5) is an outer transparent cylinder. This outer cylinder is also loaded axially by the 8 springs and can sustain 690 kPa (100 psi) of gas pressure. Use of the outer cylinder results in compressive, rather than tensile, gas loading on the inner cylinder. The apparatus can be run without the outer cylinder (for zero pressure drop across the seal) or with the outer cylinder (for pressure drops up to 690 kPa (100 psi)).across the seal. Also not shown in the photographs (but included in Figure 5) is the containment for the gas volume. This containment is effected by attaching a Bellofram rollsock seal to the inside of the moving upper shaft. The other end of this rollsock seal is attached to a stationary plug which is in turn, attached to the backing plate. The design of the rollsock seal is such that the gas volume changes little during the reciprocating shaft motion. When the gas volume is connected to an external gas reservoir, the peak pressure variations are estimated to be less than 1.70 kPa (0.25 psi) at 690 kPa (100 psi) gas pressure.

Figure 7 shows several significant parts of the stationary plunger. Through the transparent Lexan cylinder, one can see, proceeding from top to bottom, the felt wiper which contains the seal oil, plugged holes which are associated with the water cooling system, a volume of test oil (upper dark band), and the test seal (lower dark band). The parts can be seen more easily in Figure 8, which shows only the plunger.

In Figure 8, the test seal can be seen near the lower right end of the plunger. This end of the plunger (the test seal holder) can be disassembled from the body of the plunger by removing the 4 bolts at the lower right of the picture. This is accomplished by first straightening the locking tabs. Having the test seal holder replaceable allows various types of seals to be tested. For each type of seal, a holder is required in which a groove appropriate to the seal has been cut. For the holder in Figure 8, the groove has been cut for the T seal shown in the photograph.

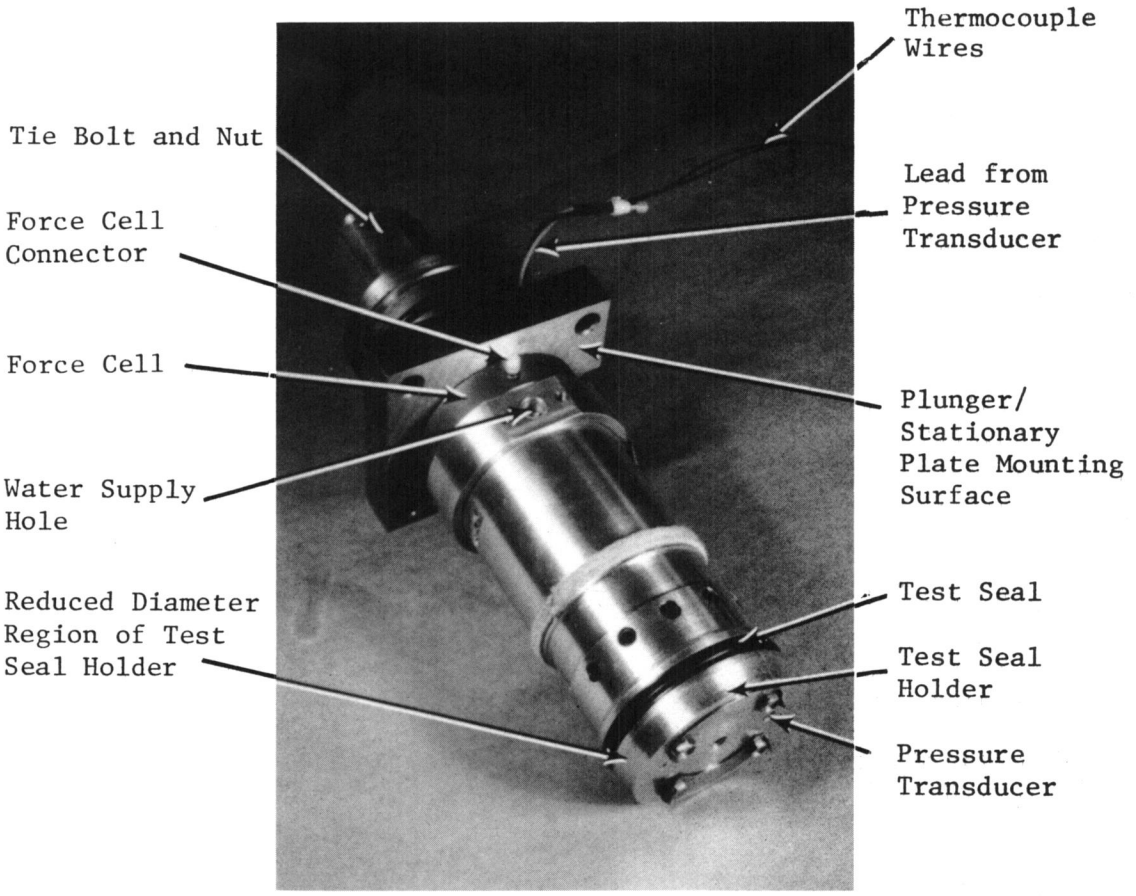

Figure 8 Close-up of the Plunger

The plunger mounts to the stationary plate at the lower surface of the plate having the holes (Figure 8). Just below this plate is a force cell (Kiag type 9071) for measuring the friction force produced by the seal. The connector for the lead is the white protrusion just above the cooling water supply hole. The force cell is preloaded between the plate and the remainder of the plunger body by a hollow tie bolt (the nut that controls the magnitude of the preload is at the upper left in Figure 8). The assembly of the plunger to produce the preload is a one-time operation--the tie bolt portion of the plunger need never be disassembled at any time during all planned use of the apparatus.

Use of the tie bolt to preload the force cell is desirable for several reasons. The first reason is that the hollow tie bolt is a convenient way to remove the cooling water from the plunger. The second reason is that with a properly designed tie bolt only one force cell need be used to measure seal friction. To see this, the following diagram, which shows the axial elastic behavior of the plunger, can be used:

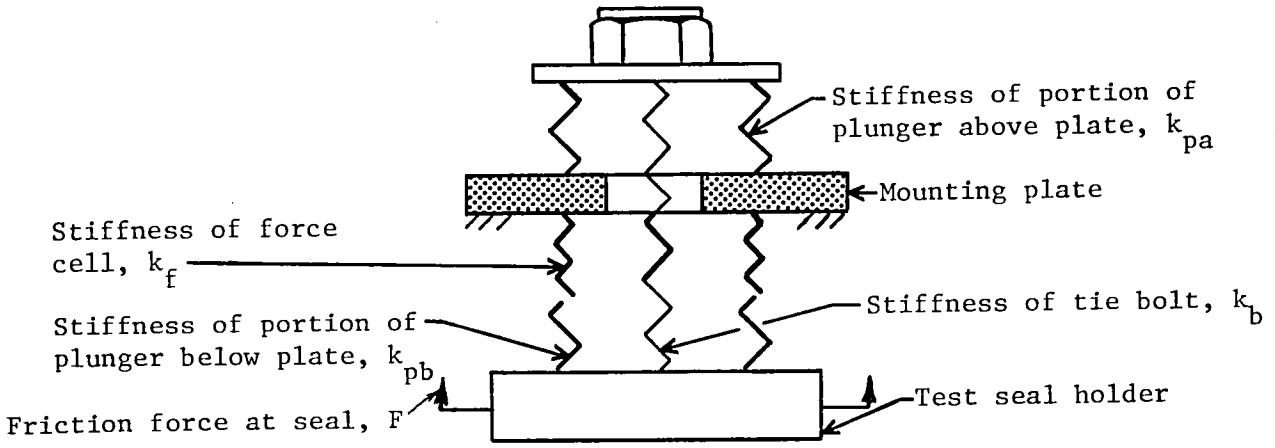

The diagram indicates four stiffnesses, those of the tie bolt, of the plunger below the plate, of the plunger above the plate, and of the force cell. A friction force, F, at the seal/cylinder interface must produce an axial displacement, d, of the test seal holder such that

$$F = \left(\frac{k_b \, k_{pa}}{k_{pa} + k_b} + \frac{k_f \, k_{pb}}{k_{pb} + k_f} \right) \cdot d$$

Also, the force, F_c, measured by the force cell is

$$F_c = \frac{k_f\, k_{pb}}{k_{pb} + k_f} \cdot d$$

so that

$$\frac{F_c}{F} = \frac{k_f\, k_{pb}/(k_{pb} + k_f)}{k_b\, k_{pa}/(k_{pa} + k_b) + k_f\, k_{pb}/(k_{pb} + k_f)}$$

or

$$\frac{F_c}{F} = \frac{1}{k_b\, k_{pa}(k_{pb} + k_f)/(k_f\, k_{pb}(k_{pa} + k_b)) + 1}$$

Now, if the design of the plunger is such that k_b is small compared to k_{pa}, the above expression reduces to

$$\frac{F_c}{F} = \frac{1}{k_b/k_f + k_b/k_{pb} + 1}$$

which further reduces to $F_c/F = 1$ if k_b/k_f and k_b/k_{pb} are small compared to 1. The plunger was designed to meet these conditions so that the applied and the measured forces are nearly identical. Evidence that this design objective has been met is presented in the preliminary results section below.

Figure 8 can be used to point out other design features of the plunger. One such feature is the reduced diameter region below the test seal. This has the function of easing the installation of the test seal on the test seal holder. Another feature is the pressure transducer for measuring the small cyclic variations of gas pressure. This measurement can be made on a real time basis and can be used to subtract the gas pressure force variations from the force measured by the load cell. The lead from the pressure transducer can be seen (white wire) emerging from the plunger at the upper center of the photograph. The other two wires are thermocouple leads for measuring temperatures in the oil above the seal and in the test seal holder near the seal groove.

The present test seal holder (that shown in Figures 1, 2, 4, 7 and 8) was designed to accept a T seal. This T seal consists of an elastomeric portion, one part of which contacts the cylinder, and two fiber back-up rings. The mounted seal is shown schematically in Figure 9.

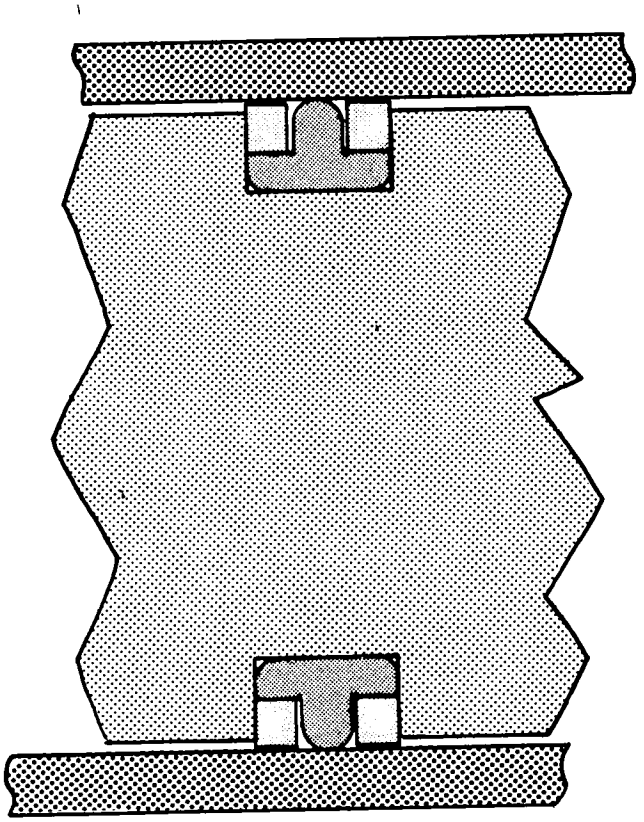

Figure 9 Schematic of "T" Seal as Installed

Figure 10 is a photograph of the seal prior to installation on the test seal holder. The elastomeric material of this seal is Viton, a fluroelastomer.

Preliminary Results

In this section, results obtained from preliminary use of the experimental apparatus are presented. These results concern the operation of the apparatus rather than the behavior of the seal. The results show that the device performs well mechanically and that its force measurement capability is as intended.

Upon completing the assembly of the rig, the first measurement made was of the stiffness of the hydrostatic bearings. A high degree of stiffness is desirable in order that dynamic forces not result in appreciable horizontal motion of the transparent cylinder with respect to the seal. The measurement was made by simply applying a steady horizontal force between the two hydrostatic bearings of the upper shaft. This force was measured with a spring scale. The displacement was measured with a dial indicator. The results showed the both upper hydrostatic bearings together have a horizontal stiffness of 1.2×10^5 N/mm (700,000 pounds per inch). The stiffness of each bearing is, therefore, at least 0.6×10^5 N/mm (350,000 pounds per inch).

To show what the effects of this stiffness are on the seal/cylinder interface, two rough calculations can be made. For these calculations, the following conservative assumptions are used:

- The horizontal stiffness of each upper hydrostatic bearing is 0.6×10^5 N/mm (350,000 pounds per inch).
- The horizontal dynamic force in the apparatus is 290 N (65 pounds). This force is calculated using the geometry of the connecting rod (the ratio of crank length to connecting rod length is 0.05), the maximum frequency (50 Hz), and the mass of the upper reciprocating shaft. This mass is less than 4.5 kg (10 pounds mass).
- The horizontal dynamic force is applied 0.13 m (5.0 inches) below the lower hydrostatic bearing of the upper shaft and these hydrostatic bearings are 0.21 m (8.1 inches) apart.
- The seal is 0.22 m (8.5 inches) above the upper hydrostatic bearing of the upper shaft.

The displacement of the transparent cylinder results from two effects--translation of the upper shaft due to the 290 N (65 pound) force, and rocking in the vertical plane due to the same 290 N (65 pound) force. The translation, t, can be computed simply from

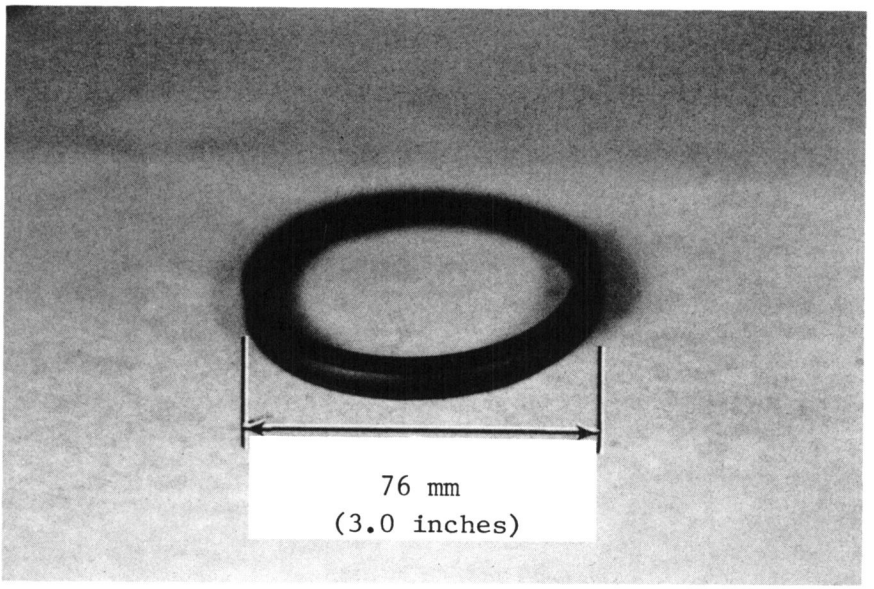

Figure 10 Test "T" Seal

$$t = \frac{290}{2(0.6 \times 10^{8})} = 2.4 \times 10^{-3} \text{ mm (0.1 mils)}$$

This motion is clearly negligible when compared to a typical seal preload. The displacement, r, due to rocking can be computed from:

$$r = \frac{290}{0.6 \times 10^{8}} \left[\frac{0.13 + 0.105}{0.21}\right]\left[\frac{0.22 + 0.105}{0.105}\right]$$

$$= 0.17 \times 10^{-2} \text{ mm (0.67 mils)}$$

This motion is also negligible when compared to a typical seal preload.

The next measurements to be made after assembly of the experimental apparatus were concerned with the smoothness of the device during operation. To obtain an evaluation of this, an accelerometer was placed on the backing plate at a height approximately corresponding to that of the seal. The sensitive axis of the accelerometer was oriented first in the vertical direction and then in the horizontal direction (such that the axis was in the plane of the backing plate). The drive motor was operated at about 900 rpm. The plunger was removed.

The results obtained are shown in Figures 11 and 12, where Figure 11 is for the horizontal acceleration and Figure 12 is for the vertical acceleration. Each figure gives an average spectrum made from 8 spectrum analyses of the measured acceleration. The analyses were made in the 0-200 Hz range and therefore cover the flywheel frequency of 15 Hz as well as the drive motor frequency of about 30 Hz.

The plots show that the vibration levels in the apparatus are relatively low. Reference to typical charts* used in vibration analysis indicates that both the horizontal and vertical vibration levels fall in the "smooth" range for machine operation. This shows that a satisfactory dynamic environment exists in the experimental apparatus for conducting the optical interferometry studies.

The plots show that the horizontal acceleration is greater than the vertical acceleration, particularly in the regions near 60 Hz and 30 Hz. This may have been anticipated, since the vertical, but not the horizontal, forces are balanced by the lower reciprocating shaft. However, these two frequencies are not directly associated with the rotation speed of the flywheel, which is about 15 Hz.

---

*One such chart is the "Vibration Computer," a paper slide rule, published by Endevco Corp.

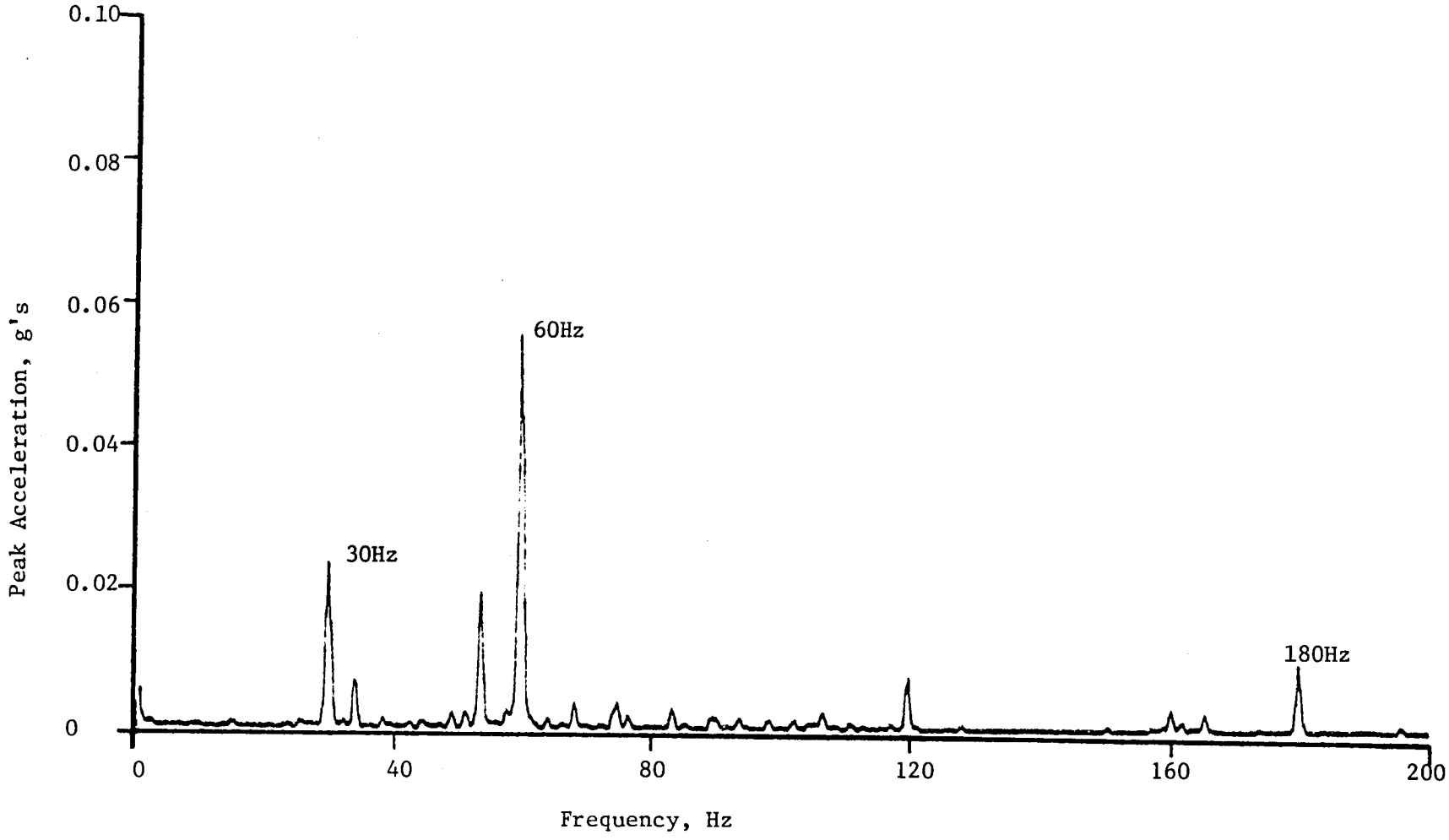

Figure 11 Average of 8 Spectra for Horizontal Acceleration

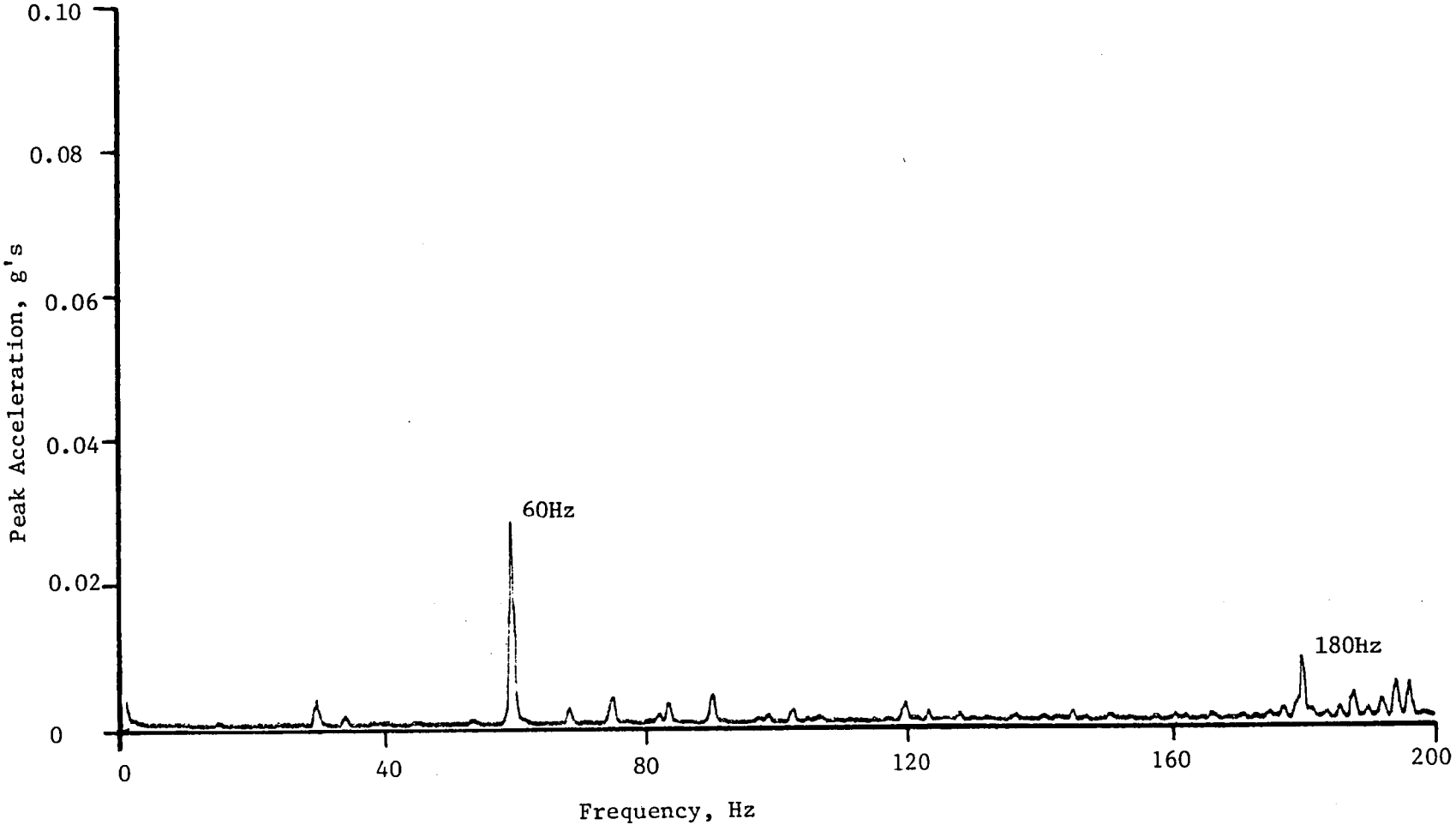

Figure 12 Average of 8 Spectra for Vertical Acceleration

The origin of the acceleration signals at these frequencies is of interest, so additional spectra, Figures 13 and 14, were produced. For these spectra, all conditions were identical to those of Figures 11 and 12; however, the coupling between the drive motor and the flywheel was disconnected. Consequently, the spectra of Figures 13 and 14 were obtained under the condition of a stationary flywheel (and stationary connecting rods) but a rotating drive motor whose output speed was about 900 rpm (15 Hz).

Comparison of Figures 11 and 13 shows that most of the horizontal acceleration at 30 Hz, 60 Hz, and 180 Hz is not due to the flywheel and reciprocating masses; in fact, the only significant flywheel/reciprocating mass signal is the one at about 53 Hz. Comparison of Figures 12 and 14 gives a similar result. For vertical vibrations, it can be observed that the flywheel/reciprocating mass portion of the apparatus contributes essentially nothing to the vibration spectrum.

One further plot was made. The intent of this plot was to determine whether the 30, 60, and 180 Hz signals were due to the drive motor or, perhaps, due to some electrical source. The plot, Figure 15, is an instantaneous spectrum made from the accelerometer with the drive motor switched off. The plot shows that significant portions of the 60 Hz and 180 Hz signals are still present. These residual portions are, therefore, not associated with mechanical vibrations produced either by the drive motor or by the flywheel/reciprocating mass combination. This indicates that the drive motor contributes much less vibration to the experimental apparatus than Figures 13 and 14 suggest. Consequently, of the vibration levels of Figure 11, half of the 60 Hz and almost all of the 180 Hz signals are not mechanically produced. Also, most of the remainder of the 60 Hz signal and most of the 30 Hz signal are produced by the drive motor.

One other mechanical aspect of rig operation is of concern. That aspect is whether a vertical force (i.e., the seal friction force) applied to the plunger at the seal is accurately measured by the force transducer. (The stiffness conditions for this to occur are considered in the section above.) To evaluate the performance of the force transducer, a reference force transducer was attached to the bottom of the plunger at the hole on the vertical centerline. To this reference transducer was fastened a spring mass combination. Schematically, the arrangement is as shown in Figure 16. The spring mass combination was arranged so that the natural frequency was about 12 Hz.

Displacement and subsequent release of the mass resulted in an oscillation which applied a sinusoidal vertical force to the reference cell. The force was also transmitted to the bottom of the plunger. Both the force measured by the reference force cell and that measured

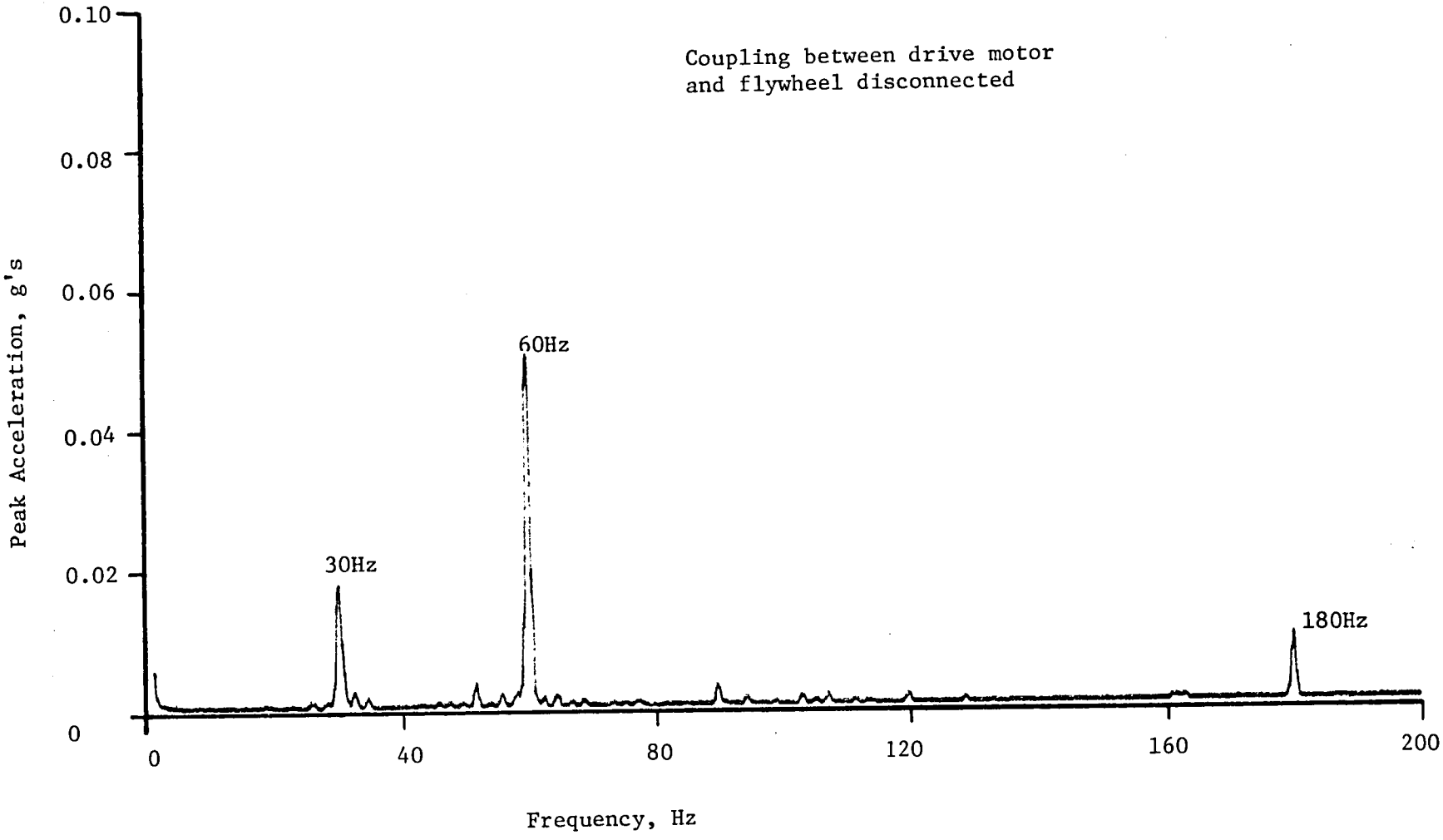

Figure 13 Average of 8 Spectra for Horizontal Acceleration

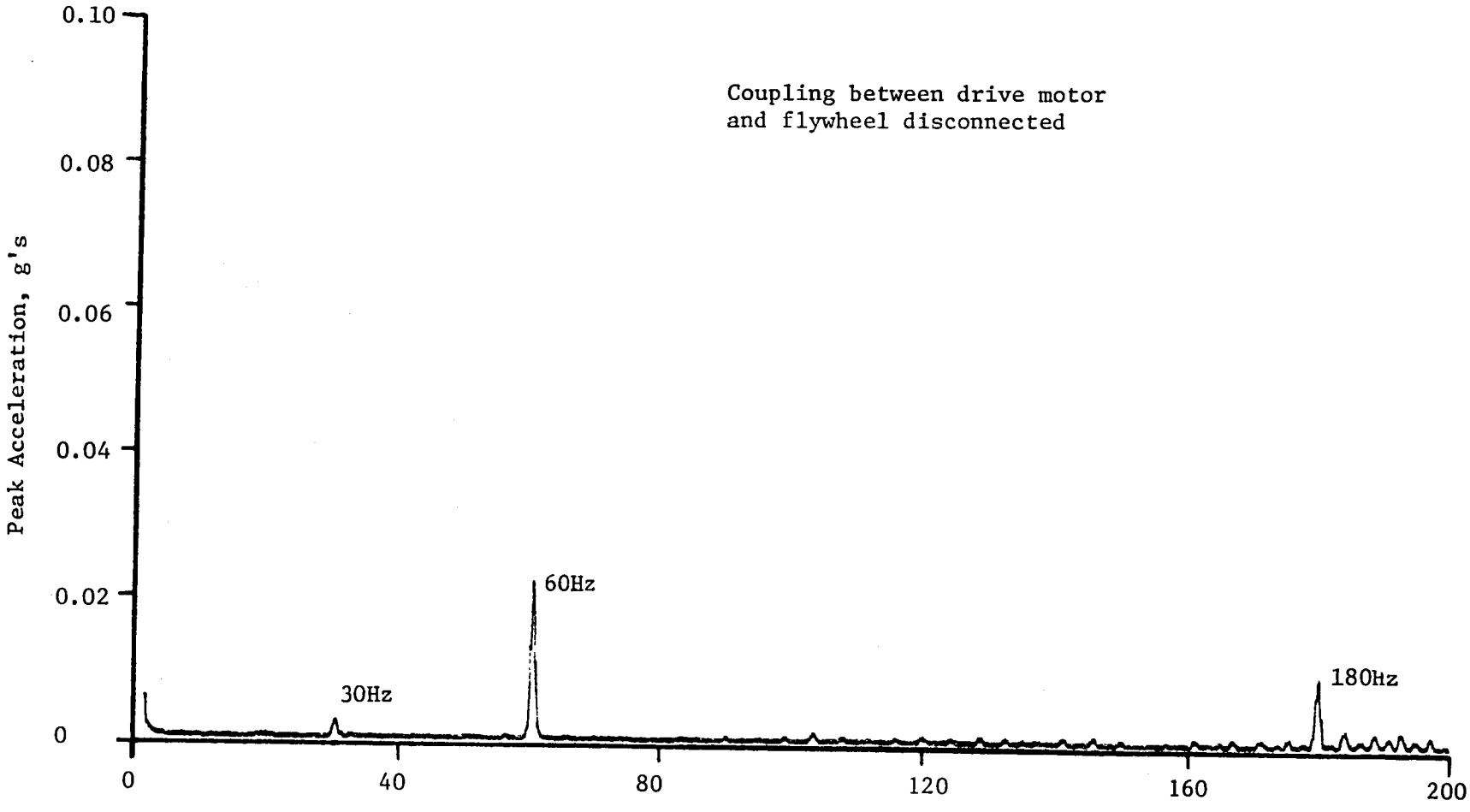

Figure 14 Average of 8 Spectra for Vertical Acceleration

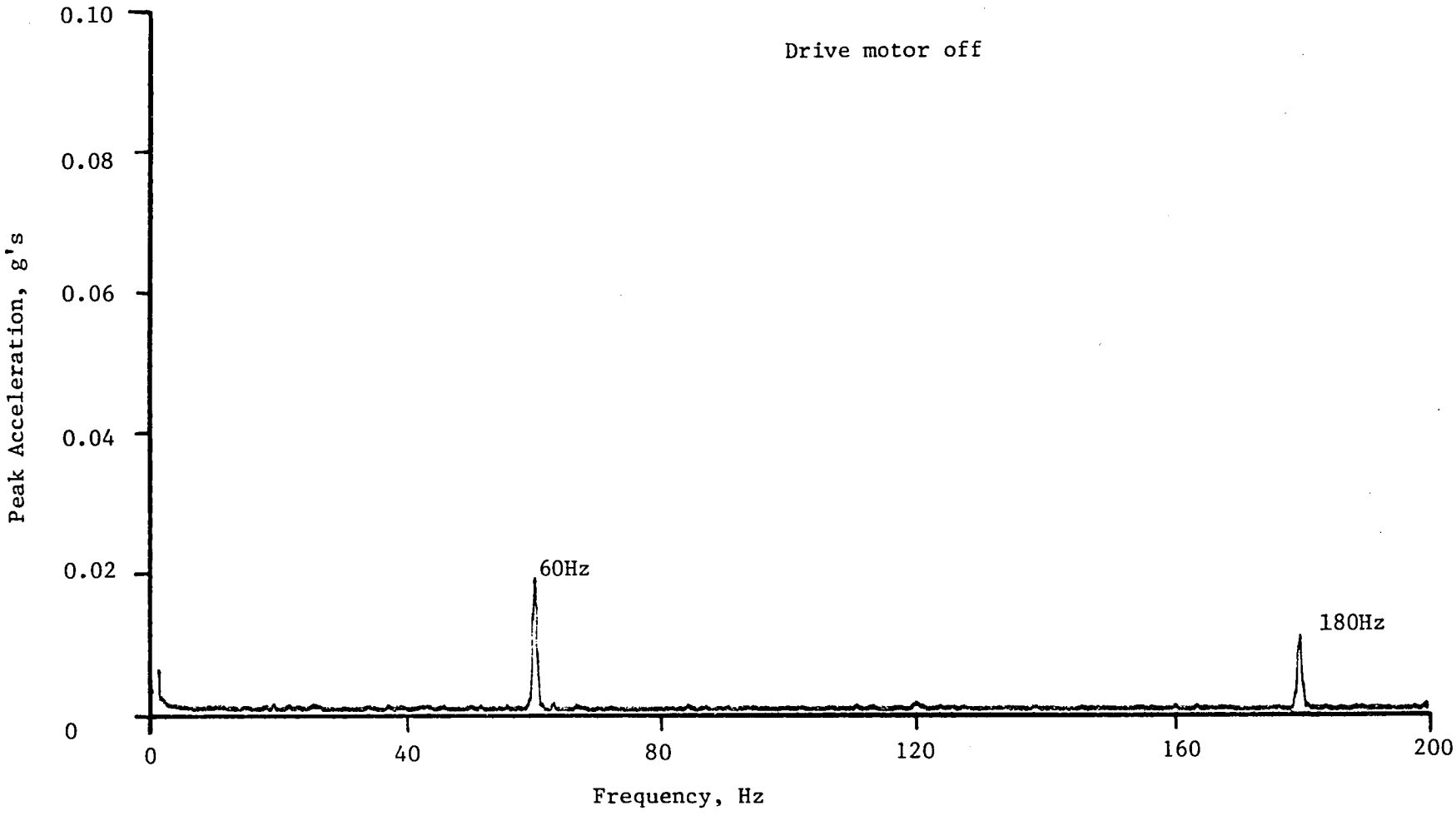

Figure 15 Instantaneous Spectrum for Vertical Acceleration

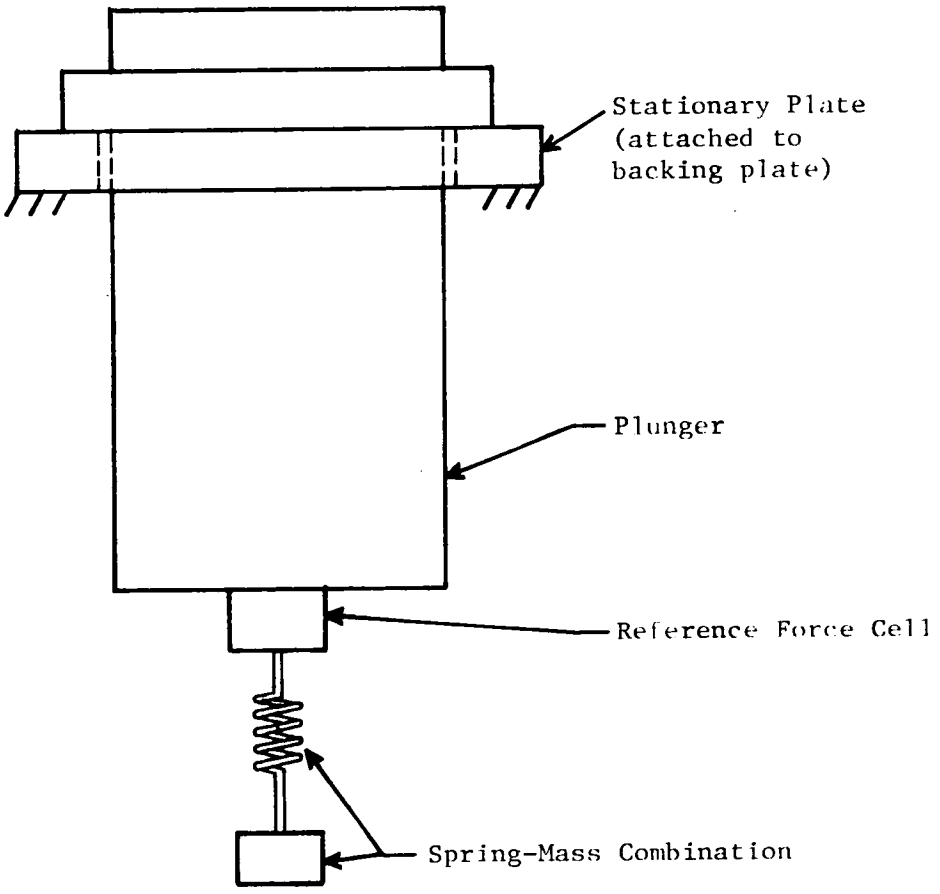

Figure 16 Location of Reference Force Cell and Spring-Mass with Respect to the Plunger

by the force cell in the plunger were recorded by photographing the voltage outputs from their electronic drivers. These drivers were set so that each load cell had the same sensitivity 2.25 mV/N (10 mV/pound). The results are given in the photographs of Figure 17.

The three sets of time traces in Figure 17 are for segments from three separate releases of the mass. The first set corresponds to a vibration amplitude such that no spring bottoming occurred. The second set involved some bottoming near the start of the trace shown. The third set was made under a condition of relatively hard spring bottoming at the start of the oscillation. In each set of traces, two curves are given--the top one is for the reference force transducer and the bottom one is for the force cell in the plunger. The vertical and horizontal scales are as shown in the figure.

All three photographs indicate very good correspondence between the forces measured by the two cells. The time traces are in phase, indicating that mass effects are not significant, even for the higher frequencies that occurred. The magnitudes correspond well, suggesting that the required stiffness relationships for the tie bolt, plunger assembly and plunger force cell have been met. It therefore, appears that the force cell in the plunger does satisfactorily measure vertical forces (i.e., seal friction forces) that are applied to the test seal holder.

Interferometry

The accurate measurement of the film thickness at the seal/cylinder interface is central to the success of the current program. Film thickness measurements are the most sensitive means for performing analytical and experimental correlations. In addition, knowledge of film thickness can be used in studying seal friction behavior and can provide insight into how leakage can be controlled.

Historically, many techniques of measurement have been used to obtain EHD film thickness. Successful methods of film thickness detection have been developed with the aid of optical equipment, capacitive probes, inductive probes (eddy current devices), and resistance measurement sensors. The optical approach, however, is the only direct scheme which can provide a full point-by-point topographical film measurement within a reciprocating seal interface. In addition, the optical approach allows gradients within the contact region to be observed and film thicknesses as small as 2 microinches to be measured reliably. For these reasons, an optical approach to film thickness measurement has been taken and the moving transparent cylinder concept has been used.

Application of optical procedures to measuring thicknesses such as those in elastohydrodynamic contacts invariably involves the interferometry technique. This technique, which relies on the interference

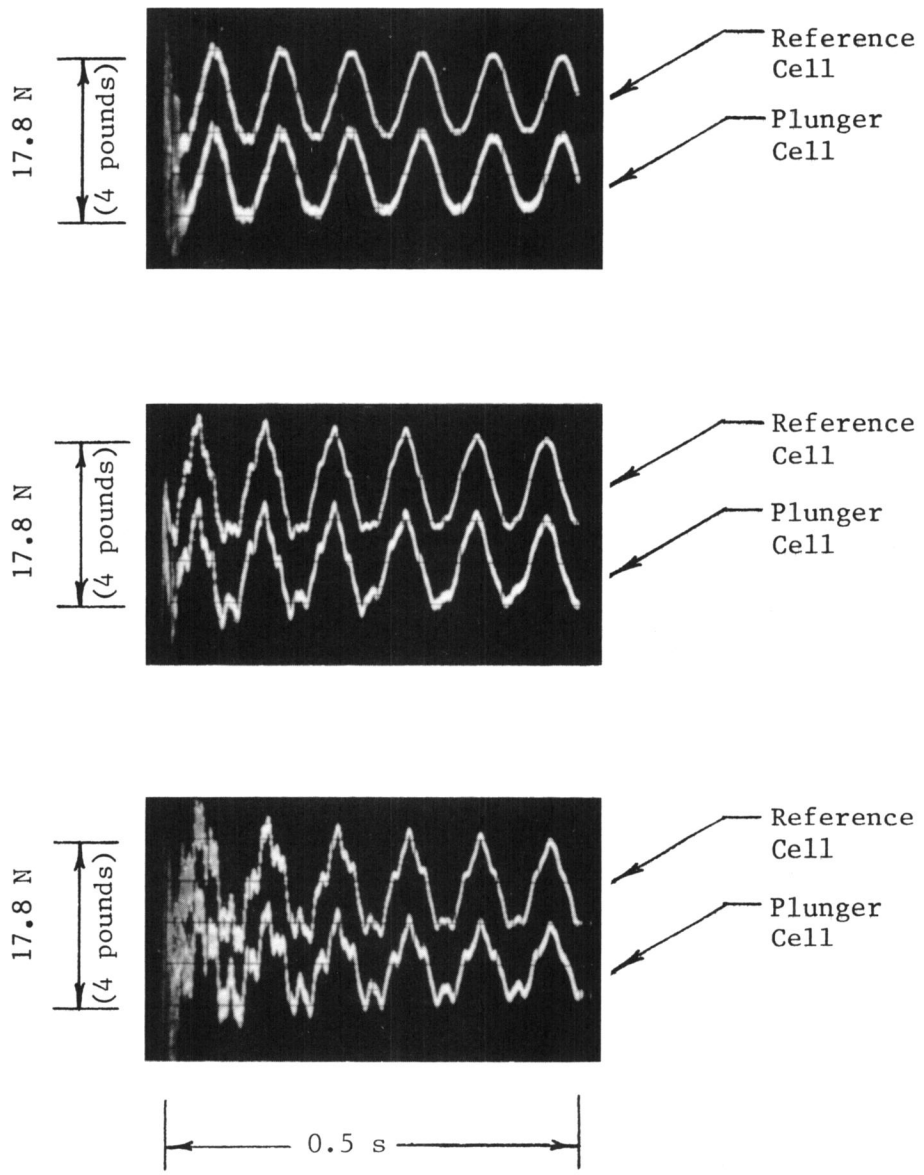

Figure 17 Comparison of Outputs from Reference Force Cell and from Plunger Force Cell

between two coherent beams of light, is described beiefly below.

Figure 18 shows a greatly expanded drawing of the seal/cylinder contact zone. The orientation of the seal and cylinder in the drawing is the same as that in the experimental apparatus--the section is made by passing a vertical plane through the vertical axis of the transparent cylinder. The drawing includes a light source which sends a light beam, A, toward the outer surface of the cylinder. This beam, which also lies in this vertical plane, has an intensity I_a. At the outer surface of the cylinder, this beam splits into two parts; one part, B, having intensity I_b, is reflected. The other part enters the cylinder wall and proceeds to the inner surface of the cylinder. At this surface, the beam splits such that one part is reflected internally in the glass and the other part passes into the oil, to the surface of the elastomer, and then back to the inner wall of the glass. The viewer, looking in the direction indicated sees beams B, C, and D, where C is form the glass/oil interface and D is from the seal/oil interface. If certain physical conditions are met, interference between beams C and D will occur. One of these conditions is that the ratio of the thickness h to the wavelength of the incident light is ½, 1, 1½, etc. If the film thickness changes with axial position, the viewer will see alternating light and dark bands. These bands are termed interference fringes. It is evident that the axial spacing of these fringes gives directly a map of the changes in film thickness throughout the contact region.

Several physical conditions must be met, in addition to the proper relationship between wavelength and film thickness, for observable fringes to exist. One of these conditions is that the beam intensities I_c and I_d be approximately equal. Another condition is that the intensities I_c and I_d be sufficiently high to allow them to be seen and photographed. A third condition is that I_b be sufficiently small (or be somehow eliminated) so that it does not overwhelm the interference between C and D. Finally, the interface between the glass and the oil and the interface between the oil and the seal must be sufficiently specular that beams C and D are well defined.

Satisfying the above conditions for an elastomeric seal is not straightforward. The most difficult problem to overcome is the creation of a specular (optically smooth) surface at the oil/seal interface. Additional, but more readily overcome, problems are to minimize the effects of beam B, and to produce sufficiently intense beams C and D. Because of these problems, a little optical interferometry is done using elastomers such as rubber, and few reports of such work can be found in the literature. In those reports that exist (see, for example, [1] - [3]*), the problems are dealt with as follows:

*Numbers in brackets denote references.

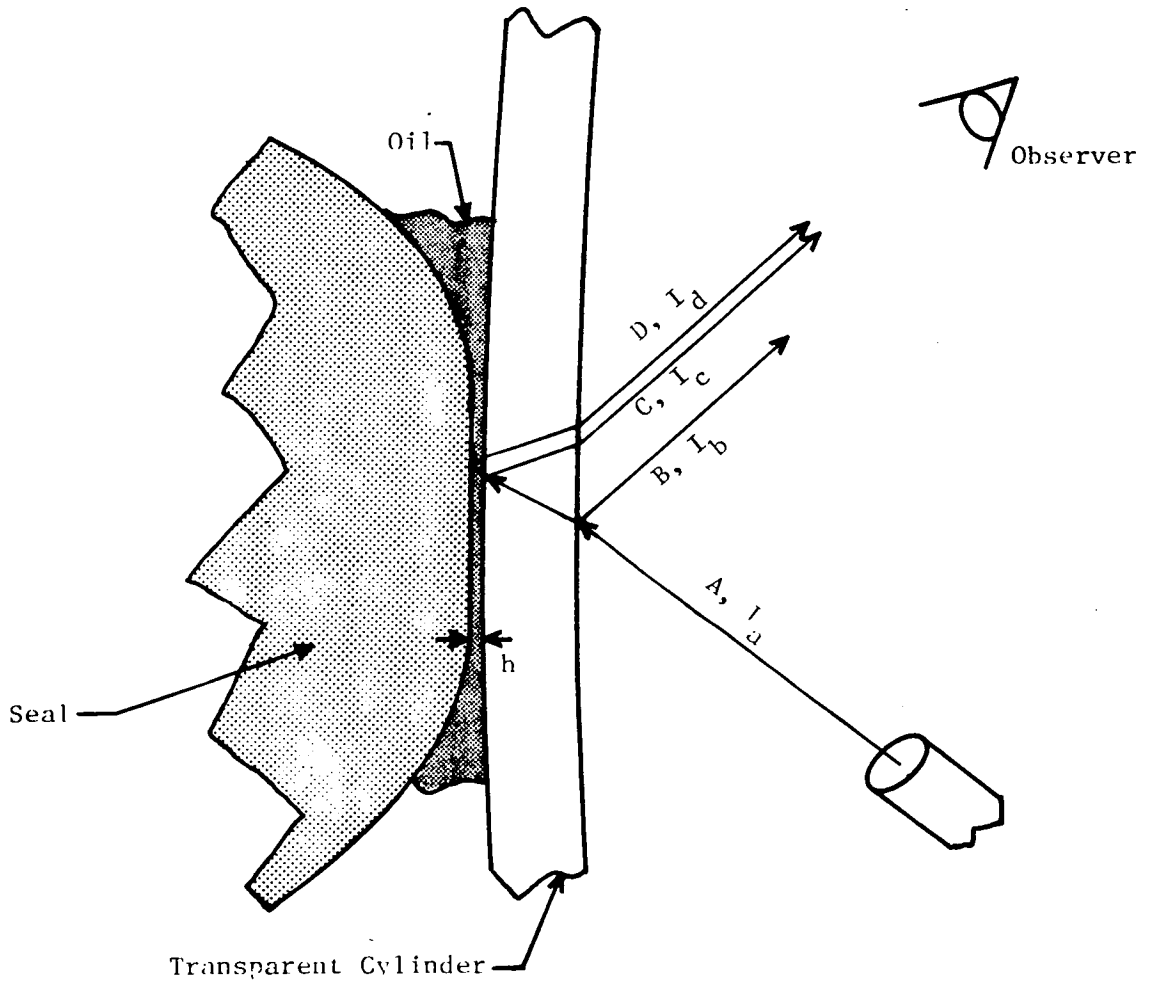

Figure 18 Schematic Drawing of Contact Zone

- Creation of a specular surface is accomplished by molding the elastomer in an optically smooth mold, thereby creating an optically smooth surface on the elastomer.
- Creation of a specular surface by coating the elastomer with a thin specular material such as a metal.
- Reducing the effects of beam B by coating the outer cylinder surface with a thin film which causes destructive interference of B in the coating.
- Increasing the intensity I_c by coating the interior wall of the cylinder and increasing the intensity I_d with a coating on the elastomer.

For the present work, none of the above techniques is entirely satisfactory. It is desirable, for example, not to have to coat either surface of the cylinder. Such coatings are expensive and the one on the inner surface is prone to scratching and wear. It is also desirable not to coat the seal surface with a material which affects its deformation characteristics. Finally, it is very desirable that the experimental apparatus employ production seals rather than seals especially produced with optically smooth surfaces. The cost for the specially produced seals can be very high, their behavior may not be typical of production seals, and the optically smooth surfaces can be prone to scratching during testing.

Experimental work conducted during the course of the present effort resulted in a technique which gives good interference fringes and which is appropriate to the experimental apparatus. Interference fringes were observed and photographed with a laboratory bench setup by using:

- A Parker Viton T Seal which was coated with shiny black lacquer. The lacquer was employed because it is flexible (to conform to the deformed rubber shape), strongly adherent to the rubber, and insoluble in the production oil used. Additionally, the lacquer coating does not crack easily or wear rapidly. It can be applied such that the thickness is small and relatively uniform.
- An optical flat having a refractive index in the range of 1.5 to 1.6. The optical flat could be moved manually to simulate the motion of the glass cylinder.
- An automatic transmission oil which is a candidate for use in actual Stirling engines. This oil (Mobil XRL 1032 AR-1) has a refractive index of 1.4605.
- A fiber optics white light source having a high intensity. The end of the fiber optics tube was mounted close to the optical flat and oriented so that the angle between the incident light A and the normal to the surface of the optical flat was about 30^{o}. This mounting method eliminates the effects of beam B by taking advantage of the (axial) distance between

beams C and B; i.e., when sighting along C and D, the beam B does not enter the field of view.

- A stereo microscope with a maximum magnification of about 50X.

The fringes obtained were of sufficient optical quality that 35 mm color slides could be taken and a 16 mm color movie could be made. A black and white photograph made from a 35mm slide is shown in Figure 19. The dark zones are interference fringes which appear as multicolor bands in the original slide. The bands are very apparent in the color movies. The bands show the presence of a lubricant film between the glass and rubber at relatively low sliding speeds (less than 0.25 m/s (10 inches/second)) and at relatively large seal preloads (contact width of the seal approximately equal to half the seal width).

Once good quality interference fringes had been produced using the laboratory bench setup, additional optical work was postponed until completion of the experimental apparatus. The optical instrumentation was then installed on the device as shown in Figure 20. In the figure, the fiber optics tube can be seen at the lower center of the photograph. The microscope is at the left center.

A low magnification photograph, taken through the microscope is given as Figure 21. The photograph was taken with the cylinder stationary. The figure shows the aluminum bands on the test seal holder, the two fiber backing rings for the T seal, and the T seal itself. At this low magnification, the contact zone cannot be seen but is approximately equidistant from the two fiber backing rings. A photograph for which a higher magnification was used is given as Figure 22. For this figure, a scale was taped to the outside of the transparent cylinder. Each of the smallest divisions is one millimeter. In Figure 22, the contact zone can be seen bounded by horizontal light lines in the dark region of the T seal.

Interferometry was attempted with both a stationary transparent cylinder and for a slowly moving transparent cylinder (the flywheel was turned by hand). Fringes were obtained, but were not sufficient quality to be photographed. The lack of optical quality was caused by the transparent Lexan cylinder, whose optical characteristics were poor. Specifically, both the inner and outer surfaces of the cylinder had circumferential scratches and grooves which appeared to have been produced by turning during manufacture. These scratches and grooves tended to dissipate both the incident and emerging light. In addition, the contact region, during motion of the cylinder, was rather irregular on a microscopic level. This caused the fringes to be numerous, close together, and non-uniform.

An attempt was made to polish the Lexan cylinder. This did improve the surface quality somewhat, but not sufficiently that a smooth contact zone resulted and that sufficient optical quality was attained.

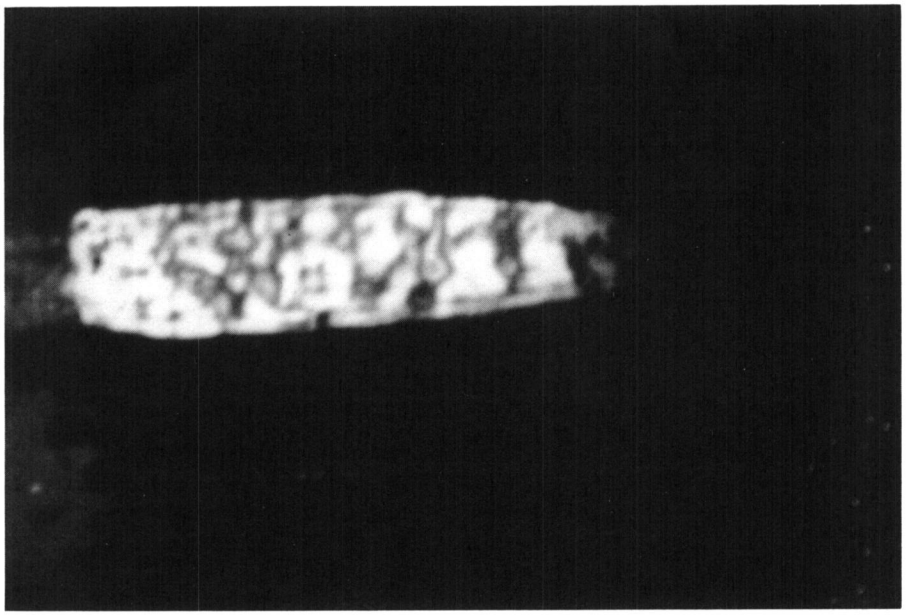

Figure 19 Interference Fringes Produced with Laboratory Bench Setup (Original Color Photograph Made Using White Light)

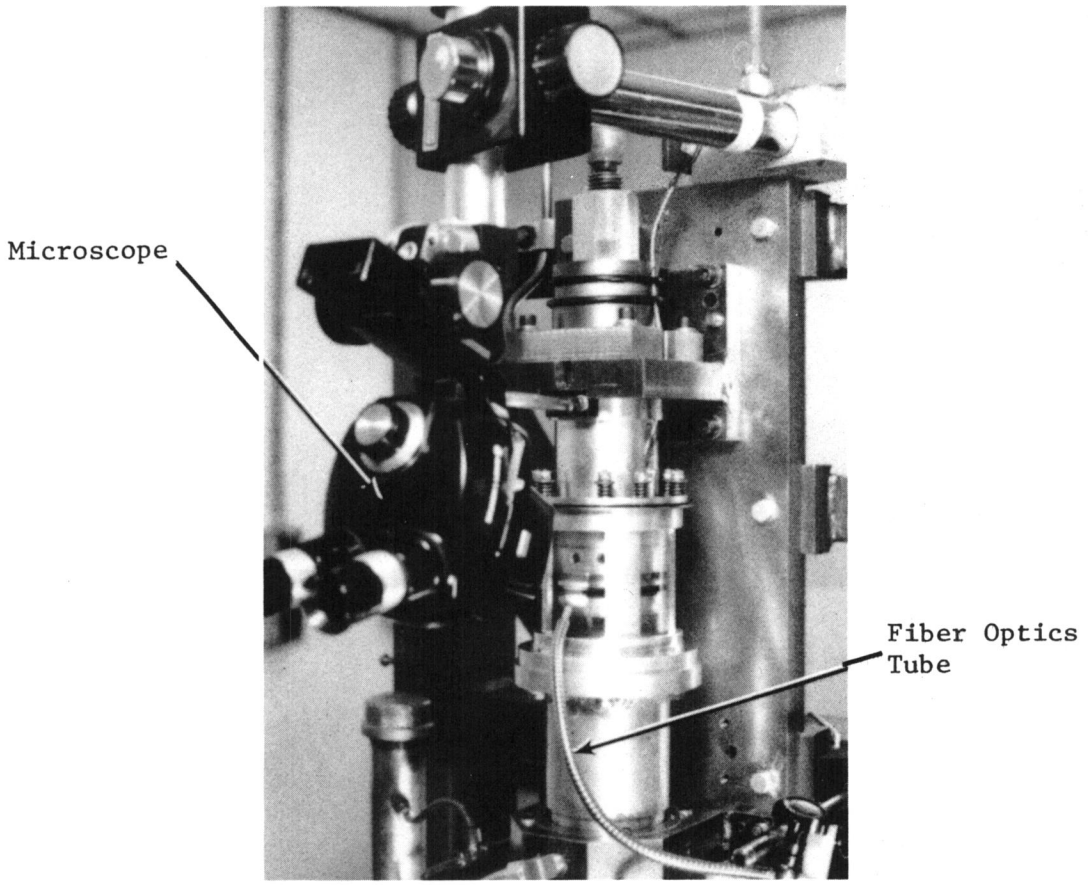

Figure 20 Experimental Apparatus With
Optical Instrumentation Installed

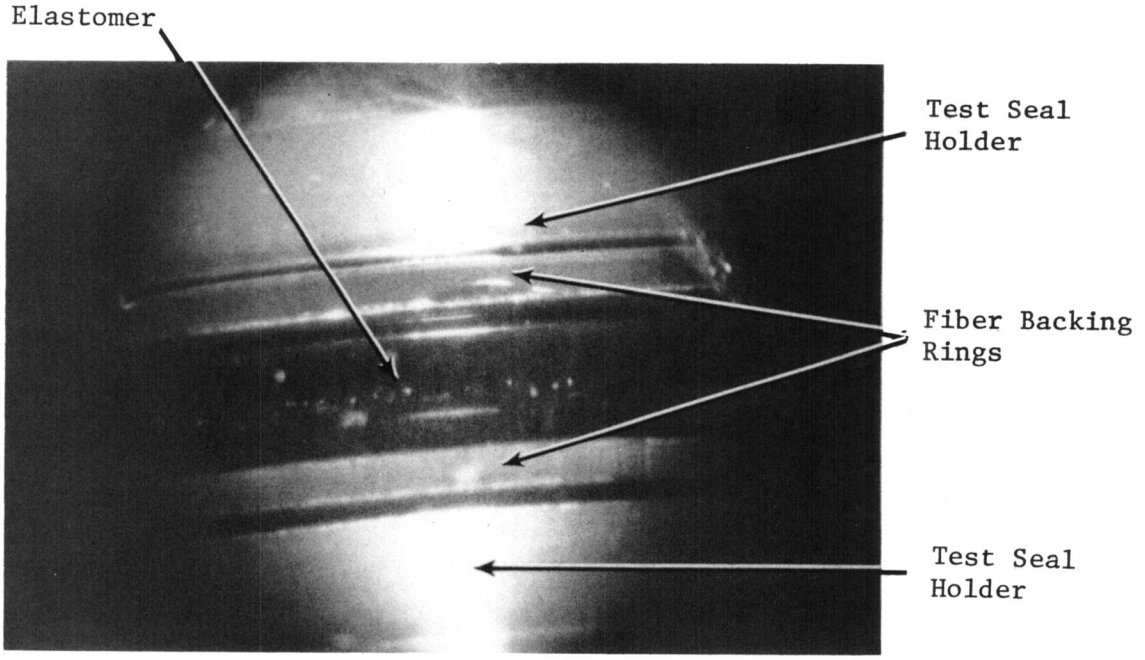

Figure 21 "T" Seal in Contact With Transparent Cylinder

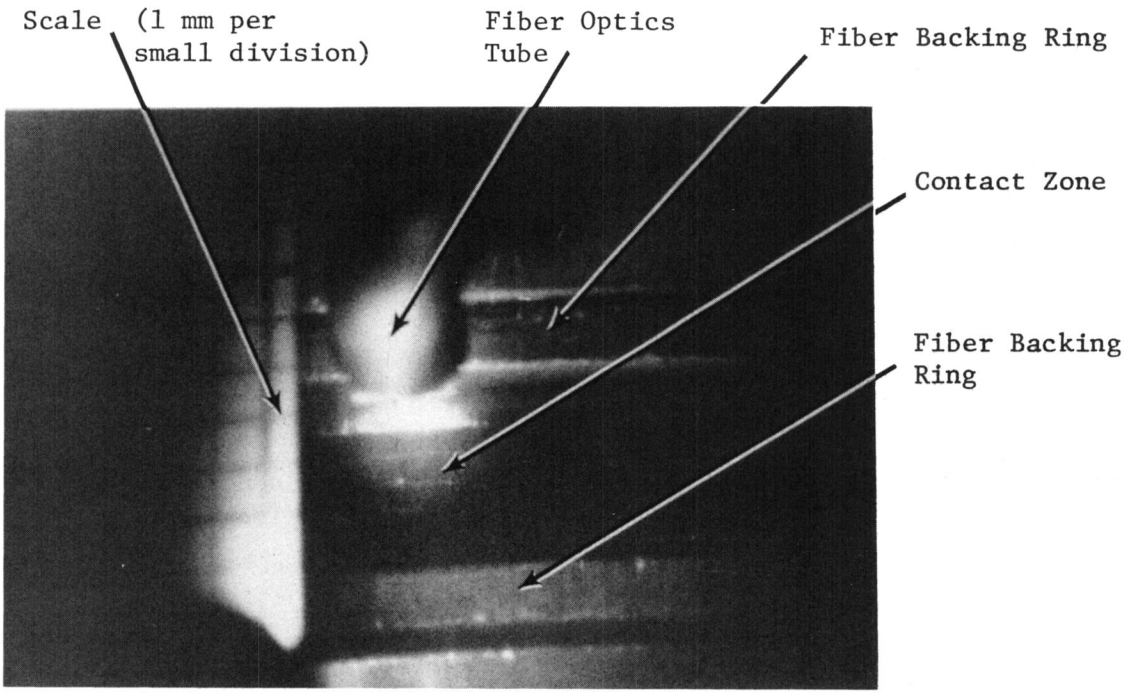

Figure 22 Close-up of "T" Seal in Contact With Transparent Cylinder

The attempt at polishing did indicate that Lexan does not polish well because of its inherent softness. In addition, the material does not maintain its degree of polish well — again due to its inherent softness.

The above work led to the conclusion that Lexan is unsuitable for use in the transparent cylinder. Two alternative materials are glass and acrylic. At the time of this writing, a glass cylinder is on order and due for installation in the experimental device before the end of March. The manufacturing of the glass, however, is risky and it is not certain that a glass cylinder having the proper dimensions and tolerances can be secured. Nevertheless, the glass cylinder is the most desirable, since the inner and outer surfaces will be optically smooth and will be very scratch resistant.

Acrylic is the second choice--it is desirable because it is relatively easy to polish and relatively scratch resistant. In the event that substantial problems arise in manufacturing the glass cylinder, this material will be used in the apparatus. However, since acrylic is susceptable to scratching, designs are being considered currently in which the acrylic member is expendable and easily replaced.

ANALYTICAL REPORT

In this section, the analytical work completed during the past year is discussed. The analytical work was directed at determining the film thickness distribution at the seal/cylinder interface. This film thickness distribution is important because it controls the net leakage during each cycle of the reciprocating motion. The film thickness distribution also affects the frictional forces produced by the sliding seal.

Determination of the film thickness distribution for a reciprocating elastomeric seal requires that two elements of seal behavior be considered. Firstly, due to the low modulus of the seal, the film thickness and the pressure distributions are coupled. These must be determined together by theories developed in elastohydrodynamic (EHD) lubrication. Secondly, the film thickness at the seal/cylinder interface fluctuates during each reciprocating cycle. This is unlike conventional EHD problems for bearings and cams where steady-state EHD theories provide accurate film thickness predictions. Because of the reciprocating motion, the film thickness is influenced by both squeeze film and sliding effects — an accurate determination of film thickness behavior therefore requires a solution of the time-dependent Reynolds equation coupled with the elasticity equation. However, a reasonable estimate of the average film thickness level in rod seals can be had by using the existing steady-state EHD theories based on some effective velocity over each cycle of the reciprocating motion. Contributions in this category include the earlier analysis by Dowson and Swales [4, 5], and later by Hooke, et. al. [6, 7].

The analytical work given in this section includes two parts. First, an approximate method is presented to estimate the mid-stroke and the end stroke film thickness. In the second part, a time-dependent EHD analysis is developed to determine the temporal behavior of the film thickness distribution during the entire cycle of the reciprocating motion. The nomenclature used for both parts of the analytical work is given in Table 1.

Estimate of the Mid-Stroke and End-Stroke Film Thickness

The variation of film profile in a rod seal during a reciprocating cycle was observed first by Blok and Koens [8] using the interferometric technique. Figure 23 shows the observed film profiles at twelve different stroke positions. At mid-stroke positions, i.e., $\omega t = \frac{\pi}{2}$, $\omega t = \frac{3\pi}{2}$, the sliding velocity is at its maximum and the film profile is similar to those predicted by the steady-state EHD analyses. At the end-stroke positions, i.e., $\omega t = 0$ and $\omega t = \pi$, the sliding velocity is zero, and surfaces are separated only by squeeze-film action. As the shaft travels from mid-stroke to end-stroke position, the minimum film shifts forward from the exit side of the contact to the entrance region. There also seems to be a considerable variation of the average

Table 1

Nomenclature for Analytical Report

a = semi-major axis of the contact ellipse

b = semi-minor axis of the contact ellipse

c = an integration constant used in Equation (32)

c' = an integration constant used in Equation (36)

c_I', c_o' = integration constant c' in inlet and exit half of the contact region respectively

$$C_1 = 16\left(\frac{p_o}{E'}\right)^2 \Big/ \left(\frac{h_o}{R}\right)$$

$$C_7 = 16\left(\frac{p_o}{E'}\right)^2 \Big/ \sqrt{48U}$$

$d_{1,k}$, $d_{2,k}$, $d_{3,k}$ = derivative coefficients for uneven grids

E_1, E_2 = elastic moduli for bodies 1 and 2

$$\frac{1}{E'} = \frac{1}{2}\left(\frac{1-\nu_1^2}{E_1} + \frac{1-\nu_2^2}{E_2}\right)$$

f = frequency of reciprocating cycle

h = film thickness

h_o = center film thickness

h_{min} = minimum film thickness

$$\bar{h}_o = \left(\frac{h_o}{R}\right) \Big/ \sqrt{48U}$$

$\bar{h}_{o,L}$ = $\bar{h}_o$ for the last time interval or last stroke position

$$H = \frac{h}{h_o}$$

$$H^* = \frac{h_{min}}{R}\left(\frac{E'R}{2\mu_o u}\right)^{1/2}$$, used by Herrebrugh [9]

H_k = H at kth grid

$H_{k,L}$ = H_k for the last stroke position

j = grid designation

k = grid designation, also used as the ellipticity ratio by Hamrock and Dowson [10]

k_o = grid number at the contact center

k_{ff} = grid number at the film termination

$M = \left(\frac{W}{E'R}\right)\left(\frac{E'R}{2\mu_o u}\right)^{1/2}$, used by Herrebrugh [9]

p = pressure

p_o = pressure at the contact center or maximum Hertzian pressure

$P = \frac{p}{p_o}$

P_k = P at kth grid

$Q_{k,j}$ = a kernel function, see Appendix B

R = radius of "0" ring

R_x, R_y = effective radius in the x and y direction respectively

S = stroke of the shaft

t = time

$T = \frac{u_o t}{b}$

u = entrainment velocity

u_o = entrainment velocity at mid-stroke = $\frac{\omega S}{4}$

$U = \frac{\mu_o u_o}{E'R}$

V = normal approach velocity

W = load per unit circumferential length of "0" ring

W_T = total load

$\bar{W} = \frac{W_T}{E'R_x^2}$

x = coordinate in the direction of motion

x_i = inlet coordinate

x_{ff} = coordinate at the film termination

$\bar{x} = \frac{x}{b}$

μ_o = viscosity

ν_1, ν_2 = Poisson's ratio of bodies 1 and 2

$\omega = 2\pi f$

ψ = equations to be solved for P_k, etc., see Equations (37)

ξ = dummy coordinate for x

$\bar{\xi} = \frac{\xi}{b}$

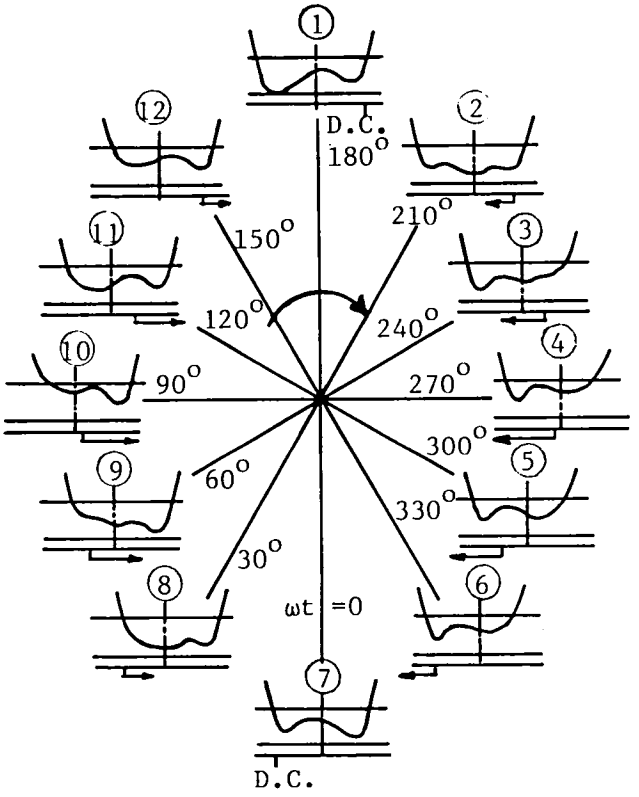

Figure 23 Twelve Successive Phases During the Cycle of a Breathing Lubricant Film

film thickness during the reciprocating cycle. It will be seen later in the detailed time-dependent EHD analysis that these observed film characteristics are completely in accord with the predicted film profiles. It should be noted that if the kinematics are the same during the forward and backward stroke, the film profiles should also have the same characteristics. Figure 24 depicts the qualitative features of the film profiles relative to the four stroke positions in Stirling cycle rod seals.

Approximate Mid-Stroke Film Predictions. Even though results of steady-state EHD analyses are not exactly applicable to a reciprocating rod seal, they are nevertheless suitable for making approximate predictions of the mid-stroke film thickness and the level of film thickness for each cycle. For this purpose, results obtained by Herrebrugh [9] for line contacts as well as those recently developed by Hamrock and Dowson [10] for low modulus point contacts have been adopted.

The numerical solution by Herrebrugh, Figure 25, gives the variation of a dimensionless film parameter H* with an EHD parameter M. Since the load parameter, W/ER, in rod seals is usually very large, the portion of the curve in Figure 25 applicable to rod seals is towards right in the heavily loaded region. In this region, the curve can be best fitted by

$$H^* = 2.45\ M^{-1/4} \tag{1}$$

where

$$H^* = \frac{h_{min}}{R}\left(\frac{E'R}{2\mu_o u}\right)^{1/2} \tag{2}$$

$$M = \left(\frac{W}{E'R}\right)\left(\frac{E'R}{2\mu_o u}\right)^{1/2} \tag{3}$$

Equation (1) can be rearranged to give

$$\frac{h_{min}}{R} = 2.45\left(\frac{2\mu_o u}{E'R}\right)^{5/8}\left(\frac{W}{E'R}\right)^{-1/4} \tag{4}$$

Since in line contacts

$$\frac{W}{E'R} = 2\pi\left(\frac{P_o}{E'}\right)^2 \tag{5}$$

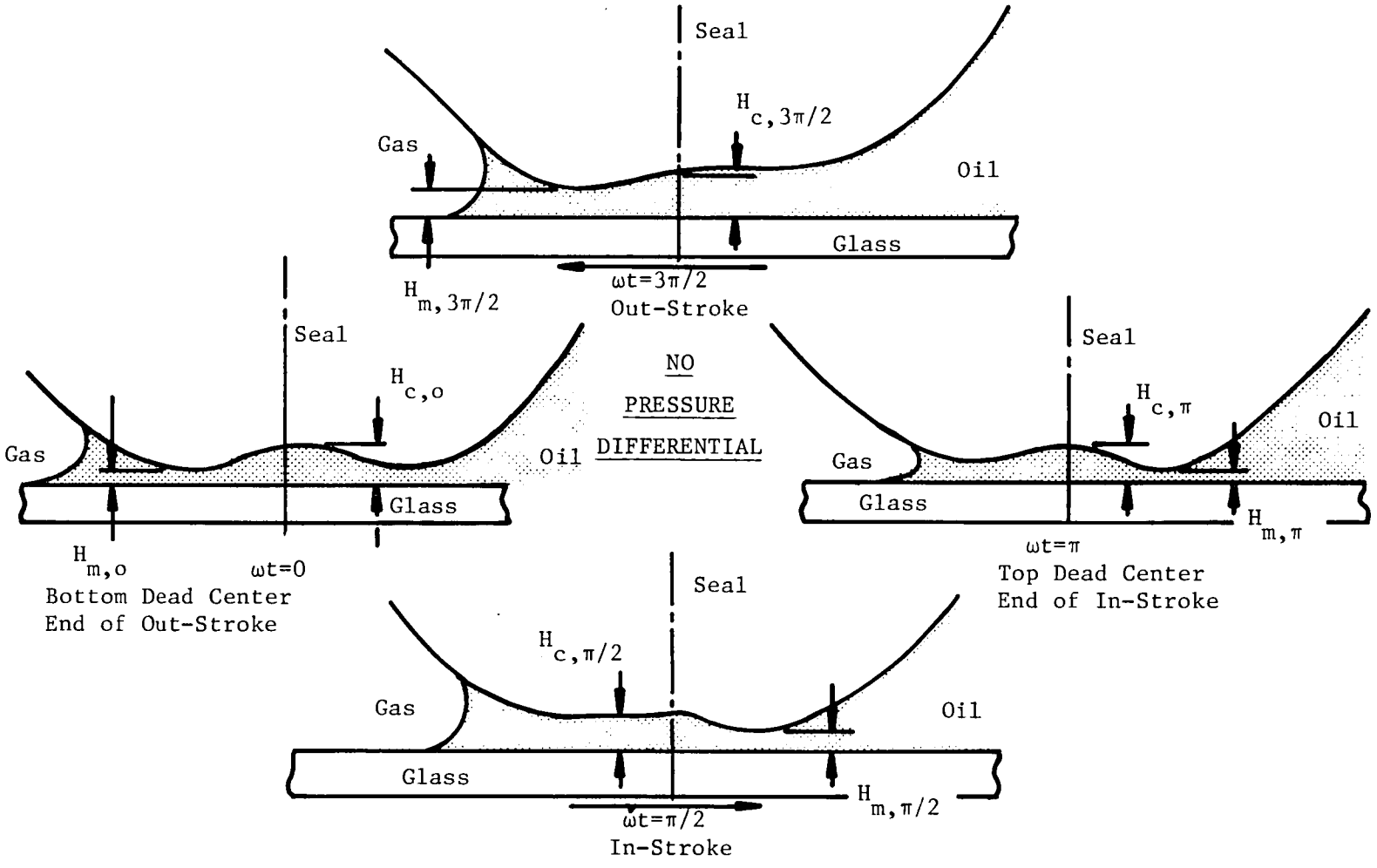

Figure 24 Film Thickness Profiles at Four Piston Positions

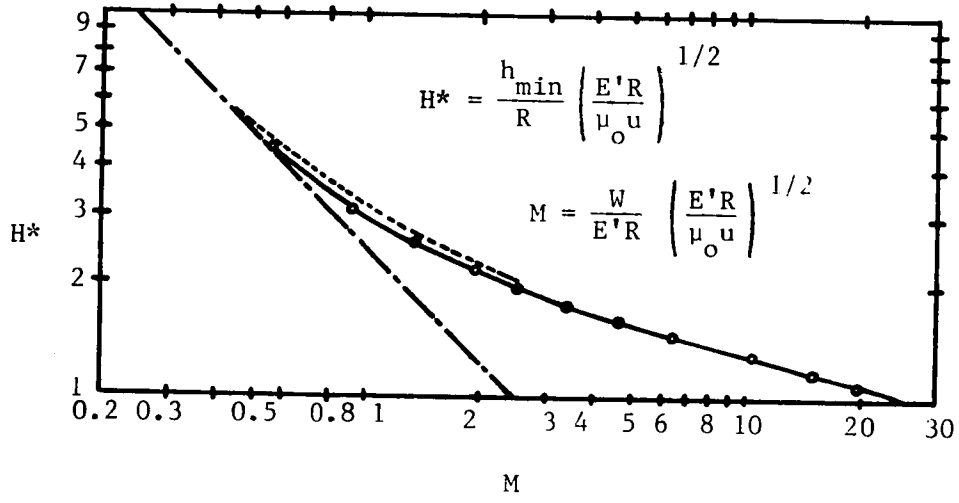

Figure 25 The Functional Relationship: $H^* = F(M)$.
Dash and dot — Gümbel-Martin;
Dashed line — Weber and Saalfeld;
Circled points — author's results.

Equation (4) in terms of a pressure parameter $\frac{p_o}{E'}$, becomes

$$\frac{h_{min}}{R} = 2.45 \left(\frac{2^{5/8}}{2\pi^{1/4}}\right)\left(\frac{\mu_o u}{E'R}\right)^{5/8} \left(\frac{p_o}{E'}\right)^{-1/2}$$

or

$$\frac{h_{min}}{R} = 2.385 \left(\frac{\mu_o u}{E'R}\right)^{5/8} \left(\frac{p_o}{E'}\right)^{-1/2} \tag{6}$$

An alternate method can also be used to estimate the minimum film at the mid-stroke by modifying the minimum film thickness formula given recently by Hamrock and Dowson [10] for low-modulus point contacts. Reference [10] gives

$$\frac{h_{min}}{R_x} = 7.43 \left(1 - 0.85\, e^{-0.31k}\right) U^{0.65} \overline{W}^{-0.21} \tag{7}$$

where

h_{min} = minimum film thickness

$k = \frac{a}{b} = 1.03 \left(\frac{R_y}{R_x}\right)^{0.64}$

a = semi-major axis of contact ellipse

b = semi-minor axis of contact ellipse

R_x = effective radius in the direction of rolling

R_y = effective radius perpendicular to rolling

$U = \frac{\mu_o u}{E'R_x}$

μ_o = viscosity

u = entrainment velocity

$$\frac{1}{E'} = \frac{1}{2}\left(\frac{1-\nu_1^2}{E_1} + \frac{1-\nu_2^2}{E_2}\right)$$

$$\overline{W} = \frac{W_T}{E'R_x^2}$$

W_T = total load of the contact

From Hertz theory for an elliptical contact, it can be shown that

$$\frac{p_o}{E'} = \frac{3}{2\pi} \frac{1}{\left(\frac{a}{b}\right)\left(\frac{b^2}{R_x^2}\right)} \left(\frac{W_T}{E'R_x^2}\right) \tag{8}$$

or

$$\frac{W_T}{E'R_x^2} = \frac{2\pi}{3} \frac{a}{b} \left(\frac{b}{R_x}\right)^2 \frac{p_o}{E'} \tag{9}$$

Substitution of [9] into [7] gives

$$\frac{h_{min}}{R_x} = 7.43 \left(1 - 0.85\, e^{-0.31k}\right) U^{0.65} (k)^{-.21} \left[\frac{2\pi}{3} \frac{p_o}{E'} \left(\frac{b}{R_x}\right)^2\right]^{-0.21} \tag{10}$$

It was suggested in Reference [10] that for low-modulus contact Equation (10) can be converted to line contact if k is taken to be 11. Setting k = 11 and using the following relation for line contacts,

$$\frac{b}{R_x} = 4 \frac{p_o}{E'} \tag{11}$$

Equation (10), for line contacts, becomes

$$\frac{h_{min}}{R_x} = 7.43 \left(1 - 0.85\, e^{-0.31 \times 11}\right)(11)^{-.21} \left(16 \cdot \frac{2\pi}{3}\right)^{-.21} U^{0.65} \left(\frac{p_o}{E'}\right)^{-.63} \tag{12}$$

or

$$\frac{h_{min}}{R_x} = 2.09\, U^{0.65} \left(\frac{p_o}{E'}\right)^{-.63} \tag{13}$$

Equation (13) is the minimum film for low-modulus line contacts based

on Hamrock and Dowson's point contact theory. Film thickness curves based on Equation (6) and Equation (13) for conditions used in the Stirling engine rod seals are plotted in Figure 26. The agreement between these two theories is seen to be reasonably good at low loads. At higher loads, the larger exponent in Equation (13), deduced from the point contact theory, yields a much lower estimate compared to Herrebrugh's theory. Nevertheless, for pressures encountered in Stirling engine seals 3.5×10^3 - 14×10^3 kPa (500-2000 psi) the discrepancy is not serious; therefore, both theories appear to be satisfactory.

Herrebrugh's theory was recently correlated experimentaly by Swales et. al. with rubber pads [5]. Comparison in Reference [5] showed that the load dependence in the experimental data is considerably smaller than in Herrebrugh's formula. Since the values of p_o/E' in Swales' experiment were considerably smaller than would be encountered in Stirling engine seals, it is believed that film predictions based on Equation (6) or Equation (13) for rod seals are likely to be on the pessimistic side.

End-Stroke Film Thickness. Based on the steady state analysis, the film thickness at both ends of the stroke would be zero because the entrainment velocity is zero. However, due to squeeze-film effects, the end-stroke film thickness will not vanish, but will attain a finite value which depends on the squeeze-film velocity.

To estimate the values of end-stroke film thickness due to squeeze-film effects, the results developed by Herrebrugh [11] for two normally approaching cylinders with an isoviscous lubricant are used. Based on his findings, the center film thickness during a normal approach of two cylinders in the heavily loaded region is

$$\frac{h_o}{R} = 4.85 \left(\frac{W}{E'R}\right)^{1/6} \left(\frac{\mu_o V}{E'R}\right)^{1/3} \tag{14}$$

where

V = normal approaching velocity

It is assumed that the film thickness at the end-stroke does not deviate greatly from the mid-stroke film thickness; i.e.,

$$h_o = h_{o,-/2} \tag{15}$$

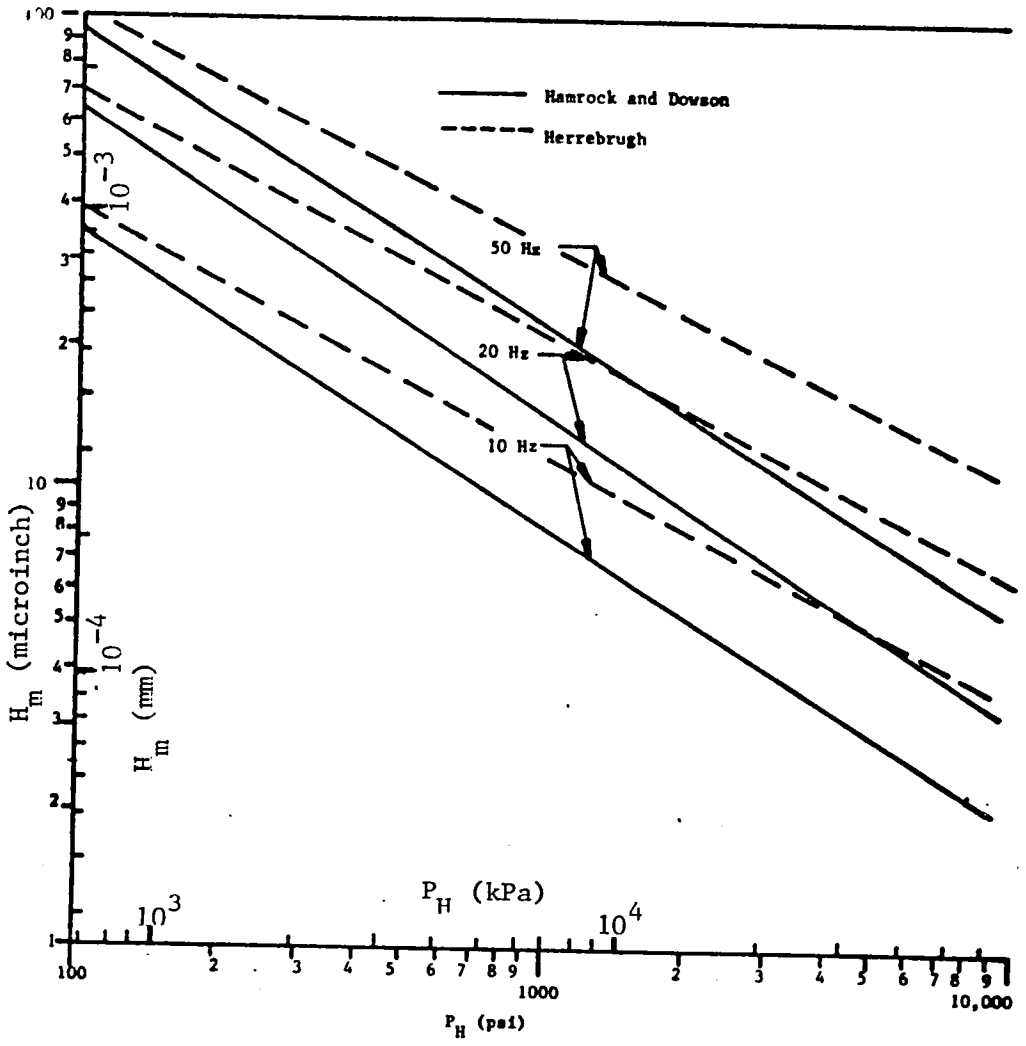

Figure 26 Comparison of Approximate Analytical Film Thickness Results

The normal approaching velocity can then be approximated by

$$V = \frac{\Delta h_o}{\Delta t} = \frac{h_{o,\frac{\pi}{2}} - h_{o,\pi}}{\Delta t} \qquad (16)$$

where the time increment can be taken as one quarter of the period; i.e.,

$$t = \frac{1}{4}\left(\frac{1}{f}\right) \qquad (17)$$

In Equation (17), f is the frequency of the strokes.

Rearranging of Equation (14) gives

$$\frac{\mu_o V}{E'R} = \left(\frac{h_o}{R}\right)^3 \frac{1}{(4.85)^3} \frac{1}{\left(\frac{W}{E'R}\right)^{1/2}} \qquad (18)$$

By substituting $\frac{\Delta h_o}{\Delta t}$ for V one obtains

$$\frac{\Delta h_o}{h_o} = \frac{E'R}{\mu_o}\left(\frac{\Delta t}{h_o}\right)\left(\frac{h_o}{R}\right)^3 \frac{1}{(4.85)^3} \frac{1}{\sqrt{2\pi}\left(\frac{p_o}{E'}\right)}$$

or

$$\frac{\Delta h_o}{h_o} = \left(\frac{E'R}{\mu_o u_o}\right)\left(\frac{u_o \Delta t}{R}\right)\left(\frac{h_o}{R}\right)^2 \frac{1}{285.8\left(\frac{p_o}{E'}\right)} \qquad (19)$$

Here, u_o is the entrainment velocity at the mid-stroke, so that

$$u_o = \left(\omega \frac{S}{2}\right)\frac{1}{2} = \pi f S/2$$

from which

$$u_o \Delta t = \pi f \frac{S}{2} \cdot \frac{1}{4f} = \frac{\pi S}{8} \qquad (20)$$

Equation (6) can now be used to express h_c/R in terms of the speed and load parameter. Substituting Equations (20) and (6) into (19) yields

$$\frac{\Delta h_o}{h_o} = \left(\frac{\pi S}{8R}\right) 2.385 \times U^{0.25} \frac{1}{285.8} \left(\frac{P_o}{E'}\right)^{-2.0} \tag{21}$$

$$= 0.00327 \left(\frac{S}{R}\right) \times U^{0.25} \left(\frac{P_o}{E'}\right)^{-2.0} \tag{22}$$

When the following ranges for $\frac{S}{R}$, U, and $\frac{P_o}{E'}$ are used,

$$\frac{S}{R} = 4 - 12$$

$$U = 2 \times 10^{-6} - 5 \times 10^{-7}$$

$$\frac{P_o}{E'} = 0.05 - 0.2$$

the ratio $\frac{\Delta h_o}{h_o}$ is found to be within the range from 0.59 - 0.0087

This shows that the squeeze-film effect can be quite substantial under conditions in rod seal lubrication. The variation of the center film h_c during the entire cycle of the reciprocating motion is expected to be small for high values of p_o/E'.

Transient Film Thickness Analysis

It was shown in the last section that the mid-stroke film thickness can be estimated by equations derived from existing low-modulus EHD theories. The reduction of film thickness at the end-stroke can be estimated by a relation deduced from Herrebrugh's normal approach EHD analysis. In this section, an analysis is developed to determine the temporal behavior of the film thickness by solving simultaneously the time-dependent Reynolds' equation and the deformation equation. Since it was anticipated that this transient EHD solution for severly loaded rod seal contacts might encounter unforseen difficulties, it was decided that the first attempt at producing the transient analysis be based on simple Hertzian contact. The analysis below, therefore, does not include the deformation due to contact pressures exerted by groove surfaces on the seal ring. The analytical effort was focused on developing a

numerical method to handle the transient EHD solution under severe pressure loading. Other deformation profiles, including those produced by groove contact pressures, can be incorporated into the perfected method at a later date.

Governing Equations. The time-dependent Reynolds' equation for a pure Hertzian contact is

$$\frac{\partial}{\partial x}\left(h^3\frac{\partial p}{\partial x}\right) = 12\mu_o\left(u(t)\,\frac{\partial h}{\partial x} + \frac{\partial h}{\partial t}\right) \tag{23}$$

The film thickness is governed by

$$h = h_o + \frac{x^2}{2R} - \frac{4}{\pi E'}\int_{x_i}^{x_{ff}} p(\xi)\,\ln\left|\frac{\xi - x}{\xi}\right|\,d\xi \tag{24}$$

where

x = coordinate along the sliding surface

h = film thickness

p = pressure

μ_o = viscosity

u = time varying velocity

h_o = center film at $x = 0$

R = seal radius

x_i = inlet boundary of the lubricant film

x_{ff} = exit boundary of the lubricant film

ξ = dummy variable for x

Introducing the following non-dimensional quantities:

$\bar{x} = \frac{x}{b}$

b = half contact width

$H = \frac{h}{h_o}$

$P = p/p_o$

p_o = maximum Hertzian pressure

$$\bar{h}_o = \frac{\left(h_o/R\right)}{\sqrt{48\frac{\mu_o u_o}{E'R}}}$$

u_o = mid-stroke entrainment velocity, half of the mid-stroke sliding velocity ($u_o = \omega S/4$)

$C_1 = 16(p_o/E')^2/(h_o/R)$

S = stroke of the piston

$T = \frac{u_o t}{b}$

ω = angular velocity = $2\pi f$

$\bar{\xi} = \xi/b$

Equation (23) and Equation (24) in non-dimensional form become

$$\frac{\partial}{\partial\bar{x}}\left(H^3\frac{\partial P}{\partial\bar{x}}\right) = \frac{1}{\bar{h}_o^2}\left[\sin\omega t\frac{\partial H}{\partial\bar{x}} + \frac{1}{\bar{h}_o}\frac{\partial(\bar{h}_o H)}{\partial T}\right] \tag{25}$$

$$H = 1 + C_1\left[\frac{\bar{x}^2}{2} - \frac{1}{\pi}\int_{\bar{x}_i}^{\bar{x}_{ff}} P(\bar{\xi})\ln\frac{|\bar{\xi}-\bar{x}|}{|\bar{\xi}|}\,d\bar{\xi}\right] \tag{26}$$

In the above, the shaft velocity is assumed to be sinusoidal. The boundary conditions for Equation (25) are:

$$P = 0 \text{ at } \bar{x} = \bar{x}_i \tag{27}$$

$$P = 0 \text{ and } \frac{dP}{d\bar{x}} = 0 \quad \text{at } \bar{x} = \bar{x}_{ff} \tag{28}$$

$$P = 1 \text{ at } \bar{x} = 0 \tag{29}$$

$$\left(\frac{h_o}{R}\right)_{\omega t = 0} = \left(\frac{h_o}{R}\right)_{\omega t = 2\pi} \tag{30}$$

For a given set of parameters $\frac{p_o}{E'}$, $\frac{\mu_o u_o}{E'R}$, and $\frac{S}{R}$, one can determine the center film thickness $\frac{\bar{h}_o}{R}$ and the film thickness and pressure profiles at each time interval using numerical schemes. The two numerical

schemes considered in solving Equation (25) and (26) and the experience gathered with each are documented below.

Numerical Treatment--Direct Discretization (Scheme "A"). This scheme is the conventional way of handling the Reynolds' equation. In Equation (25), the second order derivative of P is directly discretized at a grid point k. The discretized equation appears as

$$\psi_k = \left[- H_{k-1/2}^3 \frac{P_k - P_{k-1}}{\Delta\bar{x}_{k-1}} + H_{k+1/2}^3 \frac{P_{k+1} - P_k}{\Delta\bar{x}_k} \right] \bar{h}_o^2$$
$$- \sin\omega t \left[d_{3,k} H_{k+1} + d_{2,k} H_k - d_{1,k} H_{k-1} \right]$$
$$- \frac{1}{\Delta T} \left[H_k - \frac{\bar{h}_{o,L}}{\bar{h}_o} H_{k,L} \right] = 0 \qquad (31)$$

where

$$H_k = 1 + C_1 \left[\frac{\bar{x}_k^2}{2} - \frac{1}{\pi} \sum_{j=1}^{k_{ff}} P_j Q_{kj} \right]$$

$$C_1 = 16 (P_o/E')^2 \Big/ \left(\frac{h_o}{R}\right)$$

$\bar{x}_h$ = $\bar{x}$ coordinate at grid k

P_j = P at grid j

Q_{kj} = A Kernel function developed in Reference [10], and reproduced in Appendix B

$$H_{k-1/2} = (H_k + H_{k-1}) \Big/ 2$$

$$H_{k+1/2} = (H_k + H_{k+1}) \Big/ 2$$

$$\Delta\bar{x}_{k-1} = \bar{x}_k - \bar{x}_{k-1}$$

$$\bar{h}_o = (h_o/R) \Big/ \left(48 \frac{\mu_o u_o}{E'R} \right)^{1/2}$$

$$d_{1,k} = \frac{\Delta\bar{x}_k}{\Delta\bar{x}_{k-1}(\Delta\bar{x}_k + \Delta\bar{x}_{k-1})}$$

$$d_{2,k} = \frac{\Delta\bar{x}_k - \Delta\bar{x}_{k-1}}{\Delta\bar{x}_k \; \Delta\bar{x}_{k-1}}$$

$$d_{3,k} = \frac{\Delta\bar{x}_{k-1}}{\Delta\bar{x}_k(\Delta\bar{x}_k + \Delta\bar{x}_{k-1})}$$

$\bar{h}_{o,L} = \bar{h}_o$ for the previous time interval

$H_{k,L} = H_k$ for the previous time interval

$$\Delta T = \frac{u_o \Delta t}{b}$$

At each time step, Equation (31) is a set of equations written at grids 2 to $k_{ff}-1$ for a total of $k_{ff}-2$ equations. These $k_{ff}-2$ equations can be solved by the Newton-Raphson procedure to obtain values for $k_{ff}-2$ unknowns consisting of P_2 to P_{k_o-1}, P_{k_o+1} to $P_{k_{ff}-1}$, and $\bar{h}_o$. In this solution,

$$P_1 = 0$$

$$P_{k_o} = 1$$

$$P_{k_{ff}} = 0$$

which are the boundary conditions for Equation (31).

The location of $\bar{x}_{k_{ff}}$ is not fixed, and must be such to make the slope $\frac{dP}{d\bar{x}}$ vanish at $\bar{x}_{k_{ff}}$. This is accomplished by moving $\bar{x}_{k_{ff}}$ towards the contact center one grid point at each iteration whenever a negative pressure appears near k_{ff}.

Scheme "A" was tried and failed to yield satisfactory results particularly at high loads. It begins to experience difficulties at $\frac{p_o}{E'} = 0.01$. It is not known whether the difficulties arose because of the inherent discretization error associated with the interpolations factors $d_{1,k}$, $d_{2,k}$, $d_{3,k}$ for uneven grids or because of a possible error in the complicated algebraic expression of $\frac{\partial \psi_k}{\partial \bar{h}_o}$ which has to be evaluated in the Newton-Raphson procedure. Scheme "A" was finally abandoned in favor of an alternative approach, Scheme "B", which is described next.

Numerical Treatment--Discretization of Integrated Reynolds Equation (Scheme "B"). This scheme follows closely that developed previously by Lee and Cheng [12] for studying the effect of a single asperity entering the inlet zone of an EHD contact. In this formulation, the Reynolds equation is first integrated once with respect to $\bar{x}$, and then discretized.

Integrating Equation (25) once, one obtains

$$\bar{h}_o^2 H^3 \frac{\partial P}{\partial \bar{x}} = \sin\omega t \cdot H + \frac{1}{\bar{h}_o} \int_{\bar{x}_i}^{\bar{x}} \frac{\partial (\bar{h}_o H)}{\partial T} d\bar{\xi} + c \tag{32}$$

where c is an integration constant.

If $\frac{dP}{d\bar{x}}$ is zero at $\bar{x} = 0$, then

$$c = -\sin\omega t - \frac{1}{\bar{h}_o} \int_{\bar{x}_i}^{0} \frac{\partial (\bar{h}_o H)}{\partial T} d\bar{\xi} \tag{33}$$

For general cases, $\frac{dP}{dx}$ at $\bar{x} = 0$ is small but not exactly zero; therefore, a small residual constant c' must be provided to permit any small non-zero pressure gradient to exist at $\bar{x} = 0$. Thus, for general cases,

$$c = c' - \sin\omega t - \frac{1}{\bar{h}_o} \int_{\bar{x}_i}^{0} \frac{\partial (\bar{h}_o H)}{\partial T} d\bar{\xi} \tag{34}$$

Substituting (34) in (32), and observing that

$$\int_{\bar{x}_i}^{0} \frac{\partial(\bar{h}_o H)}{\partial T}\, d\bar{\xi} = \int_{\bar{x}_i}^{\bar{x}} \frac{\partial(\bar{h}_o H)}{\partial T}\, d\bar{\xi} + \int_{\bar{x}}^{0} \frac{\partial(\bar{h}_o H)}{\partial T}\, d\bar{\xi} \tag{35}$$

Equation (32) becomes

$$\bar{h}_o^{\,2} H^3 \frac{\partial P}{\partial \bar{x}} = \sin\omega t\ (H - 1) - \frac{1}{\bar{h}_0} \int_{\bar{x}}^{0} \frac{\partial(\bar{h}_o H)}{\partial T}\, d\bar{\xi} + c' \tag{36}$$

Equation (36) is discretized at the mid-point, k + 1/2, between two pressure nodes, P_k and P_{k+1}. The discretized equation is

$$\psi_{k+1/2} = \bar{h}_o^{\,2} \left(H^3_{k+1/2} \frac{P_{k+1} - P_k}{\Delta \bar{x}_k} \right) - \sin\omega t\ (H_{k+1/2} - 1)$$

$$+ \frac{1}{\Delta T}\ \text{SUMS}\ (K, TH, 0) + c' = 0 \tag{37}$$

where

$$\text{SUMS}\ (K,TH,0) = \frac{\Delta \bar{x}_k}{4} \left[\left(H_{k+1/2} - \frac{\bar{h}_{o,L}}{\bar{h}_o} H_{k+1/2,L}\right) + \left(H_{k+1} - \frac{\bar{h}_{o,L}}{\bar{h}_o} H_{k+1,L}\right) \right]$$

$$+ \sum_{\ell = k+1}^{k_o - 1} \frac{\Delta \bar{x}_\ell}{2} \left[\left(H_\ell - \frac{\bar{h}_{o,L}}{\bar{h}_o} H_{\ell,L}\right) + \left(H_{\ell+1} - \frac{\bar{h}_{o,L}}{\bar{h}_o} H_{\ell+1,L}\right) \right]$$

$$\text{For } k < k_o - 1 \tag{38}$$

$$\text{SUMS}\ (K,TH,0) = \frac{\Delta \bar{x}_{k\phi-1}}{4} \left[\left(H_{k\phi-1/2} - \frac{\bar{h}_{o,L}}{\bar{h}_o} H_{k\phi-1/2,L}\right) + \left(1 - \frac{\bar{h}_{o,L}}{\bar{h}_o}\right) \right]$$

$$\text{For } k = k_o - 1 \tag{39}$$

$$\text{SUMS}\ (K,TH,O) = \frac{\Delta\bar{x}_{k\phi}}{4}\left[(1 - \frac{\bar{h}_{o,L}}{\bar{h}_o}) + (H_{k\phi+1/2} - \frac{\bar{h}_{o,L}}{\bar{h}_o} H_{k\phi+1/2,L})\right]$$

For $k = k_o$ (40)

$$\text{SUMS}\ (K,TH,O) = \sum_{\ell=k_o}^{k} \frac{\Delta\bar{x}_\ell}{2}\left[(H_\ell - \frac{\bar{h}_{o,L}}{\bar{h}_o} H_{\ell,L}) + (H_{\ell+1} - \frac{\bar{h}_{o,L}}{\bar{h}_o} H_{\ell+1,L})\right]$$

$$+ \frac{\Delta\bar{x}_k}{4}\left[(H_k - \frac{\bar{h}_{o,L}}{\bar{h}_o} H_{k,L}) + (H_{k+1/2} - \frac{\bar{h}_{o,L}}{\bar{h}_0} H_{k+1/2,L})\right]$$

For $k \geq k_o+1$ (41)

By referring to the following diagram,

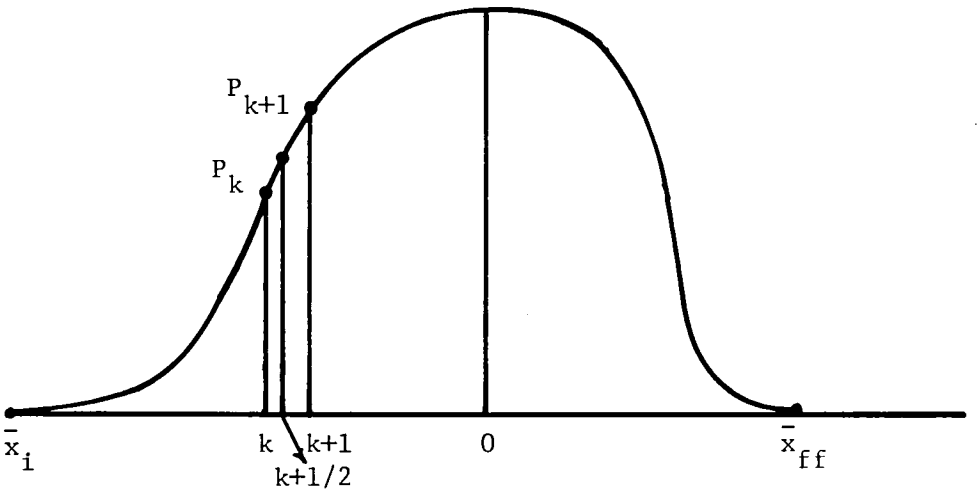

Equations (37) can be written at $k = 1$ to $k = k_{ff} - 1$ for a total number of $k_{ff} - 1$ equations. In solving Equations (37), the following

pressures are known,

$$P_1 = 0$$

$$P_{k_o} = 1$$

$$P_{k_{ff}} = 0$$

Thus, the total number of unknown pressure nodes is $k_{ff} - 3$, and they are P_2 to P_{k_o-1} and P_{k_o+1} to $P_{k_{ff}-1}$. These $k_{ff}-3$ unknown pressure nodes together with $\bar{h}_o$ and c' form the right number of unknowns for the $k_{ff}-1$ equations.

As mentioned in Scheme "A", $\bar{x}_{ff}$ must satisfy the free boundary condition $\frac{dP}{d\bar{x}} = 0$. This is accomplished at each iteration by searching for the point near the exit region where the following term vanishes

$$\sin\omega t\ (H - 1) - \frac{1}{\bar{h}_o}\int_{\bar{x}_{ff}}^{0} \frac{\partial(\bar{h}_o H)}{\partial T}\ d\bar{\xi} + c' = 0 \qquad (42)$$

It was found the inclusion of $\bar{h}_o$ as an unknown in Equations (37) in the Newton-Raphson procedure gave rise to some difficulties in convergence. This was remedied by allowing the integration constant c' in the inlet half to be different from the value of c' in the exit half. In so doing, c' is now replaced with two unknown constants, c'_I for the inlet region, and c'_o for the exit region; however, $\bar{h}_o$ is now considered as known. Thus, the total number of unknowns still matches the total number of equations.

At each time step, one begins the first iteration with an initial guess of $\bar{h}_o$, which is usually the value of $\bar{h}_o$ for the previous time step. With the first guess of $\bar{h}_o$, Equations (37) can be solved for P_k and c'_I and c'_o. If c'_I is not equal to c'_o, $\bar{h}_o$ is readjusted until c'_I matches c'_o. This procedure permits $\bar{h}_o$ values to be calculated during half of the reciprocating cycle. However, $\bar{h}_o$ thus determined in the first half cycle may not satisfy the periodic conditions, i.e.,

$$(\bar{h}_o)_{\omega t=\pi/2} = (\bar{h}_o)_{\omega t=3\pi/2}$$

The cycle must be repeated until the periodic boundary condition in time is satisfied.

The procedure seems to work well for a wide range of load and speed parameters, even for conditions beyond those occuring in Stirling engine rod seals. Results obtained from use of the procedure are given in the next section. In the Appendicies, details and use of the procedure are discussed. Specifically, the expressions for the derivatives of $\psi_{k+1/2}$ with respect to P_j for solving Equations (37) can be found in Appendix C. The computer program for Scheme "B" is entitled "RODSLJ" and is documented in Appendix A.

Results

Three input parameters are required for each run. These include:

$\frac{p_o}{E'}$: load parameter

$U = \frac{\mu_o u_o}{E'R}$: speed parameter

$\frac{S}{R}$: stroke to seal radius ratio

For the conditions to be used in the experimental rig, the range of the above dimensionless parameters was found to be:

$$\frac{p_o}{E'} = 0.05 \text{ to } 0.25$$

$$U = 10^{-7} \text{ to } 2.0 \times 10^{-6}$$

$$\frac{S}{R} = 4 \text{ to } 16$$

Table 2 lists the input data for seven runs. Runs 50, 51, and 52 are for finding the effect of speed; Runs 51, 53, and 54 for the effect of load; and Runs 51, 55, and 56 for the effect of stroke to radius ratio. Figures 27 to 34 show dimensionless film profiles at six different stroke positions during the forward stroke ($\omega t=0$ to $\omega t=\pi$) of the reciprocating cycle. Since the sealing pressure differential is not considered in the present analysis, the film profiles during the backward stroke ($\omega t=\pi$ to $\omega t=2\pi$) should be a mirror image of the forward stroke profiles, which are the only ones presented here. All film

Table 2 List of Input Data

Run No.	$\frac{p_o}{E'}$	U	$\frac{S}{R}$	$\frac{p_o}{E'}\sqrt{U}$
50	0.1	10^{-7}	8	31.6
51	0.1	5×10^{-7}	8	14.14
52	0.1	2×10^{-6}	8	7.07
53	0.25	5×10^{-7}	8	88.3
54	0.05	5×10^{-7}	8	3.54
55	0.1	5×10^{-7}	16	14.14
56	0.1	5×10^{-7}	4	14.14

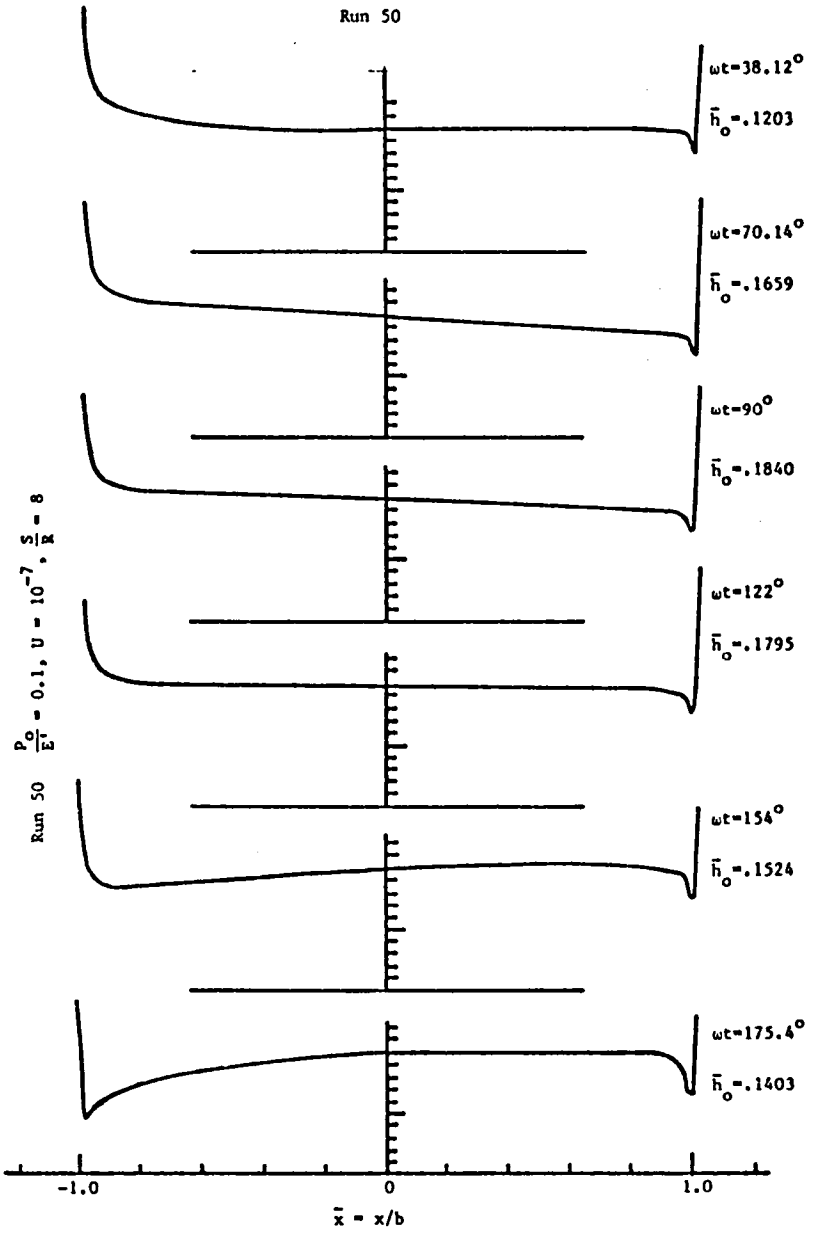

Figure 27 Film Profiles for Run 50, $\frac{P_o}{E'} = .1$, $U = 10^{-7}$, $\frac{S}{R} = 8$

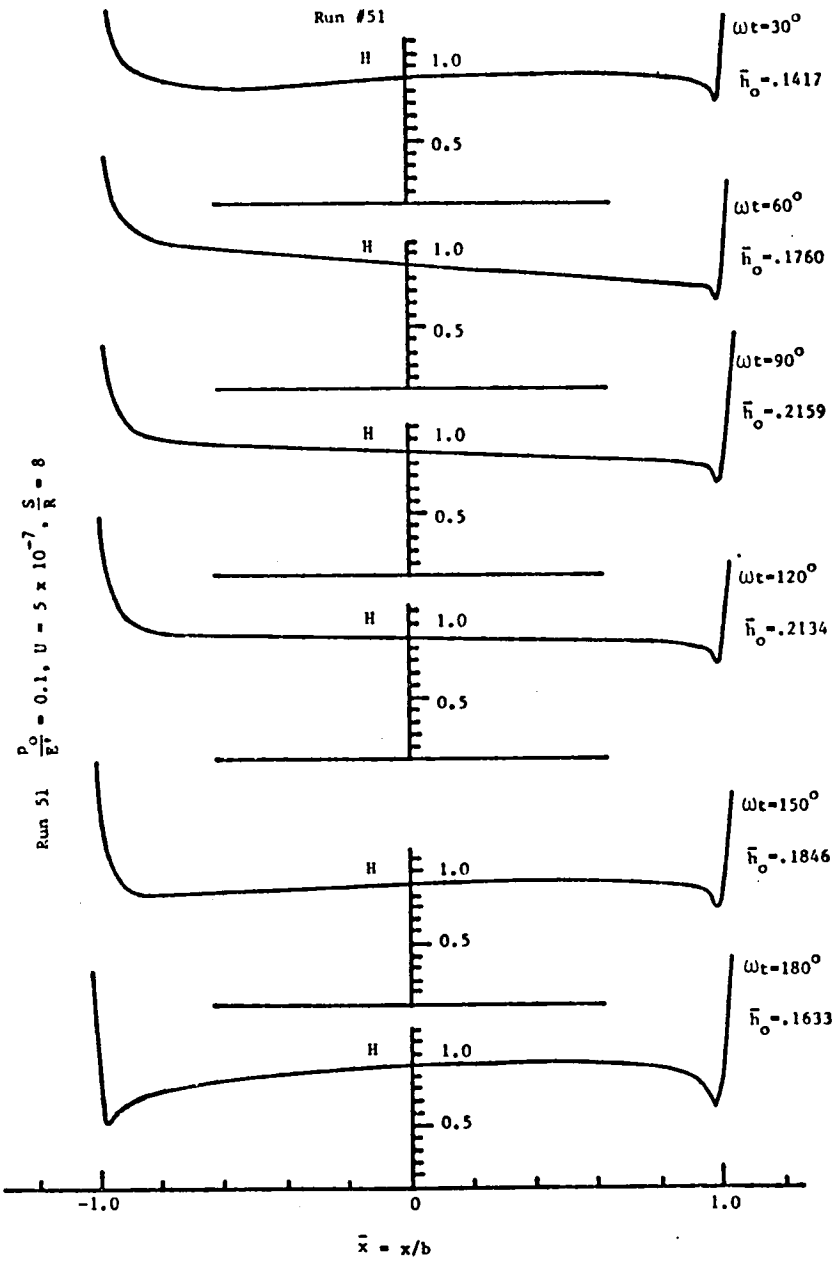

Figure 28 Film Profiles for Run 51, $\frac{p_o}{E'} = 0.1$, $U = 5 \times 10^{-7}$, $\frac{S}{R} = 8$

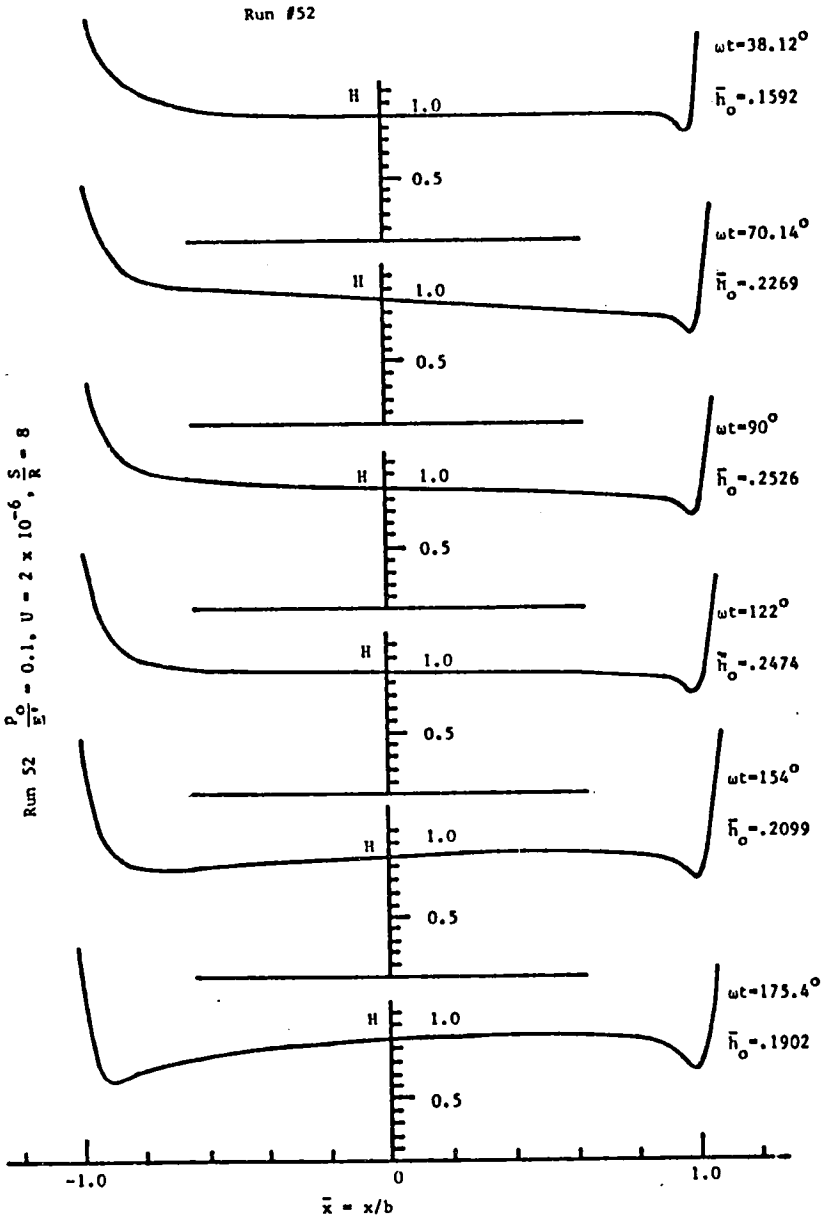

Figure 29 Film Profiles for Run 52, $\frac{p_o}{E'} = 0.1$, $U = 2 \times 10^{-6}$, $\frac{S}{R} = 8$

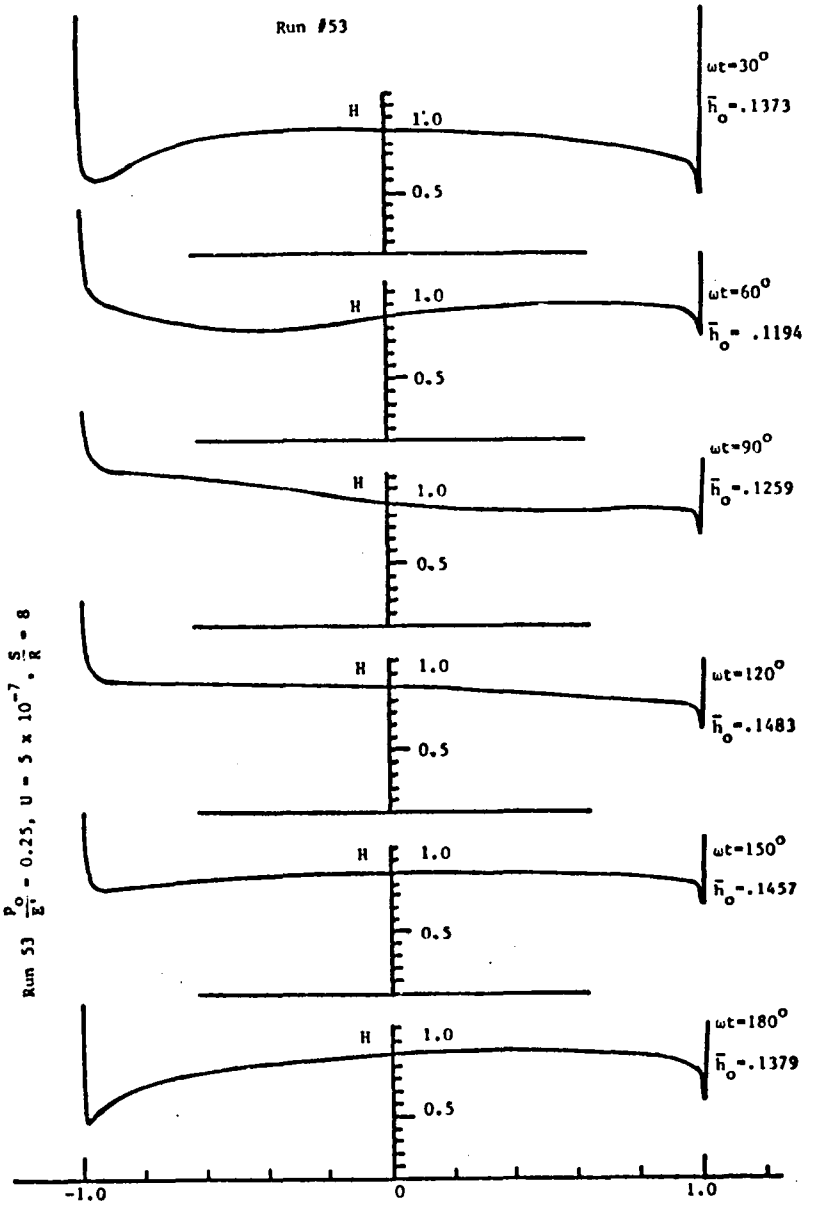

Figure 30 Film Profiles for Run 53, $\frac{P_o}{E'} = 0.25$, $U = 5 \times 10^{-7}$, $\frac{S}{R} = 8$

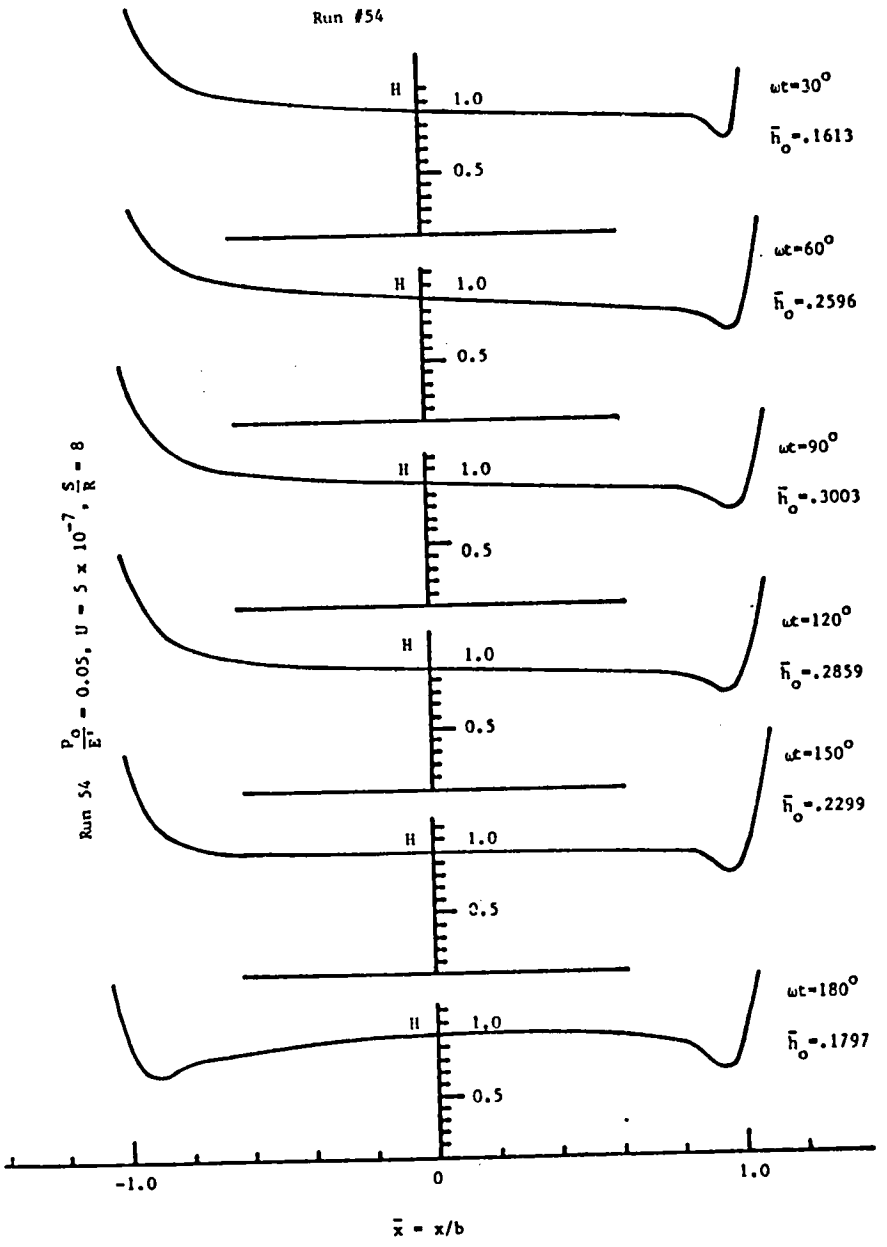

Figure 31 Film Profiles for Run 54, $\frac{P_o}{E'} = 0.05$, $U = 5 \times 10^{-7}$, $\frac{S}{R} = 8$

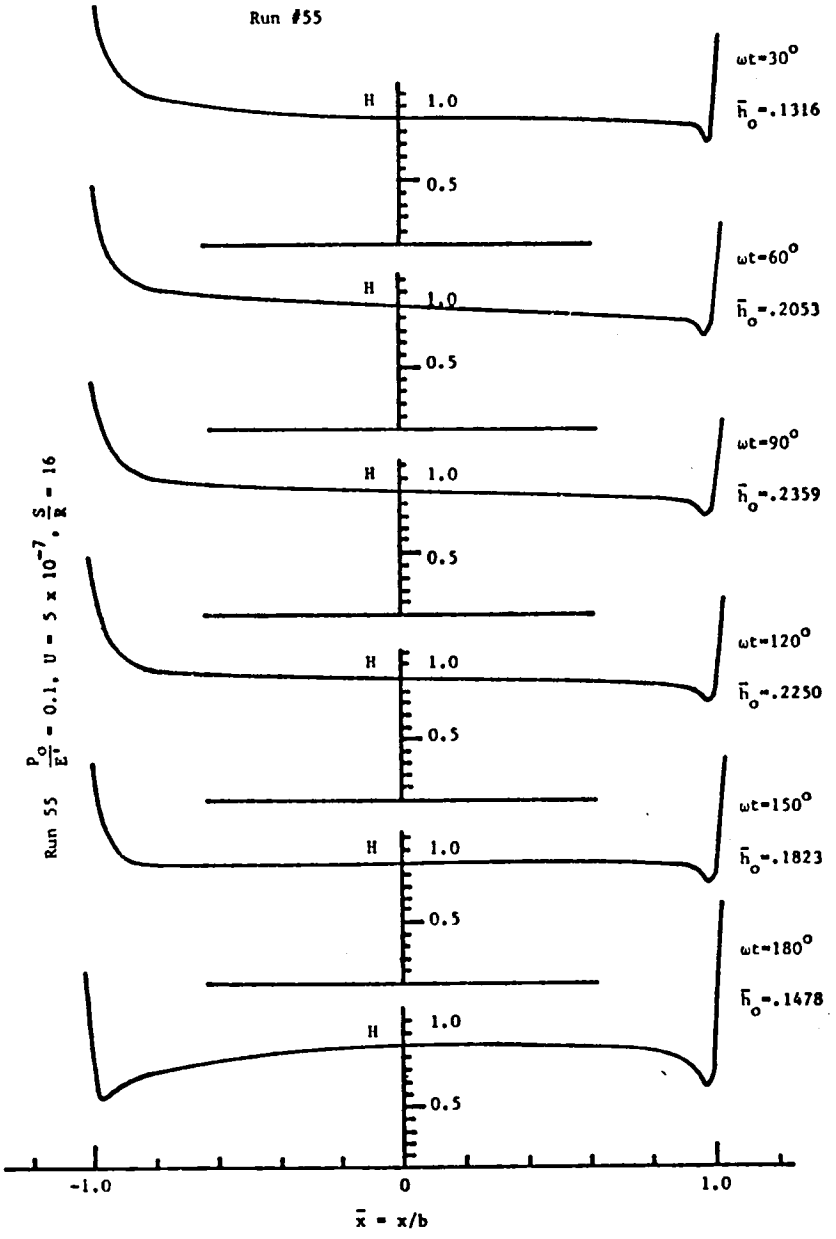

Figure 32 Film Profiles for Run 55, $\frac{p_o}{E'} = 0.1$, $U = 5 \times 10^{-7}$, $\frac{S}{R} = 16$

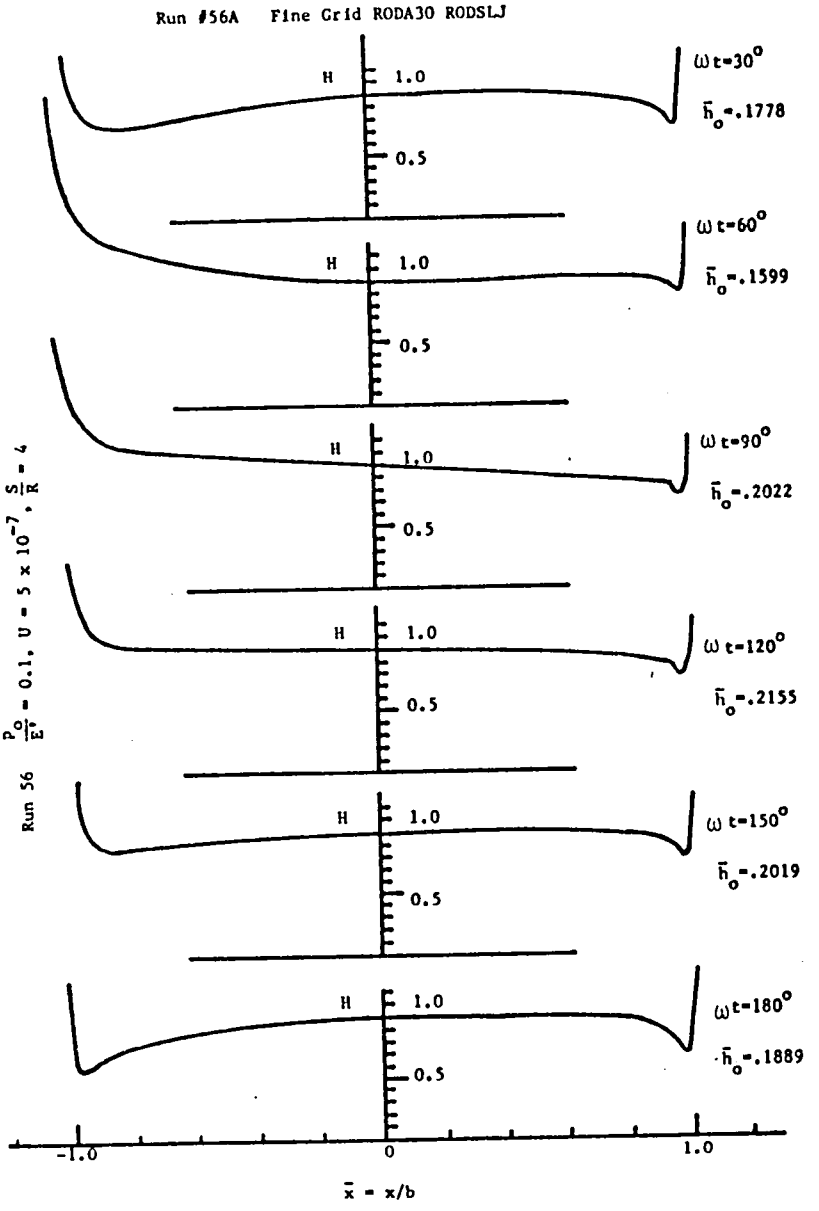

Figure 33 Film Profiles for Run 56, $\frac{P_o}{E'}$ = .1, U = 5 x 10^{-7}, $\frac{S}{R}$ = 4

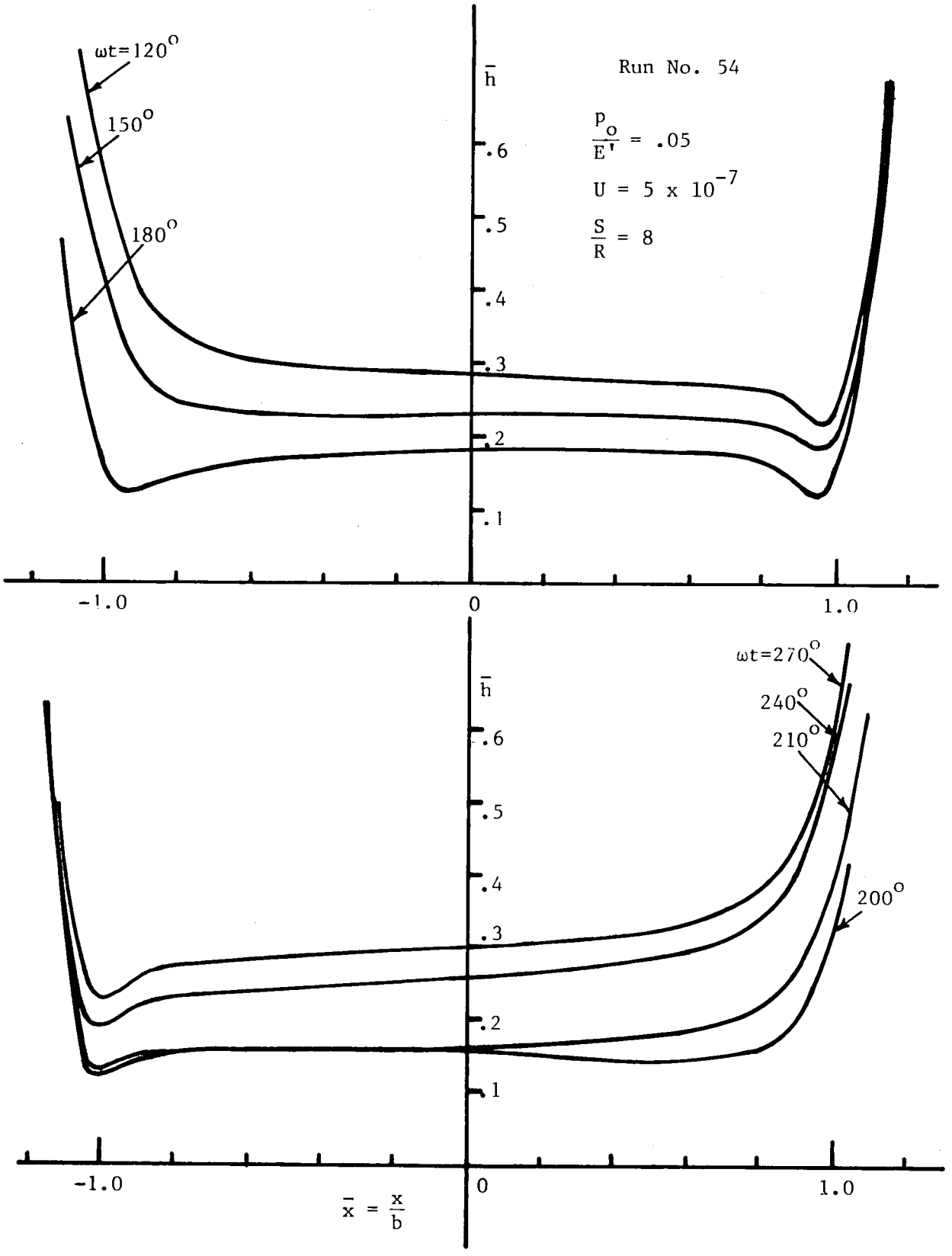

Figure 34 Film Profiles for Run No. 34

profiles are normalized with respect to the film thickness at the center. The value of $\bar{h}_o$, the non-dimensional film thickness at the center, at each stroke position is labelled for each profile.

For Run 54, the most lightly loaded case, the film profile between the last half of the forward stroke ($\omega t = \frac{\pi}{2}$ to $\omega t = \pi$) and the first half of the backward stroke ($\omega t = \pi$ to $\omega t = \frac{3\pi}{2}$) are replotted on the same scale to show their relative positions. These curves show a trend consistent with these observed by Blok and Koens [8]. It would be of interest to ascertain the exact conditions used in their experimental runs so that more quantitative comparisons can be made.

Aside from the fact that the edge protrusions are much more pronounced for heavily loaded or low speed cases, the general features of film profiles are very similar for all runs. It is interesting to note that at the end-stroke position ($\omega t = \pi$), where the sliding velocity vanishes, the film droops down more in the inlet half region, whereas in the exit half the film remains reasonably flat or even rises slightly above the center film in some cases. This feature seems to be due to the sliding action producing a very effective suction once a negative wedge is formed at the inlet. As can be seen in Figure 23, this same feature also exists in the observed film profiles at the end-strokes.

The variation of the center film thickness during half of the reciprocating cycle ($\omega t = \frac{\pi}{2}$ to $\omega t = \frac{3\pi}{2}$) is shown in Figure 35. At the mid-stroke ($\omega t = \frac{\pi}{2}$), the shaft velocity reaches a maximum and is decreasing. However, the center film thickness does not reach a maximum until about 10-15 degrees after the mid-stroke. This shift is due to the fact that part of the sliding action at the mid-stroke is nullified by the squeeze-film action $\frac{\partial H}{\partial T}$. The stronger the squeeze-film term, the larger the shift of the maximum film from the mid-stroke position. As the shaft reaches the end-stroke position ($\omega t = \pi$), the sliding action ceases, and the pressure within the film is supported entirely by the squeeze-film action. Perhaps the most interesting feature in this curve is the sudden reduction of $\bar{h}_o$ soon after the end-stroke position, where the motion reversal takes place. This reduction is attributable to the penetration of the exit protrusion into the center of the contact after the shaft reverses its direction. This penetration causes a sharp reduction $\bar{h}_o$ for low-speed or high-pressure cases. It becomes more pronounced as the squeeze-film effect becomes more influential.

Figure 36 shows influence of speed on $\bar{h}_o$. It is seen that the squeeze-

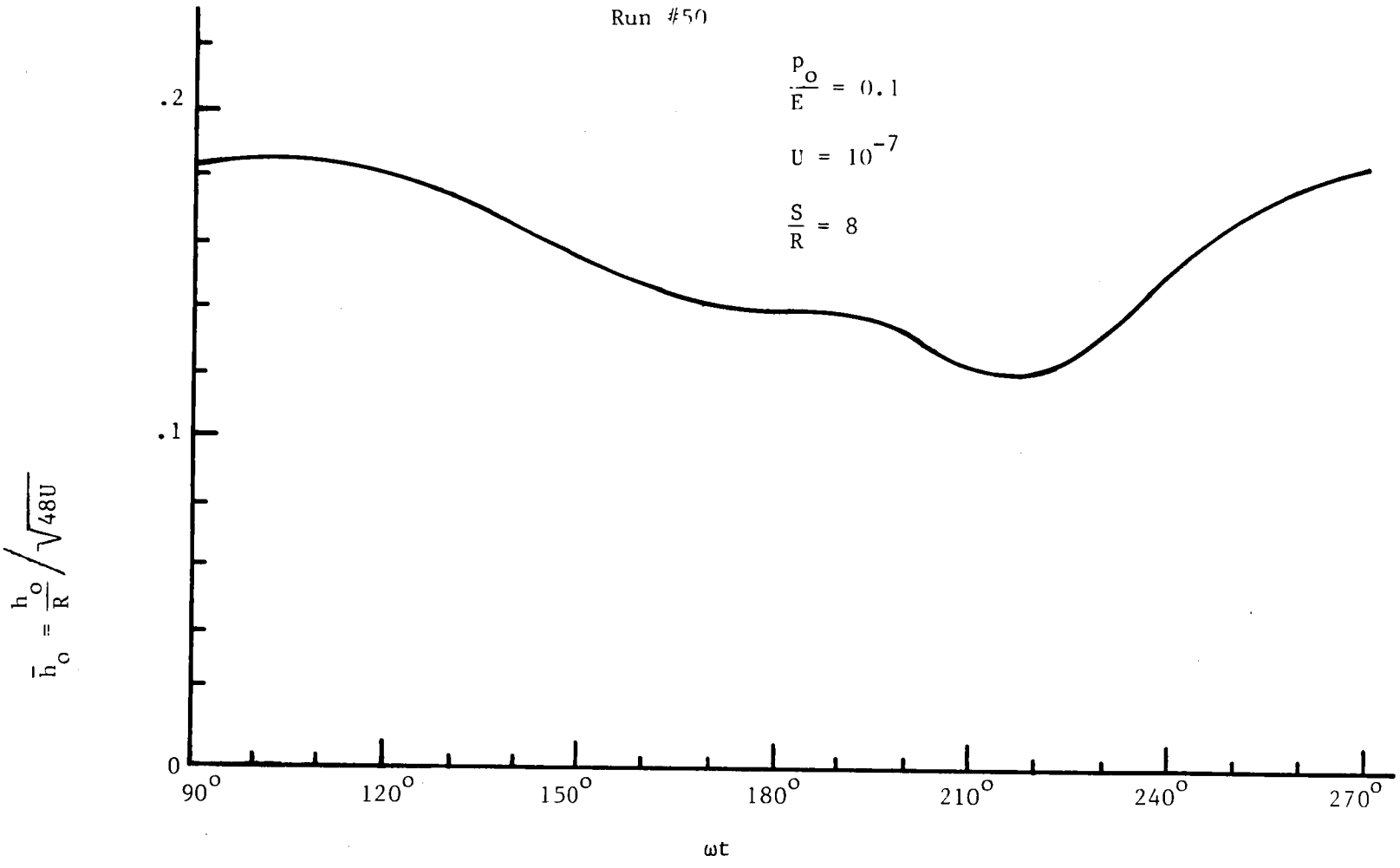

Figure 35 Variation of $\bar{h}_o$ with the Stroke Position

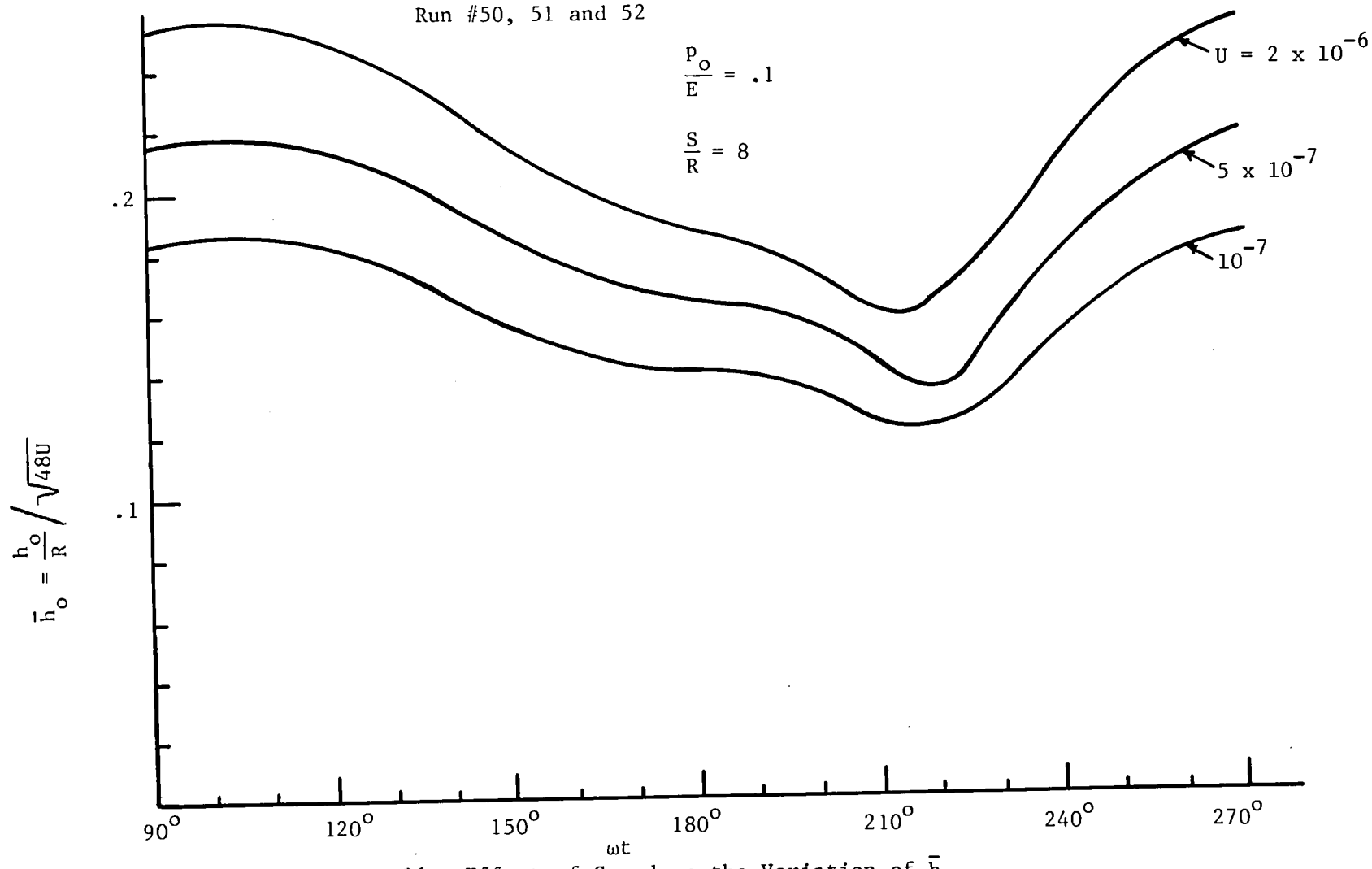

Figure 36 Effect of Speed on the Variation of $\bar{h}_o$

film action is not altered significantly even for a five-fold increase in speed. This trend agrees well with the approximate analysis of squeeze-film effect represented by Equation (20).

Figure 37 shows the effect of load parameter on $\bar{h}_o$. It is seen that the fluctuation of $\bar{h}_o$ is most strongly influenced by the change in pressure. A five-fold increase in Hertzian pressure from 0.05 to 0.25 yields more than ten times reduction of $\bar{h}_o$ during the last half of the forward cycle ($\omega t = \frac{\pi}{2}$ to $\omega t = \pi$). This result again confirms qualitatively the approximate formula Equation (20) derived from Herrebrugh's squeeze-film analysis. It should be noted that for the highest Hertzian pressure $\left(\frac{P_o}{E'} = .25\right)$ the reduction of $\bar{h}_o$ right after the end-stroke position ($\omega t = \pi$) is quite sudden. It should also be noted that the lowest film thickness at this position is accompanied by a substantial sliding velocity. If the seal surface is to fail by sliding wear, it is likely to begin first at this position.

Figure 38 shows the effect of stroke length on the variations of $\bar{h}_o$. As expected, a longer stroke would lessen the squeeze-film effect and allow $\bar{h}_o$ to approach more to the steady-state value based solely on the sliding velocity. With a shorter stroke, the squeeze-film action dominates, and the fluctuation due to the sinusoidal sliding velocity is considerably suppressed.

Concluding Remarks on Analyses

A time-dependent numerical EHD analysis for low-modulus line contacts was developed to investigate the temporal behavior of the film profiles of sliding rod seals during a reciprocating cycle. Resulting film profiles reveal all essential features of the temporal film behavior observed by Blok and Koens [8] between a rubber cylinder and a transparent reciprocating surface.

The results indicate that the squeeze-film effect dampens the film thickness fluctuations caused by the oscillatory sliding velocity. It also produces a shift of the maximum film from the mid-stroke position, where the maximum velocity occurs. Likewise, the minimum center film thickness occurs not at the end-stroke, but a few degrees thereafter. For cases of pronounced squeeze-film effect, usually associated with high-load cases, the reduction of the center film after the end-stroke is rather abrupt, particularly at a position where there is substantial sliding velocity.

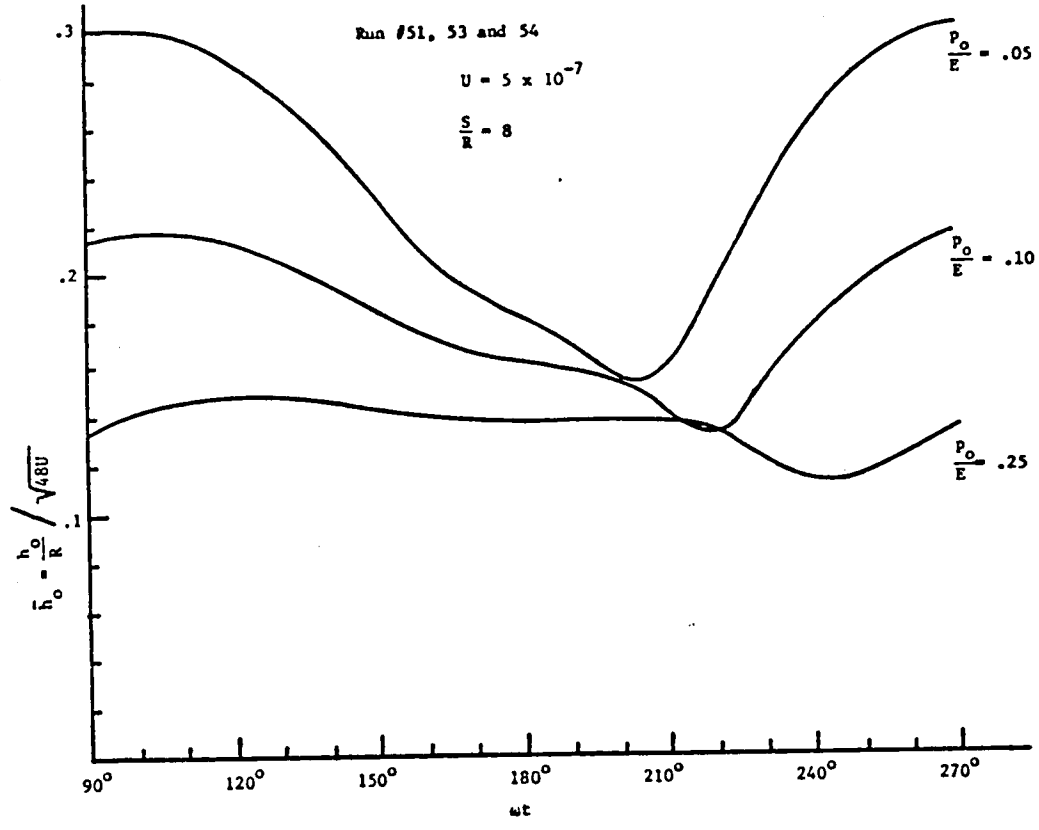

Figure 37 Effect of Load on the Variation of $\bar{h}_o$

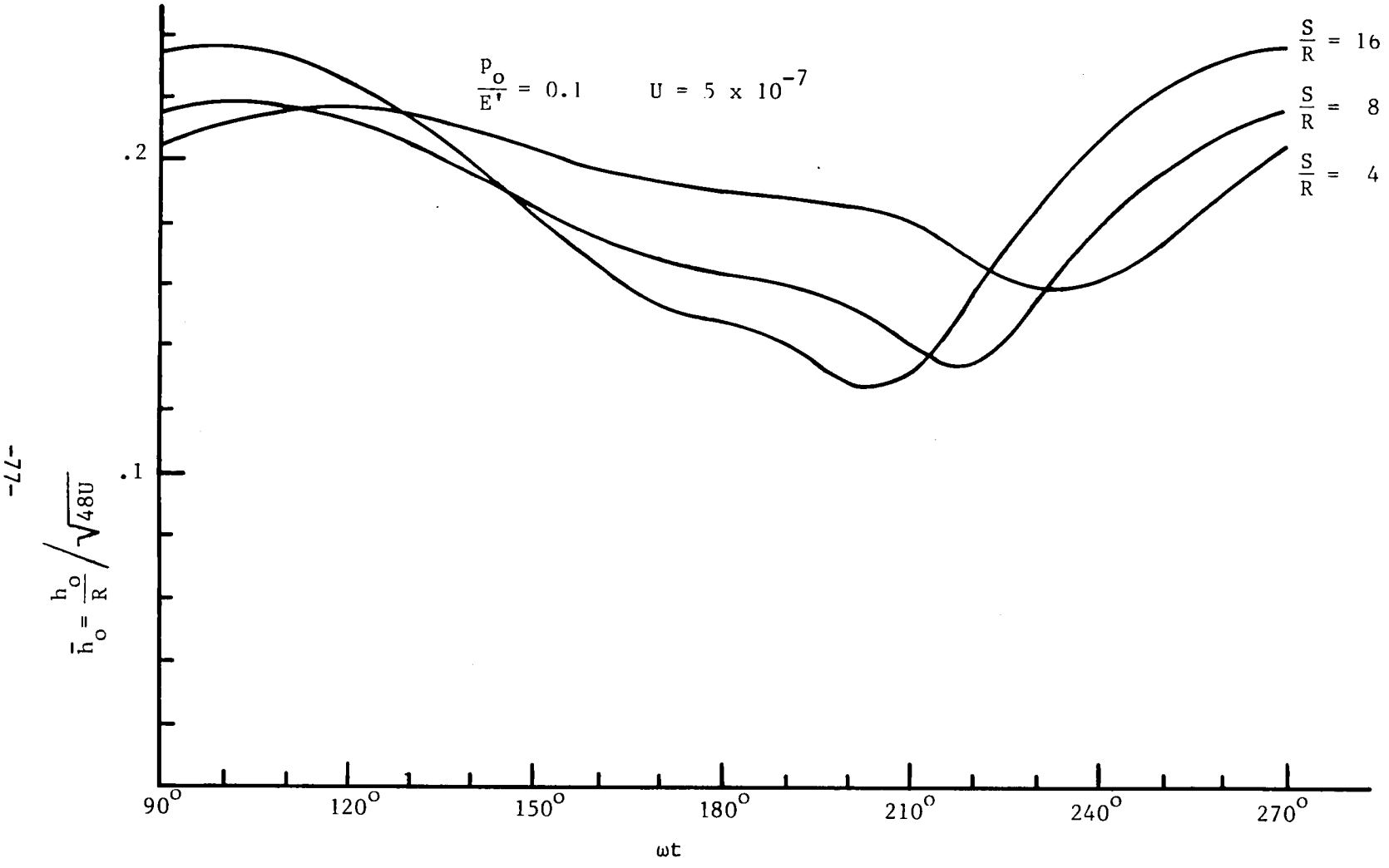

Figure 38 $\bar{h}_o$ vs ωt, Effect of Stroke to Radius Ratio

The squeeze-film effect increases strongly with an increase in contact pressure, but is almost uninfluenced by a significant change in speed. These findings correlate well with an approximate formula for the change of film thickness due to squeeze-film action based on an existing normal approach analysis [11].

The results developed in the present analysis are based on a pure Hertzian contact uninfluenced by any contact pressure between the seal ring and the groove walls or by the effects of a large sealing pressure differential. The analysis should be valid for cases where the sealing pressure differential is small compared to the contact pressure. The transient analysis developed is an essential building block for further study of the temporal film behavior of rod seals under large fluid sealing pressures. The analysis can be readily modified to include an inlet deformation profile obtained from a static finite element deformation computation. When such a profile is combined with the present analysis, the resulting analysis will be capable of treating the wall pressure effects and the pressure drop across the contact region.

CONCLUSIONS AND RECOMMENDATIONS

On the basis of work done to date, the following conclusions have been reached regarding the experimental apparatus and the analytical effort:

Experimental Apparatus

- The experimental apparatus, in design and performance, is suitable for evaluating Stirling engine rod seal behavior. The apparatus produces a well-defined reciprocating motion of the transparent cylinder. It exhibits little vibration. The built-in force cell measures properly axial forces applied to the test seal holder. In addition, the device is rugged and easy to use.
- The interferometric measurements, necessary in the evaluation of seal behavior, can be made with the device. However, the Lexan presently used for the transparent cylinder must be replaced. The new material should be optically smooth both on the inner and outer diameters and should be scratch resistant. The first choice for this material is glass and the second choice is acrylic.

Analysis

- A time dependent numerical method was developed which determines the fluid film thickness and pressure distribution at the contact zone between an elastomeric seal and a reciprocating cylinder. The method is appropriate for the high values of static contact pressure to seal modulus ratio found in Stirling engine rod seal applications. At its present stage of development, the method applies for a Hertzian static contact pressure profile and for zero pressure gradient across the seal.

- Application of the numerical method produces results which correlate well with experimental results in the literature and with appropriate approximate analyses. The results obtained show that

  a) the squeeze-film effect dampens the film thickness fluctuations caused by the oscillatory sliding velocity
  b) the maximum film does not occur at the instant of maximum velocity
  c) the minimum film does not occur at the instant of zero velocity
  d) the squeeze-film effect is affected strongly by the contact pressure but is almost independent of the sliding velocity.

Continuation of the contract work should be directed at maximizing the usefulness of the analytical and experimental tools developed to date. The following recommendations are based on this objective.

It is recommended that the experimental apparatus be used in an in-depth study of Stirling engine rod seal behavior. To do this requires that some refinement to the apparatus be done, that a test program be developed and conducted, that the resulting data be reduced appropriately, and that some runs of the analytical seal model be performed for cases corresponding to the experimental situations.

The refinement of the experimental apparatus entails the addition of hardware to synchronize a stroboscopic photographic flash with the cylinder position.

The test program should include use of the apparatus with the transparent cylinder, with an aluminum cylinder, and with a coated and uncoated seal. Using the transparent cylinder and the coated seal can provide, primarily, film thickness data for comparison with theoretical results. Parameters which can be considered include:

1. Seal type and seal material
2. Seal preload and seal groove geometry
3. Gas pressure to 690 kPa (100 psi), (zero pressure for at least one set of tests)
4. Frequency (10 to 50 Hz)
5. Temperature and lubricant type
6. Seal surface finish (variations to be obtained by changing the optical coating on the seal)

Operation of the apparatus with the glass cylinder and an uncoated seal can reveal the role of the optical coating in the results with the coated seal. To accomplish this, measurements of leakage and friction-force can be made and compared to these obtained for the coated seal.

Operation of the apparatus with the aluminum cylinder and an uncoated seal can reveal the role of cylinder surface finish on friction and leakage. In this, measurements of friction and leakage can be taken and compared to those obtained for the uncoated seal/glass cylinder combination. Also, aluminum cylinders having various surface finishes can be employed in the comparisons.

Regarding data reduction, the most important aspect is quantifying the interferometry results to determine the film thickness and the film thickness profile. Techniques for the film thickness measurement include white light with color tables, two discrete wavelengths of light, or monochromatic light with counting of fringes born. It is desirable that the most suitable technique or techniques be determined and used in the above experimental work.

Additional runs of the elastohydrodynamic seal model will be needed for those situations to be treated experimentally. Such situations, not yet considered analytically, include various combinations of seal properties, seal preload, cyclic frequency, and lubricant viscosity. Comparing similar experimental/analytical cases (to the extent that the model can represent the experimental situation) will provide insight into both the important aspects of the elastohydrodynamic seal behavior and additional capabilities desirable for eventual addition to the computer model. Capabilities already identified for eventual addition to the computer model are a general (non-Hertzian) static pressure distribution and a pressure drop across the seal.

REFERENCES

1. Blok, H. and Koens, H. J., "The Breathing Film Between a Flexible Seal and a Reciprocating Rod," Vol. 180, Pt. 3B, Proc. Instn. Mech. Engineers, 1965-1966.

2. Field, G. J. and Nau, B. S., "Optical Interference Method of Studying the Lubrication of a Compliant Bearing," ASME Paper No. 76-LubS-3, May 1976.

3. Roberts, S. D., "Lubrication Studies of Smooth Rubber Contacts," The Physics of Tire Traction, Edited by D. F. Hays and S. L. Browne. Available from Plenum Publishing Corporation, 227 West 17th Street, New York, NY 10011.

4. Swales, P. D., Dowson, D., and Latham, J. L., "Theoretical and Experimental Observations of the Behavior of Soft Elastic Materials Under Elastohydrodynamic Conditions," Proceedings of the 1972 Leeds Symposium on Elastohydrodynamic Lubrication, Paper C4/72.

5. Dowson, D. and Swales, P. D., "The Development of Elastohydrodynamic Conditions in a Reciprocating Seal," Proceedings of the 4th International Conference on Fluid Sealing 1969 (BHRA).

6. Hooke, C. J., et al, "Elastohydrodynamic Lubrication of "O" Ring Seals," Proceedings of Institution of Mechanical Engineers Vol. 181 Pt. 1, No. 9, pp. 205-210.

7. Hooke, C. J. and and O'Donoghue, J. P., "Elastohydrodynamic Lubrication of Soft, Highly Deformed Contacts," Journal of Mechanical Engineering Science, Vol 14, No. 1, 1972.

8. Blok, H. and Koens, H. J., "The 'Breathing' Film Between a Flexible Seal and a Reciprocating Rod," Symposium on Elastohydrodynamic Lubrication, Journal of Mechanical Engineers, pp. 221-223.

9. Herrebrugh, K., "Solving the Incompressible and Isothermal Problem in EHD Lubrication Through an Integral Equation," JOLT, Vol. 90, Series F, No. 1, January 1970, pp.262.

10. Hamrock, B. and Dowson, D., "EHD Lubrication of Elliptical Contacts of Low Elastic Modulus, Part I - Fully Flooded Conjunction," to appear in JOLT, Trans. of ASME, 1978.

11. Herrebrugh, K., "EHD Squeeze Films Between Two Cylinders in Normal Approach," ASME, JOLT, Vol. 92, Series F, No. 2, April 1970, pp 292.

12. Lee, K. and Cheng, H. S., "Effect of Surface Asperity on EHD Lubrication," NASA Contract Report CR-2195.

REFERENCES

1. Blok, H. and Koens, H. J., "The Breathing Film Between a Flexible Seal and a Reciprocating Rod," Vol. 180, Pt. 3B, Proc. Instn. Mech. Engineers, 1965-1966.

2. Field, G. J. and Nau, B. S., "Optical Interference Method of Studying the Lubrication of a Compliant Bearing," ASME Paper No. 76-LubS-3, May 1976.

3. Roberts, S. D., "Lubrication Studies of Smooth Rubber Contacts," The Physics of Tire Traction, Edited by D. F. Hays and S. L. Browne. Available from Plenum Publishing Corporation, 227 West 17th Street, New York, NY 10011.

4. Swales, P. D., Dowson, D., and Latham, J. L., "Theoretical and Experimental Observations of the Behavior of Soft Elastic Materials Under Elastohydrodynamic Conditions," Proceedings of the 1972 Leeds Symposium on Elastohydrodynamic Lubrication, Paper C4/72.

5. Dowson, D. and Swales, P. D., "The Development of Elastohydrodynamic Conditions in a Reciprocating Seal," Proceedings of the 4th International Conference on Fluid Sealing 1969 (BHRA).

6. Hooke, C. J., et al, "Elastohydrodynamic Lubrication of "O" Ring Seals," Proceedings of Institution of Mechanical Engineers Vol. 181 Pt. 1, No. 9, pp. 205-210.

7. Hooke, C. J. and and O'Donoghue, J. P., "Elastohydrodynamic Lubrication of Soft, Highly Deformed Contacts," Journal of Mechanical Engineering Science, Vol 14, No. 1, 1972.

8. Blok, H. and Koens, H. J., "The 'Breathing' Film Between a Flexible Seal and a Reciprocating Rod," Symposium on Elastohydrodynamic Lubrication, Journal of Mechanical Engineers, pp. 221-223.

9. Herrebrugh, K., "Solving the Incompressible and Isothermal Problem in EHD Lubrication Through an Integral Equation," JOLT, Vol. 90, Series F, No. 1, January 1970, pp.262.

10. Hamrock, B. and Dowson, D., "EHD Lubrication of Elliptical Contacts of Low Elastic Modulus, Part I - Fully Flooded Conjunction," to appear in JOLT, Trans. of ASME, 1978.

11. Herrebrugh, K., "EHD Squeeze Films Between Two Cylinders in Normal Approach," ASME, JOLT, Vol. 92, Series F, No. 2, April 1970, pp 292.

12. Lee, K. and Cheng, H. S., "Effect of Surface Asperity on EHD Lubrication," NASA Contract Report CR-2195.

13. Cheng, H. S., "Isothermal EHD Theory for the Full Range of Pressure Viscosity Coefficient," JOLT, ASME Trans. 94, Series F, 35-43.

14. Wernick, R. J., "Some Computer Results in the Direct Iteration Solution of the EHD Equations," Mechanical Technology Inc. Report MTI-62-TR-38.

APPENDIX A

COMPUTER CODE "RODSLJ"

APPENDIX A

Computer Code "RODSLJ"

Flow Chart

The computer code "RODSLJ" was written to calculate the time-dependent pressure and film thickness profiles, P_k and H_k, at various stroke positions during half of the reciprocating cycle ($\omega t=\pi/2$ to $\omega t=3\pi/2$). The flow diagram shown in Figure A-1 is based on the numerical treatment described as Scheme "B" in the Analytical Report. For a set of given input data, the calculation of P_k and H_k for the entire half cycle is nested in four loops. In the innermost loop (IT=1, ITP), P_k and H_k are calculated for a prescribed $\bar{h}_o$ to satisfy Equations (37). The second inner loop (ITM=1, ITH) is an iterative loop for solving the center film $\bar{h}_o$ to satisfy the condition, $c_I' - c_o' = 0$. The third inner loop (MT=MII, MTMAX) performs the calculation of $\bar{h}_o$, P_k, and H_k in equal time intervals from the one mid-stroke position ($\omega t=\pi/2$) to the other mid-stroke position ($\omega t=3\pi/2$). The outermost loop (IE=1, ITE) repeats the MT loop until $\bar{h}_{o,\pi/2} = \bar{h}_{o,3\pi/2}$.

The nomenclature used in the computer program is listed in Table A-1.

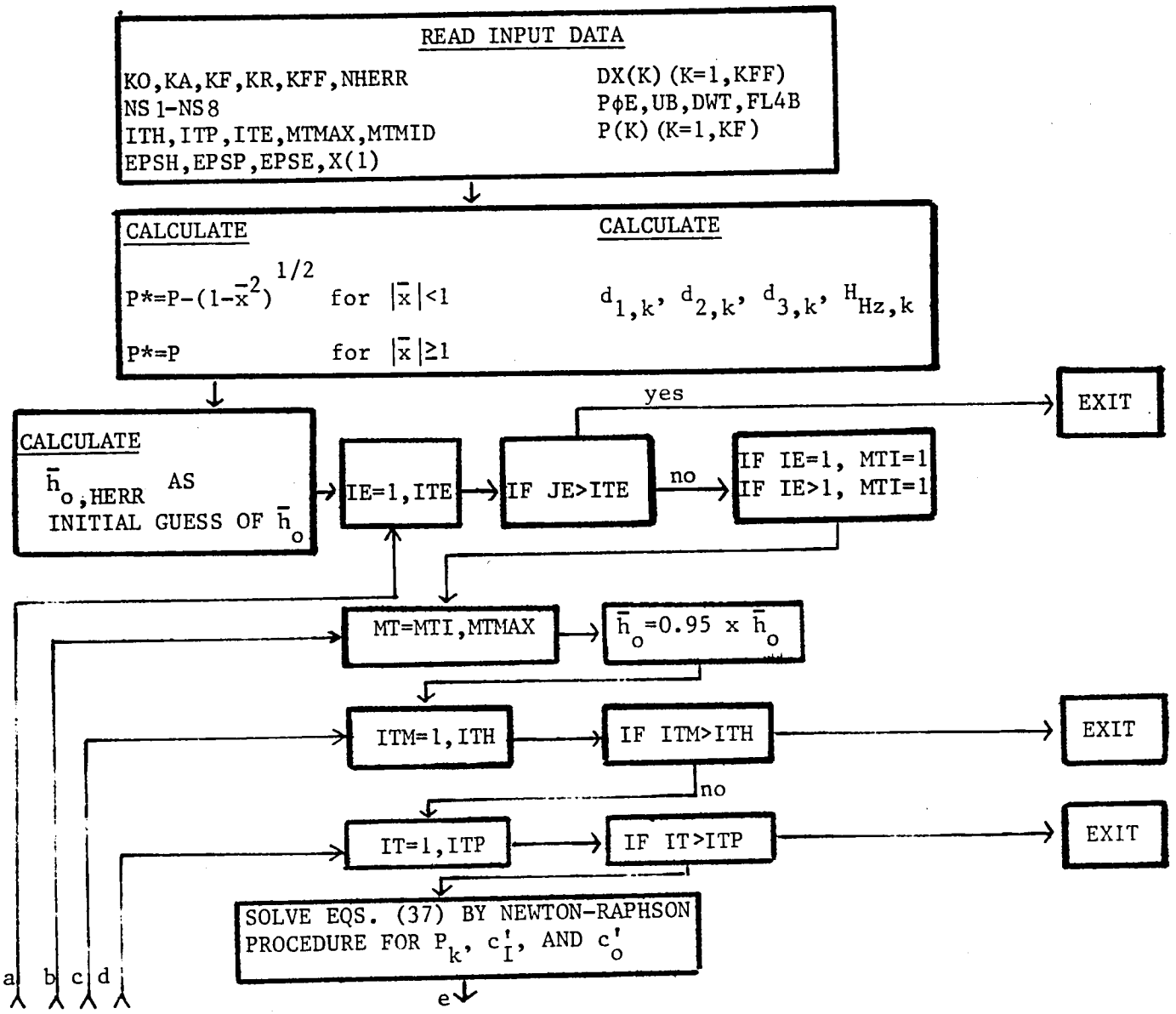

Figure A-1 Flow Diagram for Code "RODSLJ" (Continued on next page)

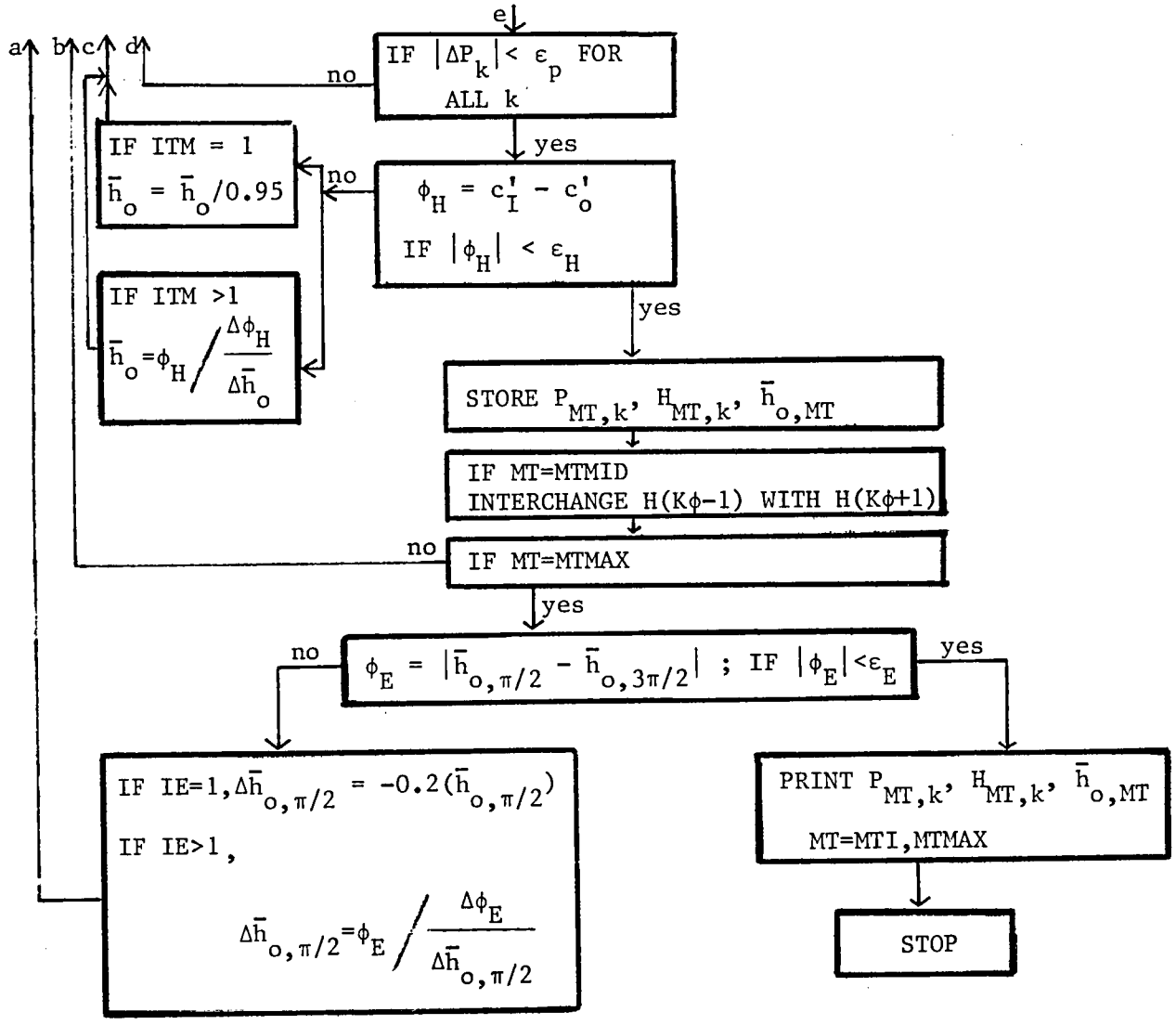

Figure A-1 Flow Diagram for Code "RODSLJ" (Continued from previous page)

Table A-1

List of Major Computer Symbols

Computer Symbol	Symbol in the Analysis
KA	k_A
Kϕ	k_o
KF	k_f
KFF	k_{ff}
DX(K)	$\Delta\bar{x}_k$
X(K)	$\bar{x}_k$
PϕE	p_o/E'
UB	U
WT	ωt
DWT	$\Delta\omega t$
FL4B	S/(4b)
P(K)	P_k
C7	C_7
DT	ΔT
Q(I,J)	$Q_{i,j}$
HϕB	$\bar{h}_o$
H(K)	H_k
CKI	c_I'
CKϕ	c_o'
HL(K)	$H_{k,L}$
HϕBL	$\bar{h}_{o,L}$
SUMS(K,TH,O)	See Eqs. (38) to (41)
MT	Time interval designation
DP(K)	$(P_{k+1} - P_k)/\Delta\bar{x}_k$

Fortran Listings of Code "RODSLJ"

```
      PROGRAM RODSLJ(INPUT,CONSOL,OUTPUT,TAPE5=INPUT,TAPE6=CONSOL,
     1 TAPE7=OUTPUT)
      DIMENSION A(60,60),C(60),WORK(60),HINT(80),SUMTK(80)
      DIMENSION HM(80),HP(80),HM2(80),HP2(80),HM3(80),HP3(80)
      DIMENSION PTEM(80),HTEM(80)
      DIMENSION PSTOR(25,80),HSTOR(25,80), HOBST(25), SUMKFF(25)
      COMMON HOB,HOBA(25),WT,DT,KA,KO,KF,KR,KFF,UB,POE
      COMMON X(80),DX(80),Q(80,80),QJA(80)
      COMMON H(80),HD(80),HS(80),HL(80),HSL(80)
      COMMON P(80),PD(80),PS(80),DP(80),DPS(80),PSAVE(80)
      COMMON FR(80),FS(80),D1(80),D2(80),D3(80)
      COMMON TA(80),TB(80),TC(80),TD(80),TE(80),TF(80),TG(80),TH(80)
      COMMON QQ(80), HZ(80)
C
C          LAST STATEMENT NO. USED, 600
C          LAST KFN USED, KF5
C
C
C                    READ BASIC INPUT DATA
C
C                                          RODSLC  WITHOUT ITERATION OF HOB
      ITMP=50
      MTP=50
      NR=5
      NW=7
      NWOUT=7
      READ(NR,1)
      WRITE(NWOUT,1)
      WRITE(NWOUT,1)
      READ(NR,2)NRUN
      DO 2000 NNR=1,NRUN
      READ(NR,2) KA,KO,KF,KR,KFF,NHERR
      WRITE(NWOUT,2)KA, KO, KF, KR, KFF
      READ(NR,2)NS1,NS2,NS3,NS4,NS5,NS6,NS7,NS8
      WRITE(NWOUT,2)NS1,NS2,NS3,NS4,NS5,NS6,NS7,NS8
      READ(NR,2)ITH,ITP,ITE,MTMAX,MTMID
      WRITE(NWOUT,2)ITH,ITP,ITE,MTMAX,MTMID
      READ(NR,3)EPSH,EPSP,EPSE,X(1)
      WRITE(NWOUT,11)EPSH,EPSP,EPSE
      WRITE(NWOUT,11)EPSH,X(1)
      KKF=KF-1
      READ(NR,3) (DX(K),K=1,KKF)
      DO 100 K=2,KF
  100 X(K)=X(K-1)+DX(K-1)
      WRITE(NWOUT,5)(K,X(K),K=1,KF)
      PI=3.141593
      READ(NR,3)POE,UB,DWT,FL4B
      READ(NR,3)(P(K),K=1,KF)
      WRITE(NWOUT,11)POE,UB,DWT,FL4B
      WRITE(NWOUT,5)(K,P(K),K=1,KF)
      C7=16.0*POE**2/SQRT(48.0*UB)
      DT=DWT*FL4B
```

```
360 C
370 C                          CALCULATE PD(K)
380 C
390         DO 105 K=1,KF
400         PD(K)=0
410         AXK=ABS(X(K))
420         IF(AXK .LT. 1.0) PD(K)=SQRT(1.0-X(K)**2)
430  105   PS(K)=P(K)-PD(K)
440         WRITE(NWOUT,5)(K,PS(K),K=1,KF)
450 C
460 C                              CALCULATE  Q(I,J)
470 C
480         CALL KERCAL
490         IF (NSS .EQ. 0)GO TO 104
500         WRITE(NWOUT,7)
510         DO 106 I=KO,KF
520  106    WRITE(NWOUT,5)(J,Q(I,J),J=KO,KF)
530  104    DO 115 K=2,KKF
540          DXS=DX(K)+DX(K-1)
550         D1(K)=DX(K)/(DX(K-1)*DXS)
560         D2(K)=(DX(K)-DX(K-1))/(DX(K)*DX(K-1))
570         D3(K)=DX(K-1)/(DX(K)*DXS)
580  115    CONTINUE
581         DO 510 K=1,KF
583  510    FS(K)=0.0
585         DO 610 K=1,KF
586         AXK=ABS(X(K))
587         SXK=SQRT(AXK**2-1.0)
588         HZ(K)=0.0
589         IF(AXK .LE. 1.0) GO TO 610
590         HZ(K)=ABS(AXK*SXK)-ALOG(AXK+SXK)
591  610    CONTINUE
630 C
640 C                             CALCULATIE INITIAL HOB
650 C
660         HERR=2.374*UB**0.125/SQRT(48.*POE)/0.8
661         DO 1990 IE=1,ITE
662         MTI=2
663         IF(IE .EQ. 1) MTI=1
664         IF(IE .EQ. 1)HOB=HERR
665         DO 665 MT=MTI,MTMAX
666         FMT=MT
667         WT=(FMT-1.0)*DWT+1.5707963
670 C
680 C                                                START TIME LOOP
690 C
700         SINWT=SIN(WT)
705         SINWT=ABS(SINWT)
710         ITM=1
711         HOB2=HOB
712         HOB1=HOB*0.95
713         KF1=1
714         HOB=HOB1
```

```
720 C
730 C                CALCULATE P(1) TO  P(KA)
740 C
741 122    KFM=KF-1
750        DO 123 K=1,KFM
760  123   PSAVE(K)=P(K)
761        CALL HCAL(1)
766        CALL HCAL(2)
771        IF(NS1 .EQ. 0)GO TO 110
776        WRITE(NWOUT,6)HOB
781        WRITE(NWOUT,5)(K,H(K),K=1,KF)
786  110   CONTINUE
791        DO 120 K=1,KF
796  120   HS(K)=H(K)-HD(K)
800        KKO=KO-1
805        DO 581 K=1,KA
810        HH=(H(K)+H(K+1))*0.5
815        TG(K)=1.0/HH**3
820        FR(K)=(HH-1.)*TG(K)
830  581   CONTINUE
835        IF(MT .EQ. 1) GO TO 585
840        HDH=HOBL/HOB
845        DO 582 K=1,KO
850  582   TH(K)=(H(K)-HDH*HL(K))
870        FS(KO)=0.0
875        DO 583 K=1,KKO
880        KK=KKO-K+1
885  583   FS(KK)=0.5*(TH(KK)+TH(KK+1))*DX(KK)+FS(KK+1)
890 585    CONTINUE
891        P(1)=0.0
892        DO 586 L=2,KA
893        P(L)=P(L-1)+(SINWT*FR(L-1)-(1.0/DT)*(FS(L-1)+FS(L))*0.5
894       1*TG(L-1))*DX(L-1)/HOB**2
895 586    CONTINUE
896  124   IT=1
897        IF(ITM .GT. 1) GO TO 590
898        CKI=0.0
899        CKO=0.0
900 590    CONTINUE
905        IF(MT .EQ. 1) GO TO 372
906        HDH=HOBL/HOB
907        DO 371 K=KO,KF
908  371   TH(K)=(H(K)-HDH*HL(K))
909  372   CONTINUE
910        NNN=KF-KO
911        DO 340 K=1,NNN
912        KK=KF-K
913        TEMP1=0.0
914        IF(MT .EQ. 1) GO TO 373
920        TEMP1=SUMS(KK,TH,1)
922  373   TEMP=(H(KK)-1.0)*SINWT-TEMP1/DT
924        IF(TEMP .GT. 0.0) GO TO 340
926        WRITE(NWOUT,18) KK,H(KK),TEMP1,TEMP
928        KFF=KK+1
930        GO TO 345
932  340   CONTINUE
940 345    CONTINUE
941        DO 417 K=KFF,KF
942 417    P(K)=0.0
```

```
1030 C
1040 C                                          CALCULATE FR(K) AND FS(K)
1050 C
1055 125    CONTINUE
1060  126   KKO=KO-1
1070        DO 130 K=1,KO
1075        HH=(H(K)+H(K+1))*0.5
1080        TG(K)=1.0/HH**3
1090        FR(K)=(HH-1.)*TG(K)
1097  130   CONTINUE
1100        IF(MT .EQ. 1) GO TO 140
1110        HDH=HOBL/HOB
1120        DO 135 K=1,KFF
1121  135   TH(K)=(H(K)-HDH*HL(K))
1131        IF(ITM .LE. ITMP)GOTO 560
1132        IF(MT .NE. MTP)GOTO 560
1133        WRITE(NWOUT,16)
1137        WRITE(NWOUT,5) (K,TH(K),K=1,KFF)
1140 560    FS(KO)=0.0
1150        DO 136 K=1,KKO
1160        KK=KKO-K+1
1170  136   FS(KK)=0.5*(TH(KK)+TH(KK+1))*DX(KK)+FS(KK+1)
1180  140   CONTINUE
1190         IF(NS4 .EQ. 0 ) GO TO 139
1191        IF(MT .EQ. 1) GO TO 139
1200        WRITE(NWOUT,5)(K,FR(K),K=1,KO)
1210        WRITE(NWOUT,5)(K,FS(K),K=1,KO)
1220   139   CONTINUE
1340        IF(NS1 .EQ. 0 ) GO TO 143
1350        WRITE(NWOUT,9)IT, CKI, CKO
1351        IF(NS6. EQ. 0) GO TO 143
1360        WRITE(NWOUT,5)(K,FS(K),K=1,KFF)
1370        WRITE(NWOUT,5)(K,H(K),K=1,KFF)
1380    143 CONTINUE
1390        NN=KFF-KA
1400 C
1410 C                                    A(1,1),A(1,2)
1420 C
1490 C
1500 C                                         C(1)
1510 C
1520 C
1530 C                         C(N),N=1,NN
1540 C
1545        KFM =KFF-1
1560        DO 170 K=1,KFM
1570        HP(K)=(H(K)+H(K+1))*0.5
1580        HP2(K)=HP(K)**2
1590        HP3(K)=HP2(K)*HP(K)
1595        DP(K)=(P(K+1)-P(K))/DX(K)
1605  170   CONTINUE
1610        DO 175 N=1,NN
1620        K=N+KA-1
1621        C(N)=-HOB**2*HP3(K)*DP(K)+SINWT*(HP(K)-1.0)
```

```
1622          IF(K .LT. KO) C(N)=C(N)-CKI
1623          IF(K .GE. KO) C(N)=C(N)-CKO
1637    561   CONTINUE
1640          IF(MT .EQ. 1) GO TO 175
1641          SUMTK(K)=SUMS(K,TH,0)
1650          C(N)=C(N)-1.0/DT*SUMTK(K)
1670    175   CONTINUE
1680  C
1690  C                              A(N,M),N=1,NN,M=1,NN
1700  C
1710          T1=1.5*C7*HOB/PI
1720          T2=HOB**2
1730          T3=C7/PI/HOB
1740          DO 200 N=1,NN
1741          K=N+KA-1
1742          A(N,1)=0.0
1743          A(N,NN)=0.0
1744          IF(K .LT. KO) A(N,1)=1.0
1745          IF(K .GE. KO) A(N,NN)=1.0
1759          NNM=NN-1
1760          DO 200 M=2,NNM
1770          J=M+KA-1
1772          IF(J .GE. KO) J=J+1
1790          DO 505 KQ=1,KFF
1800    505   QQ(KQ)=Q(KQ,J)
1860          A(N,M)=-HP2(K)*DP(K)*(QQ(K+1)+QQ(K))*T1
1870          IF(J .EQ. K+1)A(N,M)=A(N,M)+T2*HP3(K)/DX(K)
1880          IF(J .EQ. K)A(N,M)=A(N,M)-T2*HP3(K)/DX(K)
1890          A(N,M)=A(N,M)+T3*SINWT*0.5*(QQ(K)+QQ(K+1))
1891          IF(NS7 .EQ. 0) GO TO 562
1895          WRITE(NWOUT,17) N,M,A(N,M)
1900     562  IF(MT .EQ. 1)GO TO 200
1910          A(N,M)=A(N,M)-T3*SUMS(K,QQ,0)/DT
1911          IF(NS7 .EQ. 0) GO TO 200
1920          WRITE(NWOUT,17) N,M,A(N,M)
1930    200   CONTINUE
1940     201  IF(NS2 .EQ. 0)GO TO 210
1950          DO 205 KK=1,NN
1960    205   WRITE(NWOUT,5)(JJ,A(KK,JJ),JJ=1,NN)
1970          WRITE(NWOUT,14)
1980          WRITE(NWOUT,5)(KK,C(KK),KK=1,NN)
1990    210   CONTINUE
2000          IDGT=0
2010          CALL LEQT1F(A,1,NN,60,C,IDGT,WORK,IER)
2020          IF(NS1 .EQ. 0)GO TO 220
2021          NNM=NN-1
2030          WRITE(NWOUT,12)
2031          WRITE(NWOUT,11) C(1), C(NN)
2040          WRITE(NWOUT,5)(KK,C(KK),KK=2,NNM)
2050    220   CONTINUE
2060          CV=1.0
2070          CKI=CKI+C(1)
2071          CKO=CKO+C(NN)
2072          NNM=NN-1
```

```
2090          DO225 N=2,NNM
2091          K=N+KA-1
2092          IF(K .GE. KO) K=K+1
2100
2120          DPS(K)=C(N)
2121          IF(DPS(K) .LT. -3.0)GO TO 499
2130          IF(ABS(DPS(K))-EPSP) 222,222,221
2140   221    CV=0.0
2150   222    PS(K)=PS(K)+DPS(K)
2160          P(K)=PD(K)+PS(K)
2180   225    CONTINUE
2220  C
2230  C                                CHECK FOR N-R CONVERGENCE
2240  C
2250          IF(CV .EQ. 1.0) GO TO 240
2260          IF(IT .GT. ITP)GO TO 500
2270  C
2280  C                      N-R NEXT ITERATION
2290  C
2300          IT=IT+1
2310          CALL HCAL(1)
2311          NS2=0
2312          NS4=0
2315          GO TO 125
2320   240    CONTINUE
2340  C
2350  C           N-R CONVERGED, NEXT MAIN INLET ITERATION
2360  C
2390          PHI=CKI-CKO
2400          GO TO(594,595),KF1
2410  594    PF1=PHI
2411          WRITE(NWOUT,21) ITM, HOB, PHI
2420          HOB=HOB2
2430          KF1=2
2450          ITM=ITM+1
2460          GO TO 122
2470  595    PF2=PHI
2490          DPHI=(PF2-PF1)/(HOB2-HOB1)
2500          DHOB=-PHI/DPHI
2510          WRITE(NWOUT,10)ITM, HOB, PHI, DPHI, DHOB, IT
2520          HOB=HOB+DHOB
2530          IF(ABS(PHI) .LT. EPSH) GO TO 460
2540          IF(ITM .GT. ITH) GO TO 495
2541          ITM=ITM+1
2542          HOB1=HOB2
2543          PF1=PF2
2544          HOB2=HOB
2545          GO TO 122
3350   460    CONTINUE
3351          WRITE(NW,8)MT,WT,HOB
3950          WRITE(NWOUT,8)MT,WT,HOB
3951          NWQ=NWOUT
3952          IF(MT .EQ. MTMID) NWQ=NWOUT
3953          IF(MT .EQ. MTMAX) NWQ=NWOUT
```

```
3960          WRITE(NWQ,5)(K,P(K),K=1,KF)
3961          WRITE(NWQ,5)(K,H(K),K=1,KF)
3962          SUMKFF(MT)=SUMTK(KFM)
3965          HOBST(MT)=HOB
3966          DO 465 K=1,KF
3967          PSTOR(MT,K)=P(K)
3968    465   HSTOR(MT,K)=H(K)
3971          IF(NS8 .EQ. 0)GOTO 640
3972          WRITE(NWOUT,5)(K,TH(K),K=1,KFF)
3973          WRITE(NWOUT,5)(K,SUMTK(K),K=KA,KFM)
3974    640   CONTINUE
3990          CALL HCAL(2)
4000          DO 270 K=1,KF
4010          HS(K)=H(K)-HD(K)
4020          HSL(K)=HS(K)
4030          HL(K)=H(K)
4031    270   CONTINUE
4032          HOBL=HOB
4033          GO TO 121
4042  495     IF(KF5 .EQ. 1) GO TO 500
4043          WRITE(NW,26)
4044          NWOUT=6
4051          NS1=1 $NS2=0 $ NS3=1 $NS4=1 $NS6=1
4052          KF5=1
4053          GO TO 122
4054  499     IF(KF5 .EQ. 1) GO TO 500
4055          WRITE(NW,27)
4056          NWOUT=6
4060          NS1=1
4061          NS4=1
4062          KF5=1
4063          GO TO 125
4064    121   IF(MT .GT. 1) GO TO 655
4065          HIN=HOB
4066          DO 650 K=1,KF
4067    650   HINT(K)=H(K)
4068    655   IF(MT .NE. MTMAX) GO TO 660
4069          HLAST=HOB
4070          PHIA=HIN-HLAST
4071     660  IF(MT .NE. MTMID) GO TO 665
4072          DO 666 K=1,KF
4073          PTEM(K)=P(KF+1-K)
4074          HTEM(K)=H(KF+1-K)
4075     666  CONTINUE
4076          DO 667 K=1,KF
4077          P(K)=PTEM(K)
4078     667  HL(K)=HTEM(K)
4079          WRITE(NWOUT,5)(K,HL(K),K=1,KF)
4080     665  CONTINUE
4104          DO 680 K=1,KF
4105    680   HL(K)=H(K)
4106          IF(IE .EQ. 1) GO TO 670
4107          QF2=PHIA
4108          DPHIA=(QF2-QF1)/(HIN2-HIN1)
4109          DHIN=-PHIA/DPHIA
4110          WRITE(NW,22)
4111          WRITE(NW,23) IE,HIN1,HIN2,PHIA,DPHIA,DHIN
4112          QF1=QF2
```

```
4113          HIN1=HIN2
4114          HIN=HIN+DHIN
4115          HIN2=HIN
4116          IF(ABS(DHIN) .LT. EPSE) GO TO 2000
4117          HOBL=HIN
4118          HOB=HIN
4119          GO TO 1990
4120   670    HIN1=HIN
4121          HIN2=HIN/1.25
4122          QF1=PHIA
4123          WRITE(NW,24) IE,HIN,PHIA
4124          HIN=HIN2
4125          HOBL=HIN
4126          HOB=HIN
4127   1990   CONTINUE
4163   500    CONTINUE
4164   2000   CONTINUE
4165          SUMKFF(1)=0.0
4166          DO 2010 MT=1,MTMAX
4167          FMT=MT
4168          WT=(FMT-1.)*DWT+1.5707963
4169          WRITE(NW,25) MT, WT, HOBST(MT), SUMKFF(MT)
4170          WRITE(NW,5)(K, PSTOR(MT,K),K=1,KF)
4171          WRITE(NW,5)(K, HSTOR(MT,K),K=1,KF)
4172   2010   CONTINUE
4175          STOP
4176   1      FORMAT(72H
4177         1                                                    )
4178   2      FORMAT(16I5)
4179   3      FORMAT(7E10.3)
4180   4      FORMAT(/4X,4HPOE=,E12.5,5X,3HUB=,E12.5,5X,4HDWT=,E12.5/)
4181   5      FORMAT(8(1X,I2,E12.5))
4182  6       FORMAT(/4X, 4HH(K), 5X, 5HHD(K), 4HHOB=, E12.5/)
4200   7      FORMAT(/4X,6HQ(I,J)/)
4210   8      FORMAT(/4X,3HMT=,I5,5X,3HWT=,E12.5,5X,4HHOB=,E12.5/)
4220   9      FORMAT(/4X,3HIT=,I5, 4X, 4HCKI=,E12.5, 4X, 4HCKO=, E12.5/)
4230  10      FORMAT(/4X,4HITM=,I5,5X,4HHOB=,E12.5,5X,4HPHI=,E12.5,5X,
4240         1 5HDPHI=,E12.5,5X, 5HDHOB=,E12.5, 3HIT=, I2)
4250   11     FORMAT(8(1X,E12.5))
4260     12   FORMAT(4X,16HDCKI,DCKO,DPS(K)          )
4265   14     FORMAT(2X,5HC(KK))
4270   15     FORMAT(/5X,4HKFF=,I5/)
4273   16     FORMAT(2X,5HTH(K))
4277   17     FORMAT(7(1X,2I2,E12.5))
4278   18     FORMAT(I5,3E12.5)
4279  19      FORMAT(2X, 1HN, 4X,1HM, 4X, 1HK, 4X, 1HJ, 4X, 6HQ(K,J),
4280         17X,8HQ(K+1,J), 5X, 6HA(N,M))
4281  20      FORMAT(4I5, 6(1X,E12.5))
4282  21      FORMAT(/4X,4HITM=,I5,5X,4HHOB=,E12.5,5X,4HPHI=,E12.5    )
4283     22 FORMAT(/4X,2HIE,3X,4HHIN1,9X,4HHIN2,9X,4HPHIA,9X,5HDPHIA,
4284       1 8X,4HDHIN)
4285     23 FORMAT(4X,I5,5(1X,E12.5)/)
4286     24 FORMAT(/4X,3HIE=,I5,3HHIN,E12.5,4HPHIA,E12.5/)
4287     25 FORMAT(/4X, 3HMT=, I5, 5X, 3HWT=, E12.5,5X, 4HHOB=,
4288       1 E12.5, 7HSUMKFF=,E12.5/)
4289     26 FORMAT( 13HITMEXCEEDED    /)
4290     27 FORMAT(13HDPS NEGATIVE      /)
4291        END
```

```
4292        SUBROUTINE KERCAL
4293        COMMON HOB,HOBA(25),WT,DT,KA,KO,KF,KR,KFF,UB,POE
4310        COMMON X(80),DX(80),Q(80,80),QJA(80)
4320        COMMON H(80),HD(80),HS(80),HL(80),HSL(80)
4330        COMMON P(80),PD(80),PS(80),DP(80),DPS(80),PSAVE(80)
4340        COMMON FR(80),FS(80),D1(80),D2(80),D3(80)
4350        COMMON TA(80),TB(80),TC(80),TD(80),TE(80),TF(80),TG(80)
4360        DO 1 I=1, KF
4370        DO 1 J=1, KF
4380      1    Q(I,J)=0.0
4390        KKF=KF-2
4400        DO 8 K=1, KF
4410        Q(K,1)=0.0
4420        F5=X(K)
4430        DO 8 J=1, KKF, 2
4440        U=X (J)-F5
4450        U2=X(J+2)-F5
4460        AU=ABS(U)
4470        AU2= ABS(U2)
4480        IF(AU) 50, 51, 50
4490     50 AU=ALOG(AU)
4500     51 IF(AU2) 52, 6, 52
4510     52 AU2=ALOG(AU2)
4520      6 DJ=X(J+1)-X(J)
4530        F2=3.0*DJ
4540        UQ=U*U
4550        U2Q=U2*U2
4560        FK=UQ*(AU-1.5)*0.5
4570        FK2=U2Q*(AU2-1.5)*0.5
4580        FKB=U*(FK-UQ/6.0)-U2*(FK2-U2Q/6.0)
4590           Q(K,J)= ((-3.0*FK-FK2)/2.0-FKB/F2)/DJ-U*(AU-1.0)+    Q(K,J)
4600           Q(K,J+1)= (2.0*(FK+FK2)+2.0*FKB/F2)/DJ
4610           Q(K,J+2)=((-FK-3.0*FK2)/2.0-FKB/F2)/DJ+U2*(AU2-1.0)
4620      8 CONTINUE
4630        KFF=KF+1
4640        DO 100 J=1,KF
4650    100 Q(KFF,J)=Q(KR,J)
4660        DO 300 K=1, KF
4670        DO 300 J=1, KF
4680    300 Q(K,J)=Q(K,J)-Q(KFF,J)
4690        RETURN
4700        END
```

```
4710        SUBROUTINE HCAL (KFORK)
4720        COMMON HOB,HOBA(25),WT,DT,KA,KO,KF,KR,KFF,UB,POE
4730        COMMON X(80),DX(80),Q(80,80),QJA(80)
4740        COMMON H(80),HD(80),HS(80),HL(80),HSL(80)
4750        COMMON P(80),PD(80),PS(80),DP(80),DPS(80),PSAVE(80)
4760        COMMON FR(80),FS(80),D1(80),D2(80),D3(80)
4770        COMMON TA(80),TB(80),TC(80),TD(80),TE(80),TF(80),TG(80),TH(80)
4771        COMMON QQ(80),HZ(80)
4780        PI=3.141593
4790        C7=16.0*POE**2/SQRT(48.*UB)
4800         C8=C7/HOB
4810        IF(KFORK .EQ. 2) GOTO 20
4820        DO 10 K=1,KF
4821        IF(ABS(X(K)) .LE. 1.00001) GO TO 5
4830        H(K)=0.
4840        DO 1 J=1,KF
4850      1 H(K)=H(K)+(P(J)-PD(J))*Q(K,J)
4860        H(K)=1. +C8*(0.5*HZ(K)-H(K)/PI)
4861        GO TO 10
4862      5 H(K)=0.0
4863        DO 6 J=1,KF
4864      6 H(K)=H(K)+(P(J)-PD(J))*Q(K,J)
4865        H(K)=1.0-C8*H(K)/PI
4866     10 CONTINUE
4870         GO TO 30
4880  20    DO 25 K=1,KF
4890        HD(K)=0.
4900        DO 21 J=1,KF
4910  21    HD(K)=HD(K)+PD(J)*Q(K,J)
4920  25    HD(K)=1.0+C8*(0.5*X(K)**2-HD(K)/PI)
4930  30    RETURN
4940        END
```

```
4950        FUNCTION SUMN(K1,K2,A)
4960        DIMENSION A(80)
4970        COMMON HOB,HOBA(25),WT,DT,KA,KO,KF,KR,KFF,UB,POE
4980        COMMON X(80),DX(80),Q(80,80),QJA(80)
4990        KK2=K2-1
5000        SUM=0.0
5010        DO 10 K=K1,KK2
5020   10   SUM=SUM+DX(K)*A(K)
5030        SUMN=SUM
5040        RETURN
5050        END
5060
```

```
5070        FUNCTION SUMS(K1,A,NEXIT)
5080        DIMENSION A(80)
5090        COMMON HOB,HOBA(25),WT,DT,KA,KO,KF,KR,KFF,UB,POE
5100        COMMON X(80),DX(80),Q(80,80),QJA(80)
5110        KKO=KO-1
5120        KK1=K1+1
5130        KK2=K1-1
5140        IF(K1 .LT. KKO) GO TO 10
5150        IF(K1 .EQ. KKO) GO TO 20
5160        IF(K1 .EQ. KO) GO TO 30
5170        IF(K1 .GT. KO) GO TO 40
5180        SUMS=0.0
5190        RETURN
5200   10   SUM=DX(K1)/4.0*(0.5*A(K1)+1.5*A(K1+1))
5210        DO 100 K=KK1,KKO
5220   100  SUM=SUM+DX(K)/2.0*(A(K)+A(K+1))
5230        SUMS=SUM
5240        RETURN
5250   20   SUMS=DX(K1)/4.0*(0.5*A(K1)+1.5*A(K1+1))
5260        RETURN
5270   30   SUMS=-DX(KO)/4.0*(1.5*A(KO)+0.5*A(KO+1))
5280        RETURN
5290   40   SUM=0.0
5300        DO 200 K=KO,KK2
5310   200  SUM=SUM-DX(K)/2.0*(A(K)+A(K+1))
5315        IF(NEXIT .EQ. 1) GO TO 210
5320        SUM=SUM-DX(K)/4.0*(1.5*A(K1)+0.5*A(K1+1))
5321   210  SUMS=SUM
5330        RETURN
5340        END
```

Input Instructions

Card 1 Format(72H • • •)
Identification card for the run

Card 2 Format(16I5)
NRUN — Number of runs to be made

Card 3 Format(16I5)
KA — k_A, the grid which divides the contact into two regions. For $k < k_A$, the pressure is determined by integrating the Reynold's equation directly [13]. For $k > k_A$, the Newton-Raphson method is used.

Kϕ — k_o, the grid number at the contact center.

KF — k_f, the last grid.

KR — k_R, the grid at which H = 1.

KFF — k_{ff}, the grid at which the film terminates.

NHERR — Not used in RODSLJ, set NHERR = 1.

Card 4 Format(16I5)
NS1 to NS8 — diagnostic controls, set NS1 to NS8 = 0.

Card 5 Format(16I5)
ITH — Maximum iterations allowed for ITM. Recommended ITH = 15.

ITP — Maximum iterations allowed for IT. Recommended ITP = 25.

ITE — Maximum iterations allowed for IE. Recommended ITE = 4.

MTMAX — (MTMAX-1) represents the total number of time intervals within half of the reciprocating cycle.

MTMID — The time step MT corresponding to $\omega t=\pi$, or the end-stroke position.

Card 6 Format(7E10.3)
EPSH — Maximum error allowed for ϕ_H, ($\phi_H=|c_I' - c_o'|$). Recommended EPSH = 0.0005.

EPSP — Maximum error allowed for ΔP_k. Recommended EPSP = 0.0005.

EPSE — Maximum error allowed for ϕ_E, ($\phi_E=|\bar{h}_{o,\pi} - \bar{h}_{o,3\pi/2}|$). Recommended EPSE = 0.005.

X(1) — The $\bar{x}$ coordinate for the first grid.

Card 7 Format(7E10.3)
DX(K)(K=1,(KF-1))— A set of cards for $\Delta\bar{x}_k = \bar{x}_{k+1} - \bar{x}_k$.

Card 8 Format(7E10.3)
PϕE — p_o/E'

UB — $\frac{\mu_o u_o}{E'R}$

DWT — $\Delta\omega t$ (radians)

FL4B — S/4b

Card 9 Format(7E10.3)
P(K)(K=1,KF)— A set of cards for the intitial guess of pressure profile P_k.

Sample Input Data

The following is a set of sample input data for run 51 listed in Table 2.

```
10 RODA 30
20      1
30      3    21    41    21    32     1
40      0     0     0     0     0     0     0     0
50     15    25     4    19    10
60         .0005       .0005        .005     -1.5
70           0.2         0.2         0.03      0.03      0.01      0.01      0.01
80          0.01        0.01         0.01      0.01      0.01      0.02      0.02
90          0.06        0.06          0.2       0.2       0.2       0.2       0.2
100          0.2         0.2          0.2      0.06      0.06      0.02      0.02
110         0.01        0.01         0.01      0.01      0.01      0.01      0.01
120         0.01        0.03         0.03       0.2       0.2
130         0.10    5.00E-07     .1745327      5.00
140          0.0         0.0          0.0       0.0      0.01       .02       .035
150         .055         .09         .1410      .200      .2431       .28      .3411
160         .3919       .5102          0.6       0.8      .9165      .9797       1.0
170         .9797       .9165          0.8       0.6      .5102      .3919      .3411
180         0.275       0.235         0.18      0.10     0.035        0.0        0.0
190          0.0         0.0          0.0       0.0       0.0        0.0
```

Sample Output Data

A sample of output data based on the input data for Run 51 is included. The first part lists the values of $\bar{h}_o$ for different stroke positions for each iteration IE. For this sample run, the IE loop converges after three iterations. Thus, results of $\bar{h}_o$ for IE = 3 are taken to be the final solution for Run 51. In the second part of the output, there are two arrays of data listed under each stroke position ωt. The first array is the pressure profile, and it is followed by the film thickness profile.

The value listed as SUMKFF represents SUMS(KFF,TH,O) which can be used in the future for calculating the leakage rate at each stroke position.

WT= .15708E+01 HOB= .22225E+00

WT= .17453E+01 HOB= .22136E+00

WT= .19199E+01 HOB= .21965E+00

WT= .20944E+01 HOB= .21360E+00

WT= .22689E+01 HOB= .20479E+00

WT= .24435E+01 HOB= .19579E+00

WT= .26180E+01 HOB= .18469E+00

WT= .27925E+01 HOB= .17439E+00

WT= .29671E+01 HOB= .16704E+00

WT= .31416E+01 HOB= .16331E+00

WT= .33161E+01 HOB= .16118E+00

WT= .34907E+01 HOB= .15442E+00

WT= .36652E+01 HOB= .14173E+00

WT= .38397E+01 HOB= .13967E+00

WT= .40143E+01 HOB= .15446E+00

WT= .41888E+01 HOB= .17601E+00

WT= .43633E+01 HOB= .19485E+00

WT= .45379E+01 HOB= .20817E+00

WT= .47124E+01 HOB= .21591E+00

WT= .17453E+01 HOB= .21902E+00

WT= .19199E+01 HOB= .21828E+00

WT= .20944E+01 HOB= .21348E+00

WT= .22689E+01 HOB= .20572E+00

WT= .24435E+01 HOB= .19572E+00

WT= .26180E+01 HOB= .18465E+00

WT= .27925E+01 HOB= .17436E+00

WT= .29671E+01 HOB= .16702E+00

WT= .31416E+01 HOB= .16329E+00

WT= .33161E+01 HOB= .16116E+00

WT= .34907E+01 HOB= .15440E+00

WT= .36652E+01 HOB= .14171E+00

WT= .38397E+01 HOB= .13966E+00

WT= .40143E+01 HOB= .15446E+00

WT= .41888E+01 HOB= .17601E+00

WT= .43633E+01 HOB= .19485E+00

WT= .45379E+01 HOB= .20817E+00

WT= .47124E+01 HOB= .21591E+00

HEAD PHIA DPHIA DHIN

.21591E+00 .35670E-07 .99999E+00 .35671E-07

WT= .17453E+01 HOB= .19258E+00

WT= .19199E+01 HOB= .20439E+00

WT= .20944E+01 HOB= .20760E+00

WT= .22689E+01 HOB= .20356E+00

WT= .24435E+01 HOB= .19477E+00

WT= .26180E+01 HOB= .18412E+00

WT= .27925E+01 HOB= .17401E+00

WT= .29671E+01 HOB= .16675E+00

WT= .31416E+01 HOB= .16303E+00

WT= .33161E+01 HOB= .16087E+00

WT= .34907E+01 HOB= .15404E+00

WT= .36652E+01 HOB= .14138E+00

WT= .38397E+01 HOB= .13947E+00

WT= .40143E+01 HOB= .15438E+00

WT= .41888E+01 HOB= .17599E+00

WT= .43633E+01 HOB= .19485E+00

WT= .45379E+01 HOB= .20817E+00

WT= .47124E+01 HOB= .21591E+00

HDIF2 FILL DFHIA DHIN

.17780E+00 -.38108E-01 .99999E+00 .38108E-01

MT= 1 WT= .15708E+01 HOB= .22225E+00SUMKFF= 0.

1	0.	2	.25333E-02	3	.17787E-01	4	.34373E-01	5	.63862E-01	6	.70476E-01	7	.95872E-01	8	.11622E+00
9	.13[illegible]E+00	10	.16535E+00	11	.19346E+00	12	.22295E+00	13	.25289E+00	14	.31150E+00	15	.36498E+00	16	.49[illegible]E+00
17	.59[illegible]E+00	18	.79789E+00	19	.91541E+00	20	.97962E+00	21	.10000E+01	22	.98024E+00	23	.91700E+00	24	.80698E+00
25	.69[illegible]E+00	26	.51197E+00	27	.39566E+00	28	.34846E+00	29	.28673E+00	30	.24332E+00	31	.18154E+00	32	.98405E-01
33	.17[illegible]E-01	34	-.13671E-01	35	0.	36	0.	37	0.	38	0.	39	0.	40	0.
41	0.														
1	.55[illegible]E+02	2	.25248E+02	3	.63380E+01	4	.45935E+01	5	.32293E+01	6	.28640E+01	7	.25448E+01	8	.22714E+01
9	.20[illegible]E+01	10	.18452E+01	11	.16794E+01	12	.15524E+01	13	.14517E+01	14	.13111E+01	15	.12260E+01	16	.11242E+01
17	.10[illegible]E+01	18	.10394E+01	19	.10219E+01	20	.10106E+01	21	.10000E+01	22	.99234E+00	23	.98058E+00	24	.97061E+00
25	.96[illegible]E+00	26	.93139E+00	27	.91896E+00	28	.90893E+00	29	.87929E+00	30	.85008E+00	31	.80883E+00	32	.78399E+00
33	.83[illegible]E+00	34	.97593E+00	35	.12232E+01	36	.15632E+01	37	.19603E+01	38	.34454E+01	39	.53017E+01	40	.24610E+02
41	.5[illegible]E+02														

MT= 2 WT= .17453E+01 HOB= .21902E+00SUMKFF= -.23305E-01

1	0.	2	.24907E-02	3	.17498E-01	4	.33957E-01	5	.63315E-01	6	.77906E-01	7	.95298E-01	8	.11567E+00
9	.13[illegible]E+00	10	.16492E+00	11	.19313E+00	12	.22272E+00	13	.25277E+00	14	.31152E+00	15	.36508E+00	16	.49749E+00
17	.59[illegible]E+00	18	.79793E+00	19	.91544E+00	20	.97964E+00	21	.10000E+01	22	.98019E+00	23	.91693E+00	24	.80080E+00
25	.68[illegible]E+00	26	.51163E+00	27	.39483E+00	28	.34761E+00	29	.28691E+00	30	.24451E+00	31	.18336E+00	32	.98924E-01
33	.16[illegible]E-01	34	.16492E-01	35	0.	36	0.	37	0.	38	0.	39	0.	40	0.
41	0.														
1	.56[illegible]E+02	2	.25609E+02	3	.64175E+01	4	.46472E+01	5	.32632E+01	6	.28929E+01	7	.25693E+01	8	.22934E+01
9	.20[illegible]E+01	10	.18614E+01	11	.16939E+01	12	.15659E+01	13	.14645E+01	14	.13231E+01	15	.12376E+01	16	.11355E+01
17	.10[illegible]E+01	18	.10492E+01	19	.10283E+01	20	.10155E+01	21	.10000E+01	22	.98824E+00	23	.97226E+00	24	.95658E+00
25	.93[illegible]E+00	26	.91549E+00	27	.89896E+00	28	.88998E+00	29	.86332E+00	30	.83552E+00	31	.79412E+00	32	.76657E+00
33	.82[illegible]E+00	34	.93546E+00	35	.12091E+01	36	.15555E+01	37	.19592E+01	38	.34678E+01	39	.53526E+01	40	.24952E+02
41	.5[illegible]E+02														

MT= 3 WT= .19199E+01 HOB= .21828E+00SUMKFF= -.57953E-02

1	0.	2	.23767E-02	3	.16738E-01	4	.32802E-01	5	.61714E-01	6	.76202E-01	7	.93543E-01	8	.11394E+00
9	.13[illegible]E+00	10	.16347E+00	11	.19193E+00	12	.22180E+00	13	.25212E+00	14	.31131E+00	15	.36509E+00	16	.49754E+00
17	.59[illegible]E+00	18	.79789E+00	19	.91541E+00	20	.97962E+00	21	.10000E+01	22	.98021E+00	23	.91695E+00	24	.80087E+00
25	.68[illegible]E+00	26	.51172E+00	27	.39523E+00	28	.34796E+00	29	.28638E+00	30	.24313E+00	31	.18135E+00	32	.97685E-01
33	.16[illegible]E-01	34	-.14241E-01	35	0.	36	0.	37	0.	38	0.	39	0.	40	0.
41	0.														
1	.53[illegible]E+02	2	.25665E+02	3	.63907E+01	4	.46110E+01	5	.32197E+01	6	.28476E+01	7	.25229E+01	8	.22455E+01
9	.20[illegible]E+01	10	.18151E+01	11	.16488E+01	12	.15222E+01	13	.14225E+01	14	.12846E+01	15	.12022E+01	16	.11065E+01
17	.10[illegible]E+01	18	.10323E+01	19	.10181E+01	20	.10094E+01	21	.10000E+01	22	.99236E+00	23	.97988E+00	24	.96785E+00
25	.94[illegible]E+00	26	.92937E+00	27	.91333E+00	28	.90318E+00	29	.87371E+00	30	.84436E+00	31	.80245E+00	32	.77486E+00
33	.81[illegible]E+00	34	.95303E+00	35	.12266E+01	36	.15737E+01	37	.19786E+01	38	.34923E+01	39	.53835E+01	40	.25047E+02
41	.5[illegible]E+02														

MT= 4 WT= .20944E+01 HOB= .21348E+00SUMKFF= .13941E-01

1	[illegible]	2	.22037E-02	3	.13656E-01	4	.31065E-01	5	.59242E-01	6	.73569E-01	7	.90843E-01	8	[illegible]				
9	[illegible]	10	.16139E+00	11	.19032E+00	12	.22070E+00	13	.25151E+00	14	.31142E+00	15	.36552E+00	16	[illegible]				
17	[illegible]	18	.29793E+00	19	.91542E+00	20	.97966E+00	21	.10000E+01	22	.98028E+00	23	.91701E+00	24	.80099E+00				
25	[illegible]	26	.51190E+00	27	.39562E+00	28	.34828E+00	29	.28613E+00	30	.24240E+00	31	.18034E+00	32	.97306E-01				
33	[illegible]	34	-.12403E-01	35	0.	36	0.	37	0.	38	0.	39	0.	40	0.				
41	0																		
1	[illegible]	2	.26193E+02	3	.64534E+01	4	.46293E+01	5	.32042E+01	6	.28239E+01	7	.24927E+01	8	.22105E+01				
9	[illegible]	10	.17757E+01	11	.16092E+01	12	.14836E+01	13	.13854E+01	14	.12514E+01	15	.11724E+01	16	.10834E+01				
17	[illegible]	18	.10184E+01	19	.10096E+01	20	.10047E+01	21	.10000E+01	22	.99648E+00	23	.98718E+00	24	.97843E+00				
25	[illegible]	26	.94173E+00	27	.92553E+00	28	.91445E+00	29	.88251E+00	30	.85165E+00	31	.80873E+00	32	.78411E+00				
33	[illegible]	34	.96873E+00	35	.12475E+01	36	.16019E+01	37	.20159E+01	38	.35639E+01	39	.54983E+01	40	.25612E+02				
41	[illegible]																		

MT= 5 WT= .22689E+01 HOB= .20572E+00SUMKFF= .27556E-01

1	[illegible]	2	.19253E-02	3	.13704E-01	4	.28138E-01	5	.55193E-01	6	.69271E-01	7	.86442E-01	8	.10700E+00				
9	.13093E+00	10	.15802E+00	11	.18771E+00	12	.21891E+00	13	.25049E+00	14	.31153E+00	15	.36610E+00	16	.49835E+00				
17	[illegible]	18	.79791E+00	19	.91546E+00	20	.97959E+00	21	.10000E+01	22	.98026E+00	23	.91697E+00	24	.80099E+00				
25	[illegible]	26	.51187E+00	27	.39568E+00	28	.34820E+00	29	.28558E+00	30	.24148E+00	31	.17913E+00	32	.96353E-01				
33	.29087E-01	34	-.11046E-01	35	0.	36	0.	37	0.	38	0.	39	0.	40	0.				
41	0																		
1	[illegible]	2	.27074E+02	3	.65679E+01	4	.46699E+01	5	.31879E+01	6	.27935E+01	7	.24510E+01	8	.21606E+01				
9	[illegible]	10	.17176E+01	11	.15502E+01	12	.14258E+01	13	.13299E+01	14	.12016E+01	15	.11279E+01	16	.10496E+01				
17	[illegible]	18	.10008E+01	19	.99895E+00	20	.10001E+01	21	.10000E+01	22	.10012E+01	23	.99547E+00	24	.99025E+00				
25	[illegible]	26	.95525E+00	27	.93874E+00	28	.92673E+00	29	.89258E+00	30	.86015E+00	31	.81573E+00	32	.79140E+00				
33	[illegible]	34	.98700E+00	35	.12747E+01	36	.16415E+01	37	.20705E+01	38	.36755E+01	39	.56814E+01	40	.26541E+02				
41	[illegible]																		

MT= 6 WT= .24435E+01 HOB= .19572E+00SUMKFF= .40094E-01

1	[illegible]	2	.16180E-02	3	.11649E-01	4	.24729E-01	5	.50108E-01	6	.63765E-01	7	.80714E-01	8	.10135E+00				
9	.25725E+00	10	.15360E+00	11	.18439E+00	12	.21678E+00	13	.24943E+00	14	.31200E+00	15	.36715E+00	16	.49904E+00				
17	[illegible]	18	.79803E+00	19	.91549E+00	20	.97967E+00	21	.10000E+01	22	.98032E+00	23	.91700E+00	24	.80107E+00				
25	[illegible]	26	.51196E+00	27	.39585E+00	28	.34820E+00	29	.28510E+00	30	.24065E+00	31	.17809E+00	32	.95703E-01				
33	[illegible]	34	-.92613E-02	35	0.	36	0.	37	0.	38	0.	39	0.	40	0.				
41	0																		
1	[illegible]	2	.28348E+02	3	.67365E+01	4	.47312E+01	5	.31659E+01	6	.27507E+01	7	.23916E+01	8	.20890E+01				
9	[illegible]	10	.16343E+01	11	.14662E+01	12	.13439E+01	13	.12516E+01	14	.11321E+01	15	.10659E+01	16	.10021E+01				
17	[illegible]	18	.97674E+00	19	.98442E+00	20	.99453E+00	21	.10000E+01	22	.10072E+01	23	.10056E+01	24	.10045E+01				
25	[illegible]	26	.97064E+00	27	[illegible]	28	.93985E+00	29	.90259E+00	30	.86809E+00	31	.82172E+00	32	.79774E+00				
33	[illegible]	34	.10071E+01	35	[illegible]	36	.16937E+01	37	.21446E+01	38	.38323E+01	39	.59416E+01	40	[illegible]				
41	[illegible]																		

MT= 7 WT= .26180E+01 HOB= .18465E+00SUMKFF= .48946E-01

1	[illegible]	2	.12461E-02	3	.92645E-02	4	.20495E-01	5	.43369E-01	6	.56304E-01	7	.72789E-01	8	.93398E-01
9	[illegible]	10	.14732E+00	11	.17970E+00	12	.21383E+00	13	.24805E+00	14	.31269E+00	15	.36856E+00	16	.49977E+00
17	[illegible]	18	.79817E+00	19	.91554E+00	20	.97977E+00	21	.10000E+01	22	.98038E+00	23	.91701E+00	24	.80113E+00
25	[illegible]	26	.51197E+00	27	.39597E+00	28	.34798E+00	29	.28399E+00	30	.23890E+00	31	.17591E+00	32	.94201E-01
33	[illegible]	34	-.67663E-02	35	0.	36	0.	37	0.	38	0.	39	0.	40	0.
41	[illegible]														
1	[illegible]	2	.29913E+02	3	.69273E+01	4	.47858E+01	5	.31133E+01	6	.26713E+01	7	.22910E+01	8	.19732E+01
9	[illegible]	10	.15062E+01	11	.13390E+01	12	.12217E+01	13	.11361E+01	14	.10309E+01	15	.97637E+00	16	.93287E+00
17	[illegible]	18	.94312E+00	19	.96478E+00	20	.98713E+00	21	.10000E+01	22	.10145E+01	23	.10177E+01	24	.10209E+01
25	[illegible]	26	.98685E+00	27	.96774E+00	28	.95176E+00	29	.90966E+00	30	.87212E+00	31	.82324E+00	32	.80081E+00
33	[illegible]	34	.10324E+01	35	.13506E+01	36	.17582E+01	37	.22363E+01	38	.40265E+01	39	.62642E+01	40	.29532E+02
41	[illegible]														

MT= 8 WT= .27925E+01 HOB= .17436E+00SUMKFF= .51364E-01

1	[illegible]	2	.87684E-03	3	.65641E-02	4	.15280E-01	5	.34306E-01	6	.45920E-01	7	.61383E-01	8	.81608E-01
9	[illegible]	10	.13771E+00	11	.17261E+00	12	.20949E+00	13	.24607E+00	14	.31358E+00	15	.37042E+00	16	.50036E+00
17	[illegible]	18	.79834E+00	19	.91565E+00	20	.97983E+00	21	.10000E+01	22	.98037E+00	23	.91691E+00	24	.80108E+00
25	[illegible]	26	.51181E+00	27	.39589E+00	28	.34715E+00	29	.28135E+00	30	.23495E+00	31	.17112E+00	32	.90937E-01
33	[illegible]	34	-.30973E-02	35	0.	36	0.	37	0.	38	0.	39	0.	40	0.
41	[illegible]														
1	[illegible]	2	.31508E+02	3	.70720E+01	4	.47803E+01	5	.29861E+01	6	.25132E+01	7	.21089E+01	8	.17750E+01
9	[illegible]	10	.13006E+01	11	.11400E+01	12	.10342E+01	13	.96184E+00	14	.88176E+00	15	.84607E+00	16	.83299E+00
17	[illegible]	18	.89998E+00	19	.94150E+00	20	.97791E+00	21	.10000E+01	22	.10217E+01	23	.10288E+01	24	.10355E+01
25	[illegible]	26	.99752E+00	27	.97403E+00	28	.95281E+00	29	.90233E+00	30	.86068E+00	31	.81002E+00	32	.79269E+00
33	[illegible]	34	.10551E+01	35	.13913E+01	36	.18231E+01	37	.23302E+01	38	.42288E+01	39	.66010E+01	40	.31253E+02
41	[illegible]														

MT= 9 WT= .29671E+01 HOB= .16702E+00SUMKFF= .48080E-01

1	[illegible]	2	.45541E-03	3	.35265E-02	4	.88070E-02	5	.21649E-01	6	.30598E-01	7	.43558E-01	8	.62169E-01
9	[illegible]	10	.12107E+00	11	.16077E+00	12	.20291E+00	13	.24369E+00	14	.31540E+00	15	.37382E+00	16	.50175E+00
17	[illegible]	18	.79879E+00	19	.91592E+00	20	.97983E+00	21	.10000E+01	22	.98026E+00	23	.91672E+00	24	.80090E+00
25	[illegible]	26	.51163E+00	27	.39552E+00	28	.34521E+00	29	.27656E+00	30	.22842E+00	31	.16408E+00	32	.87043E-01
33	[illegible]	34	-.13270E-02	35	-.44577E-02	36	0.	37	0.	38	0.	39	0.	40	0.
41	[illegible]														
1	[illegible]	2	.32695E+02	3	.70684E+01	4	.46389E+01	5	.27245E+01	6	.22199E+01	7	.17912E+01	8	.14430E+01
9	[illegible]	10	.97742E+00	11	.83838E+00	12	.76028E+00	13	.71619E+00	14	.68451E+00	15	.68363E+00	16	.72390E+00
17	[illegible]	18	.86769E+00	19	.92606E+00	20	.97127E+00	21	.10000E+01	22	.10246E+01	23	.10323E+01	24	.10385E+01
25	[illegible]	26	.98952E+00	27	.95475E+00	28	.92350E+00	29	.86050E+00	30	.81434E+00	31	.76389E+00	32	.75527E+00
33	[illegible]	34	.10477E+01	35	.13980E+01	36	.18546E+01	37	.23880E+01	38	.43771E+01	39	.68585E+01	40	.32604E+02
41	[illegible]														

MT= 10 WT= .31416E+01 HOB= .16329E+00SUMKFF= .42561E-01

		2	.58496E-05	3	.10985E-03	4	.61054E-03	5	.26038E-02	6	.50123E-02	7	.99954E-02	8	.20943E-01
9	33933E-01	10	.88138E-01	11	.14990E+00	12	.21019E+00	13	.25936E+00	14	.33192E+00	15	.38624E+00	16	.50713E+00
17	[illegible]	18	.79937E+00	19	.91614E+00	20	.97980E+00	21	.10000E+01	22	.98007E+00	23	.91660E+00	24	.80056E+00
25	60035E+00	26	.51176E+00	27	.39255E+00	28	.33693E+00	29	.26015E+00	30	.20804E+00	31	.14546E+00	32	.83261E-01
33	.49265E-01	34	.17989E-01	35	.90616E-02	36	.37814E-02	37	.18259E-02	38	.37005E-03	39	.51213E-04	40	.24407E-05
41															
1	.24426E+02	2	.33272E+02	3	.69053E+01	4	.43652E+01	5	.23353E+01	6	.17957E+01	7	.13393E+01	8	.98041E+00
9	.24209E+00	10	.59241E+00	11	.54258E+00	12	.55458E+00	13	.58024E+00	14	.63027E+00	15	.66558E+00	16	.73006E+00
17	.77635E+00	18	.87155E+00	19	.92913E+00	20	.97231E+00	21	.10000E+01	22	.10199E+01	23	.10236E+01	24	.10190E+01
25	.97255E+00	26	.94459E+00	27	.86909E+00	28	.81336E+00	29	.73116E+00	30	.68804E+00	31	.66139E+00	32	.70182E+00
33	.84985E+00	34	.10839E+01	35	.14426E+01	36	.18992E+01	37	.24387E+01	38	.44673E+01	39	.70050E+01	40	.33353E+02
41	.[illegible]														

MT= 11 WT= .33161E+01 HOB= .16116E+00SUMKFF= -.19066E-01

		2	.45178E-03	3	.34576E-02	4	.83580E-02	5	.20175E-01	6	.28388E-01	7	.40340E-01	8	.57680E-01
9	82035E-01	10	.11439E+00	11	.15378E+00	12	.19609E+00	13	.23729E+00	14	.31081E+00	15	.37059E+00	16	.50122E+00
17	[illegible]	18	.79999E+00	19	.91657E+00	20	.97997E+00	21	.10000E+01	22	.97982E+00	23	.91610E+00	24	.79941E+00
25	.[illegible]	26	.50838E+00	27	.38917E+00	28	.33963E+00	29	.27716E+00	30	.23445E+00	31	.17122E+00	32	.80176E-01
33	55176E-02	34	-.10609E-01	35	0.	36	0.	37	0.	38	0.	39	0.	40	0.
41															
1	.23511E+02	2	.33891E+02	3	.72946E+01	4	.47637E+01	5	.27611E+01	6	.22305E+01	7	.17778E+01	8	.14087E+01
9	.11342E+01	10	.91364E+00	11	.76730E+00	12	.68709E+00	13	.64473E+00	14	.62455E+00	15	.63928E+00	16	.73299E+00
17	.93383E+00	18	.95557E+00	19	.99416E+00	20	.10065E+01	21	.10000E+01	22	.98282E+00	23	.94915E+00	24	.90666E+00
25	.92862E+00	26	.79506E+00	27	.75049E+00	28	.73014E+00	29	.69148E+00	30	.65550E+00	31	.60115E+00	32	.57074E+00
33	.64358E+00	34	.87478E+00	35	.12637E+01	36	.17471E+01	37	.23079E+01	38	.43884E+01	39	.69740E+01	40	.33710E+02
41	.[illegible]														

MT= 12 WT= .34907E+01 HOB= .15440E+00SUMKFF= -.18799E-01

1		2	.82563E-03	3	.65525E-02	4	.15126E-01	5	.33943E-01	6	.45508E-01	7	.60982E-01	8	.81330E-01
9	10703E+00	10	.13818E+00	11	.17350E+00	12	.21056E+00	13	.24700E+00	14	.31377E+00	15	.36773E+00	16	.49843E+00
17	[illegible]	18	.79746E+00	19	.91550E+00	20	.97977E+00	21	.10000E+01	22	.98011E+00	23	.91637E+00	24	.80009E+00
25	[illegible]	26	.50942E+00	27	.39048E+00	28	.34176E+00	29	.28143E+00	30	.24003E+00	31	.17694E+00	32	.84041E-01
33	.[illegible]	34	0.	35	0.	36	0.	37	0.	38	0.	39	0.	40	0.
41															
1	.[illegible]	2	.35494E+02	3	.78826E+01	4	.52891E+01	5	.32567E+01	6	.27207E+01	7	.22622E+01	8	.18838E+01
9	15932E+01	10	.13456E+01	11	.11627E+01	12	.10404E+01	13	.95450E+00	14	.85160E+00	15	.79437E+00	16	.75457E+00
17	[illegible]	18	.81365E+00	19	.92469E+00	20	.97657E+00	21	.10000E+01	22	.10085E+01	23	.99336E+00	24	.97127E+00
25	[illegible]	26	.89284E+00	27	.86039E+00	28	.84739E+00	29	.81767E+00	30	.78406E+00	31	.72762E+00	32	.69297E+00
33	[illegible]	34	.10106E+01	35	.13983E+01	36	.18902E+01	37	.24673E+01	38	.46224E+01	39	.73098E+01	40	.35177E+02
41	.[illegible]														

MT= 13 WT= .36652E+01 HOB= .14171E+00SUMKFF= .24493E-01

		2	.13072E-02	3	.97123E-02	4	.21174E-01	5	.44705E-01	6	.58088E-01	7	.75172E-01	8	.96532E-01
		10	.15219E+00	11	.18528E+00	12	.21977E+00	13	.25398E+00	14	.31780E+00	15	.37159E+00	16	.50313E+00
		18	.79723E+00	19	.91476E+00	20	.97946E+00	21	.10000E+01	22	.98060E+00	23	.91718E+00	24	.80132E+00
		26	.51200E+00	27	.39370E+00	28	.34525E+00	29	.28723E+00	30	.24862E+00	31	.18967E+00	32	.99349E-01
		34 0.		35 0.		36 0.		37 0.		38 0.		39 0.		40 0.	
		2	.38710E+02	3	.88301E+01	4	.60552E+01	5	.38954E+01	6	.33270E+01	7	.28395E+01	8	.24338E+01
		10	.18406E+01	11	.14283E+01	12	.14787E+01	13	.13679E+01	14	.12253E+01	15	.11428E+01	16	.10516E+01
		18	.91983E+00	19	.93032E+00	20	.96811E+00	21	.10000E+01	22	.10314E+01	23	.10396E+01	24	.10437E+01
		26	.10007E+01	27	.97621E+00	28	.96748E+00	29	.94610E+00	30	.91670E+00	31	.86064E+00	32	.81683E+00
		34	.11067E+01	35	.15110E+01	36	.20336E+01	37	.26511E+01	38	.49722E+01	39	.78795E+01	40	.38157E+02

MT= 14 WT= .38397E+01 HOB= .13966E+00SUMKFF= .26756E-01

		2	.16643E-02	3	.12167E-01	4	.25783E-01	5	.52401E-01	6	.66772E-01	7	.84592E-01	8	.10623E+00
		10	.16052E+00	11	.19207E+00	12	.22489E+00	13	.25763E+00	14	.31965E+00	15	.37352E+00	16	.50415E+00
		18	.79906E+00	19	.91561E+00	20	.97972E+00	21	.10000E+01	22	.98060E+00	23	.91736E+00	24	.80176E+00
		26	.51347E+00	27	.39560E+00	28	.34669E+00	29	.29028E+00	30	.25447E+00	31	.19949E+00	32	.11072E+00
		34 0.		35 0.		36 0.		37 0.		38 0.		39 0.		40 0.	
		2	.39331E+02	3	.91756E+01	4	.63958E+01	5	.42391E+01	6	.36710E+01	7	.31821E+01	8	.27725E+01
		10	.21621E+01	11	.19373E+01	12	.17744E+01	13	.16508E+01	14	.14876E+01	15	.13922E+01	16	.12808E+01
		18	.11008E+01	19	.10369E+01	20	.10113E+01	21	.10000E+01	22	.10091E+01	23	.10118E+01	24	.10223E+01
		26	.10049E+01	27	.98770E+00	28	.98187E+00	29	.97028E+00	30	.94867E+00	31	.89882E+00	32	.85079E+00
		34	.11046E+01	35	.15025E+01	36	.20236E+01	37	.26422E+01	38	.49785E+01	39	.79132E+01	40	.38564E+02

MT= 15 WT= .40143E+01 HOB= .15446E+00SUMKFF= -.34718E-01

		2	.19759E-02	3	.14278E-01	4	.29205E-01	5	.57331E-01	6	.71991E-01	7	.89853E-01	8	.11119E+00
		10	.16374E+00	11	.19402E+00	12	.22558E+00	13	.25727E+00	14	.31802E+00	15	.37177E+00	16	.50271E+00
		18	.79958E+00	19	.91615E+00	20	.98002E+00	21	.10000E+01	22	.98027E+00	23	.91692E+00	24	.80108E+00
		26	.51270E+00	27	.39476E+00	28	.34522E+00	29	.28905E+00	30	.25430E+00	31	.20023E+00	32	.10982E+00
		34 0.		35 0.		36 0.		37 0.		38 0.		39 0.		40 0.	
		2	.35782E+02	3	.85545E+01	4	.60491E+01	5	.41031E+01	6	.35881E+01	7	.31427E+01	8	.27668E+01
		10	.21970E+01	11	.17825E+01	12	.18236E+01	13	.17009E+01	14	.15353E+01	15	.14372E+01	16	.13210E+01
		18	.11649E+01	19	.10917E+01	20	.10441E+01	21	.10000E+01	22	.97444E+00	23	.95086E+00	24	.93985E+00
		26	.91536E+00	27	.90006E+00	28	.89469E+00	29	.88741E+00	30	.87094E+00	31	.82784E+00	32	.78287E+00
		34	.10169E+01	35	.13802E+01	36	.18537E+01	37	.24151E+01	38	.45330E+01	39	.71913E+01	40	.34934E+02

MT= 16 WT= .41888E+01 HOB= .17601E+00SUMKFF= -.86244E-01

		2	.22142E-02	3	.15799E-01	4	.31519E-01	5	.60364E-01	6	.75049E-01	7	.92745E-01	8	.11367E+00
	.13275E+00	10	.16472E+00	11	.19403E+00	12	.22466E+00	13	.25557E+00	14	.31539E+00	15	.36905E+00	16	.50067E+00
17	.59354E+00	18	.79906E+00	19	.91602E+00	20	.97996E+00	21	.10000E+01	22	.98005E+00	23	.91661E+00	24	.80044E+00
25	.60056E+00	26	.51150E+00	27	.39315E+00	28	.34380E+00	29	.28720E+00	30	.25119E+00	31	.19470E+00	32	.10243E+00
33	.10822E-01	34	0.	35	0.	36	0.	37	0.	38	0.	39	0.	40	0.

	.37544E+02	2	.31602E+02	3	.77156E+01	4	.55162E+01	5	.38033E+01	6	.33478E+01	7	.29520E+01	8	.26157E+01
	.23415E+01	10	.20994E+01	11	.19021E+01	12	.17536E+01	13	.16375E+01	14	.14782E+01	15	.13828E+01	16	.12690E+01
17	.12099E+01	18	.11393E+01	19	.10866E+01	20	.10434E+01	21	.10000E+01	22	.96496E+00	23	.92981E+00	24	.90242E+00
25	.87106E+00	26	.86117E+00	27	.84363E+00	28	.83799E+00	29	.82870E+00	30	.81121E+00	31	.76993E+00	32	.73097E+00
33	.77046E+00	34	.95651E+00	35	.12820E+01	36	.17022E+01	37	.21990E+01	38	.40669E+01	39	.64070E+01	40	.30782E+02
	.67057E+02														

MT= 17 WT= .43633E+01 HOB= .19485E+00SUMKFF= -.92078E-01

		2	.23866E-02	3	.16874E-01	4	.33115E-01	5	.62396E-01	6	.77077E-01	7	.94645E-01	8	.11529E+00
	.13893E+00	10	.16533E+00	11	.19400E+00	12	.22401E+00	13	.25440E+00	14	.31354E+00	15	.36708E+00	16	.49911E+00
17	.59215E+00	18	.79852E+00	19	.91576E+00	20	.97982E+00	21	.10000E+01	22	.98006E+00	23	.91663E+00	24	.80038E+00
25	.60049E+00	26	.51132E+00	27	.39317E+00	28	.34455E+00	29	.28789E+00	30	.25155E+00	31	.19719E+00	32	.11112E+00
33	.98580E-02	34	-.31938E-01	35	0.	36	0.	37	0.	38	0.	39	0.	40	0.

	.61232E+02	2	.28678E+02	3	.71061E+01	4	.51185E+01	5	.35677E+01	6	.31538E+01	7	.27931E+01	8	.24853E+01
	.22355E+01	10	.20087E+01	11	.18247E+01	12	.16849E+01	13	.15746E+01	14	.14217E+01	15	.13294E+01	16	.12181E+01
	.11632E+01	18	.11046E+01	19	.10654E+01	20	.10333E+01	21	.10000E+01	22	.97034E+00	23	.93770E+00	24	.90840E+00
	.87258E+00	26	.85998E+00	27	.84087E+00	28	.83467E+00	29	.82246E+00	30	.80420E+00	31	.76618E+00	32	.72626E+00
33	.73436E+00	34	.87072E+00	35	.11893E+01	36	.15853E+01	37	.20420E+01	38	.37422E+01	39	.58632E+01	40	.27902E+02
	.60678E+02														

MT= 18 WT= .45379E+01 HOB= .20817E+00SUMKFF= -.74088E-01

		2	.24982E-02	3	.17574E-01	4	.34118E-01	5	.63646E-01	6	.78324E-01	7	.95817E-01	8	.11430E+00
	.13976E+00	10	.16578E+00	11	.19408E+00	12	.22372E+00	13	.25380E+00	14	.31254E+00	15	.36599E+00	16	.49821E+00
17	.59187E+00	18	.79823E+00	19	.91559E+00	20	.97975E+00	21	.10000E+01	22	.98012E+00	23	.91627E+00	24	.80053E+00
25	.60077E+00	26	.51135E+00	27	.39353E+00	28	.34578E+00	29	.28783E+00	30	.24887E+00	31	.19101E+00	32	.10459E+00
33	.11843E-01	34	-.25156E-01	35	0.	36	0.	37	0.	38	0.	39	0.	40	0.

	.57394E+02	2	.26919E+02	3	.67261E+01	4	.48646E+01	5	.34102E+01	6	.30212E+01	7	.26816E+01	8	.23911E+01
	.21544E+01	10	.19393E+01	11	.17639E+01	12	.16299E+01	13	.15237E+01	14	.13757E+01	15	.12861E+01	16	.11780E+01
17	.11266E+01	18	.10774E+01	19	.10475E+01	20	.10246E+01	21	.10000E+01	22	.97817E+00	23	.95246E+00	24	.92728E+00
25	.89415E+00	26	.88050E+00	27	.86204E+00	28	.85534E+00	29	.83744E+00	30	.81478E+00	31	.77460E+00	32	.73965E+00
33	.77849E+00	34	.89556E+00	35	.11902E+01	36	.15588E+01	37	.19857E+01	38	.35766E+01	39	.55621E+01	40	.26195E+02
	.56881E+02														

```
   MT=   19      WT=  .47124E+01      HOB=  .21591E+00SUMKFF= -.46652E-01

 1 0.           2  .25296E-02  3  .17753E-01  4  .34376E-01  5  .63940E-01  6  .78593E-01  7  .96036E-01  8  .11644E+00
 9   .13972E+00 10  .16567E+00 11  .19383E+00 12  .22335E+00 13  .25331E+00 14  .31192E+00 15  .36536E+00 16  .49769E+00
17   .62146E+00 18  .79802E+00 19  .91548E+00 20  .97967E+00 21  .10000E+01 22  .98015E+00 23  .91686E+00 24  .80067E+00
25   .60112E+00 26  .51147E+00 27  .39420E+00 28  .34688E+00 29  .28739E+00 30  .24632E+00 31  .18631E+00 32  .10079E+00
33   .14666E-01 34 -.19919E-01 35 0.          36 0.          37 0.          38 0.          39 0.          40 0.
41 0.
 1   .35359E+02  2  .25982E+02  3  .65160E+01  4  .47211E+01  5  .33180E+01  6  .29425E+01  7  .26143E+01  8  .23334E+01
 9   .21043E+01 10  .18957E+01 11  .17254E+01 12  .15951E+01 13  .14917E+01 14  .13472E+01 15  .12596E+01 16  .11539E+01
17   .11047E+01 18  .10603E+01 19  .10360E+01 20  .10183E+01 21  .10000E+01 22  .98393E+00 23  .96389E+00 24  .94419E+00
25   .91458E+00 26  .90017E+00 27  .88287E+00 28  .87507E+00 29  .85205E+00 30  .82621E+00 31  .78512E+00 32  .75463E+00
33   .73306E+00 34  .91882E+00 35  .11995E+01 36  .15528E+01 37  .19634E+01 38  .34957E+01 39  .54090E+01 40  .25296E+02
41   .35375E+02
```

APPENDIX B

DERIVATION OF $Q_{k,j}$

APPENDIX B

Derivation of $Q_{k,j}$

The kernel functions $Q_{k,j}$ were developed originally in Reference [14] and are reproduced as follows:

$$Q_{k,j} = K_1(k_o,j) - K_1(k_o,j) \qquad \text{for } j = 1$$

$$Q_{k,j} = K_2(k,j-1) - K_2(k_o,j-1) \qquad \text{for } j = 2, 4, 6, \ldots, k_f-1$$

$$Q_{k,j} = \left[K_1(k,j) + K_3(k,j-2)\right] - \left[K_1(k_o,j) + K_3(k_o,j-2)\right] \qquad \text{for } j = 3, 5, 7, \ldots, k_f-2$$

$$Q_{k,j} = K_3(k,j-2) - K_3(k_o,j-2) \qquad \text{for } j = k_f$$

where

$$K_1(k,j) = \frac{1}{2\delta_j}(-3v_j - v_{j+2}) - \frac{\bar{v}_j}{3\delta_j^2} - u_j(\ell n|u_j| - 1)$$

$$K_2(k,j) = \frac{2}{\delta_j}(v_j + v_{j+2}) + \frac{2\bar{v}_j}{3\delta_j^2}$$

$$K_3(k,j) = \frac{1}{2\delta_j}(-v_j - 3v_{j+2}) - \frac{\bar{v}_j}{3\delta_j^2} + u_{j+2}(\ell n|u_{j+2}| - 1)$$

and

$$\delta_j = \bar{\xi}_{j+1} - \bar{\xi}_j$$

$$u_j = \bar{\xi}_j - \bar{x}_k$$

$$v_j = \frac{u_j^2}{2}\left(\ell n|u_j| - \frac{3}{2}\right)$$

$$\bar{v}_j = u_j\left[v_j - \frac{u_j^2}{6}\right] - u_{j+2}\left[v_{j+2} - \frac{u_{j+2}^2}{6}\right]$$

APPENDIX C

DERIVATION OF $\frac{\partial \psi_{k+1/2}}{\partial P_j}$ FOR EQUATIONS (37)

APPENDIX C

Derivation of $\frac{\partial \psi_{k+1/2}}{\partial P_j}$ for Equations (37)

Equations (37) are linearized to form the following system of equations which are solved for P_{k_A} to P_{k_o-1}, P_{k_o+1} to $P_{k_{ff}-1}$, c'_I, and c'_o.

$$\frac{\partial \psi_{k+1/2}}{\partial c'_I}\,\Delta c'_I + \sum_{j=k_A}^{k_o-1}\left(\frac{\partial \psi_{k+1/2}}{\partial P_j}\right)^n \Delta P_j^{n+1} + \sum_{j=k_o+1}^{k_{ff}-1}\left(\frac{\partial \psi_{k+1/2}}{\partial P_j}\right)^n \Delta P_j^{n+1} + \frac{\partial \psi_{k+1/2}}{\partial c'_o}\,\Delta c'_o = \left(-\psi_{k+1/2}\right)^n$$

$$k = k_A, \ldots, k_{ff}-1 \qquad \text{(C-1)}$$

where

$$\left.\begin{aligned}\frac{\partial \psi_{k+1/2}}{\partial c'_I} &= 1\\ \frac{\partial \psi_{k+1/2}}{\partial c'_o} &= 0\end{aligned}\right\} \quad \text{for } k = k_A \text{ to } k = k_o-1 \qquad \text{(C-2)}$$

$$\left.\begin{aligned}\frac{\partial \psi_{k+1/2}}{\partial c'_I} &= 0\\ \frac{\partial \psi_{k+1/2}}{\partial c'_o} &= 1\end{aligned}\right\} \quad \text{for } k = k_o \text{ to } k = k_{ff}-1 \qquad \text{(C-3)}$$

Also,

$$\frac{\partial \psi_k}{\partial P_j} = 3\bar{h}_o^2\, H_{k+1/2}^2 \left(\frac{P_{k+1} - P_k}{\Delta \bar{x}_k}\right)\left(-\frac{(QQ)_{k+1/2}\, C_7}{\pi \bar{h}_o}\right)$$

$$+ \delta \frac{\bar{h}_o^2 H_{k+1/2}^3}{\Delta \bar{x}_k} + \sin\omega t \, (QQ)_{k+1/2} \frac{C_7}{\pi \bar{h}_o}$$

$$- \frac{1}{\Delta T} \, SUMS(K,QQ,O) \tag{C-4}$$

where $(QQ)_k = Q_{k,j}$ for $j \neq k_A$

$$(QQ)_k = \sum_{\ell=1}^{k_A} \frac{P_\ell}{P_{k_A}} Q_{k,\ell} \text{ for } j \neq k_A$$

$$\left.\begin{aligned} &\delta = 1 \quad \text{for } j = k+1 \\ &\delta = -1 \quad \text{for } j = k \\ &\delta = 0 \quad \text{for } j \neq k \text{ or } j \neq k+1 \\ &C_7 = 16\left(\frac{P_o}{E'}\right)^2 \Big/ \sqrt{48U} \end{aligned}\right\} \tag{C-5}$$

1. Report No.	2. Government Accession No.	3. Recipient's Catalog No.
NASA CR-159543		

4. Title and Subtitle	5. Report Date
Experimental and Analytical Tools for Evaluation of Stirling Engine Rod Seal Behavior	February, 1979
	6. Performing Organization Code

7. Author(s)	8. Performing Organization Report No.
Krauter, A. I., and Cheng, H. S. (Northwestern University)	SRC-78TR-39
	10. Work Unit No.

9. Performing Organization Name and Address	11. Contract or Grant No.
Shaker Research Corporation Northway 10 Executive Park Ballston Lake, NY 12019	DEN3-22
	13. Type of Report and Period Covered Contractor Report February 1978--February 1979

12. Sponsoring Agency Name and Address	14. Sponsoring Agency Code
U. S. Department of Energy Division of Transportation Energy Conservation Washington, DC 20545	DOE/NASA/0022-79/1

15. Supplementary Notes

Interim Report, Prepared under Interagency Agreement ED-77-A-31-1040 Project Manager:
NASA-Lewis Research Center R. E. Cunningham, MS 6-1
Cleveland, OH 44135

16. Abstract

This report concerns the first year of a two year experimental and analytical program. The program is directed at the elastohydrodynamic behavior of sliding elastomeric rod seals for the Stirling engine. During the year, experimental and analytical tools were developed for evaluating seal leakage, seal friction, and the fluid film thickness at the seal/cylinder interface. Experimentally, a rugged apparatus containing a moving transparent cylinder (guided by precision hydrostatic bearings) and a stationary elastomeric test seal has been constructed. A pressure gradient of 690 kPa (100 psi) can be applied across the seal. Frequencies from 10 Hz to 50 Hz with a 25 mm (1 in.) total stroke can be employed. Film thickness is measured with optical interferometry, fluid leakage by level and pressure changes, and power (friction) loss by a force cell. Analytically, a computer model of the elastohydrodynamic behavior of the rod seal for reciprocating motion was produced. The model permits the large initial radial squeeze, which is typically used for elastomeric seals, to exist. The model, based on a time domain analysis, determines both the pressure distribution and the oil film thickness distribution in the seal/cylinder contact zone. Conclusions and recommendations concern use during the ensuing year of these experimental and analytical tools.

17. Key Words (Suggested by Author(s))	18. Distribution Statement
Seal Rod Seal Stirling engine Interferometry Friction Leakage	Unlimited

19. Security Classif. (of this report)	20. Security Classif. (of this page)	21. No. of Pages	22. Price*
Unclassified	Unclassified		

* For sale by the National Technical Information Service, Springfield, Virginia 22161